NASA/TP—2001–210962

Estimating Cosmic-Ray Spectral Parameters From Simulated Detector Responses With Detector Design Implications

L.W. Howell
Marshall Space Flight Center, Marshall Space Flight Center, Alabama

National Aeronautics and
Space Administration

Marshall Space Flight Center • MSFC, Alabama 35812

April 2001

Acknowledgments

The author gives special appreciation to John Watts, Jim Adams, and Mark Christl of the Cosmic-Ray Group, Space Science Department, Marshall Space Flight Center, Huntsville, AL; Tom Parnell, Research Associate at the University of Alabama in Huntsville, Huntsville, AL; and Jonathon Ormes, Laboratory for High Energy Astrophysics, Goddard Space Flight Center, Greenbelt, MD, for their many technical discussions and ideas and their suggested simulation studies of practical interest to the cosmic-ray community, along with their editorial remarks pertaining to this technical publication.

The author is grateful to Jim Weigang, Wilton, CT, for providing the APL (A Programming Language) code of the Nelder-Mead downhill simplex algorithm. This program, which Jim developed along the lines of the simplex algorithm as it appears in *Numerical Recipes*, is used extensively in this simulation work. Jim was an independent consultant at the time he provided this code, but now is an employee of Winklevoss Consultants, Greenwich, CT. The author also expresses thanks to Allan J. Miller of CSIRO Mathematical & Information Sciences, South MDC, Victoria 3169, Australia, for providing very efficient and accurate FORTRAN subroutines for the cumulative normal distribution, the gamma function, and a gamma random number generator that are part of a dynamic link library used by the overall APL simulation program. The author also thanks Leigh Clayton, member of the APL Development Team at Soliton Associates Limited, Toronto, Canada, for providing guidance and associated APL computer code for setting the random number seeds in the simulation to ensure maximum randomness between "missions" and for providing a more efficient uniform random number generator than the one previously used.

Special thanks to Joseph Landman, SGI Americas Technology Center, Farmington Hills, MI, and Glen Barnett, Australian Graduate School of Management, New South Wales 2052, Australia for "software tuning" suggestions that led to significant speed improvements in evaluating the integral portion of the objective function when using the gamma detector response function. Glen Barnett and Mike Day, London, England, provided valuable comments and suggestions on maximum likelihood estimation and related computer coding. Mike Day also recommended the present mathematical form of the broken power law probability density function given in eq. (34) that has significant simulation run-time benefits when compared to other mathematical forms previously used. The author is grateful to Herman Rubin, Department of Statistics, Purdue University, West Lafayette, IN, for suggestions that helped in the analytical development of the Cramer-Rao bounds and his general discussions on maximum likelihood estimation.

Available from:

NASA Center for AeroSpace Information
7121 Standard Drive
Hanover, MD 21076–1320
(301) 621–0390

National Technical Information Service
5285 Port Royal Road
Springfield, VA 22161
(703) 487–4650

TABLE OF CONTENTS

LIST OF FIGURES

LIST OF FIGURES (Continued)

LIST OF TABLES

LIST OF ACRONYMS

cdf	cumulative distribution function
GEANT	"geometry and tracking" Particle Physics Simulation Program
GCR	galactic cosmic ray
LB	lower boundary
ML	maximum likelihood
pdf	probability density function
TP	Technical Publication

TECHNICAL PUBLICATION

ESTIMATING COSMIC-RAY SPECTRAL PARAMETERS FROM SIMULATED DETECTOR RESPONSES WITH DETECTOR DESIGN IMPLICATIONS

1. INTRODUCTION

This Technical Publication (TP) develops statistical methods for estimating the three spectral parameters of the broken power law energy spectrum. Estimation of these parameters and quantification of the surrounding uncertainty of the estimates are of considerable importance to designers of cosmic-ray detectors.

Analytical methods were developed in conjunction with a Monte Carlo simulation to explore the combination of the expected cosmic-ray environment with a generic space-based detector and its planned life cycle, allowing us to explore various detector features and their subsequent impact on estimating the spectral parameters. This study thereby permits instrument developers to make important trade studies in design parameters as a function of the science objectives, which is particularly important for space-based detectors where physical parameters, such as dimension and weight, impose rigorous practical limits to the design envelope.

A simple power law model consisting of a single spectral index (α_1) is believed to be an adequate description of the galactic cosmic-ray (GCR) proton flux at energies below 10^{13} eV, with a hypothesized transition at knee energy (E_k) to a steeper spectral index $\alpha_2 > \alpha_1$ above E_k. Methods for estimating these three spectral parameters are developed in this TP. Because many of the features and analytical tools related to a simple power law have natural extensions to the analysis of this so-called broken power law, these methodologies will be discussed in detail first.

2. SIMPLE POWER LAW

The simple power law suggests that the number of protons detected above an energy (E) for an assumed collecting power (product of size and observing time) is given by:[1]

$$N_0(>E) = N_A\left(\frac{E}{E_A}\right)^{-\alpha_1+1}, \tag{1}$$

where E is in units TeV, α_1 is believed to be $\approx$2.8, and N_A and E_A are numbers determined from the detector size and exposure time in the environment, respectively. For a typical space-based detector of 1 m^2 with a 3-yr program life, N_A and E_A are 160 and 500 TeV, respectively, implying that this detector is expected to observe 160 proton events above 500 TeV over its expected life cycle. In statistical terms, N_0 is assumed to represent an average number of events while the actual number to be observed on any given mission would follow the Poisson probability distribution with mean number N_0. The number of particles detected is taken to depend only on the geometrical factor of the assumed detector and its material composition. The detection efficiency is a convolution of the geometry and material composition and is taken to be independent of energy.

The associated cumulative probability distribution function (cdf) for E over some energy interval of interest $[E_1,E_2]$ is then given by

$$\Phi_0(E) = 1 - \frac{N_0(>E) - N_0(>E_2)}{N_0(>E_1) - N_0(>E_2)} \quad \text{for} \quad E_1 \le E \le E_2$$

$$= 1 - \frac{N_A\left(\frac{E}{E_A}\right)^{-\alpha_1+1} - N_A\left(\frac{E_2}{E_A}\right)^{-\alpha_1+1}}{N_A\left(\frac{E_1}{E_A}\right)^{-\alpha_1+1} - N_A\left(\frac{E_2}{E_A}\right)^{-\alpha_1+1}}$$

$$= 1 - \frac{E^{-\alpha+1} - E_2^{1-\alpha_1}}{E_1^{1-\alpha_1} - E_2^{1-\alpha_1}} \; . \tag{2}$$

Thus, the corresponding probability density function (pdf) for E is

$$\phi_0(E) = \frac{d\Phi_0(E)}{dE}$$

$$= \frac{\alpha_1 - 1}{E_1^{1-\alpha_1} - E_2^{1-\alpha_1}} E^{-\alpha_1} \quad \text{for} \quad E_1 \le E \le E_2 \ . \tag{3}$$

To randomly sample GCR proton event energies from the simple power spectrum over the interval $[E_1,E_2]$, $u_i=\Phi_0(E_i)$ is solved in terms of E_i to obtain

$$E_i = \Phi_0^{-1}(u_i) = \left[E_1^{1-\alpha_1} + u_i(E_2^{1-\alpha_1} - E_1^{1-\alpha_1})\right]^{\frac{1}{1-\alpha_1}} , \tag{4}$$

where u_i is a simulated random number from a standard uniform distibution and Φ_0^{-1} represents the inverse function of Φ_0, which is a conventional notation that will be used in subsequent sections. The mean of the simple power law distribution is determined by the expected value operator <E> which gives

$$\mu_E = < \mathrm{E} > = \int_{E_1}^{E_2} E\phi_0(E)dE$$

$$= \left(\frac{\alpha_1 - 1}{\alpha_1 - 2}\right) \frac{E_1^{2-\alpha_1} - E_2^{2-\alpha_1}}{E_1^{1-\alpha_1} - E_2^{1-\alpha_1}} \ . \tag{5}$$

The variance is given as $\sigma^2_E = <\mathrm{E}^2> - (<\mathrm{E}>)^2$, where the general form of $<\mathrm{E}^m>$ is

$$< \mathrm{E}^{\mathrm{m}} > = \int_{E_1}^{E_2} E^m \phi_0(E)dE$$

$$= \left(\frac{\alpha_1 - 1}{\alpha_1 - m - 1}\right) \frac{E_1^{m+1-\alpha_1} - E_2^{m+1-\alpha_1}}{E_1^{1-\alpha_1} - E_2^{1-\alpha_1}} \ . \tag{6}$$

At this time, note the critical point that $<\mathrm{E}^2>$ becomes infinite, as do all other higher moments, as E_2 goes to infinity, as is easily seen in eq. (7):

$$\lim_{b\to\infty} \int_a^b x^2 x^{-\lambda}\, dx = \infty \quad \text{for all } \lambda \le 3 \text{ and } a > 0 \ . \tag{7}$$

This observation suggests the need for a careful look at the effects of the large variance and other higher moments associated with all power law distributions, even when E_2 is kept finite. A measure of the relative dispersion of the energies of the incident protons, which is independent of units, is defined by $V=\sigma_E/\mu_E$ for the simple power law and is called the coefficient of variation in the statistical literature. An important concept in detector design is the energy resolution ρ of the detector that provides a measure of the relative accuracy of a cosmic-ray detector, which is the fractional error in measurements of a monoenergetic beam. The resolution ρ is defined as the standard deviation divided by the mean response with typical values of 30 to 40 percent.

As will be shown in this TP, the precision with which the spectral parameter α_1 can be estimated from a set of detector responses (energy deposits), measured in terms of its standard deviation, is a function of both the variance of the incident energies and the uncertainty induced by the detector. The dominating component of this measurement precision will be shown to be attributable to the variance of the incident energies σ_E, which in turn can only be controlled through collecting power. Since V and ρ are dimensionless and provide a measure of relative dispersion for the power law distribution and detector, respectively, an instructive comparison will show that $V>>\rho$. To illustrate these points, a detector-life cycle having parameters N_A=160 and E_A=500 TeV will observe 52,200 events on average in the energy range E_1=20 TeV to E_2=5,500 TeV from a simple power law spectrum when α_1 is 2.8, which gives a mean GCR event energy μ_E =44.5 TeV, a standard deviation σ_E=74.10 TeV, and a coefficient of variation V=166.5 percent. In comparison, the resolution ρ of most detectors is between 30 and 40 percent. E_2 is chosen for this detector-life cycle combination as 5,500 TeV, since the expected number of events above this energy are negligible, while E_1 is taken to be 20 TeV for purposes of this discussion.

Since the number of events and their incident energies will vary because of the finite detector size and exposure time, the statistical behavior of the GCR event energies in combination with a detector having energy resolution ρ and the subsequent spectral parameter estimates over multiple missions will be studied. Thus, for each mission, a random number N of GCR events from a Poisson distribution with mean 52,200 to represent the number of simulated events that the detector will observe in the energy range 20 to 5,500 TeV on any given mission will be generated.

Next, the incident energy of each of these N events using eq. (4) is simulated. For example, for one such simulated mission, N=51,883 and the mean and standard deviation of the simulated GCR incident energies are calculated to be 43.85 and 66.39 TeV, respectively. To illustrate the large fluctuations associated with power law distributions, the same number of events (51,883) are simulated from a normal distribution having a mean of 44.5 and standard deviation 74.1 so as to match the power law's mean and standard deviation for this energy range when α_1=2.8 and observe that the sample mean and standard deviation are 44.51 and 74.17, respectively, for a single sample mission, which are much closer to the population mean and variance than those from the power law random samples. This process is repeated for 100 missions, and the standard deviation for each mission is plotted in figure 1.

Note the large fluctuations of the standard deviations for the power law samples from mission to mission, while in contrast, the standard deviations of missions generated from a normal distribution are very stable. As will be seen in subsequent sections, this is why the variation in detector responses is dominated by the variation of GCR event energies, while the additional variation induced by the detector's energy resolution plays a rather minor role. This in turn contributes the dominant component of the standard deviation of the spectral parameter estimator.

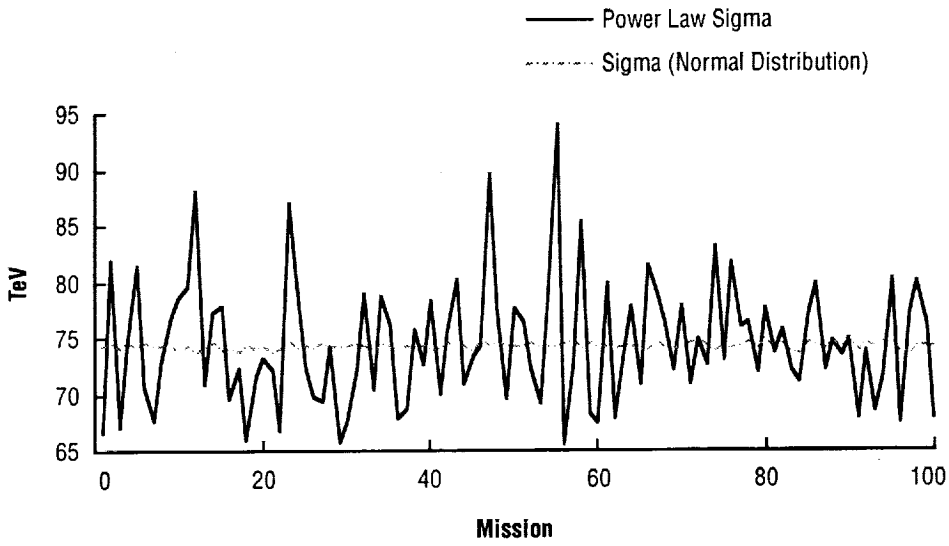

Figure 1. Standard deviation of simulated incident energies from power law (ragged curve) for 100 missions compared with that from normal distribution having same mean and variance.

The variation of the sample standard deviation s, measured by its standard deviation, is given by

$$\sigma_s = \sqrt{\frac{\mu_4 - \mu_2^2}{4\mu_2 N}} \quad , \tag{8}$$

where μ_r is the rth central moment about the mean,[2] defined for the simple power law as

$$\mu_r = \int (E - u_E)^r \phi_0(E) dE \quad . \tag{9}$$

Thus, the large variation in mission standard deviations is due to the term μ_4, which again is only finite by setting E_2 to a finite value, but nevertheless is responsible for the erratic behavior of the mission-to-mission sample standard deviations as depicted in figure 1. This erratic behavior of the observed mission standard deviations will necessarily be true for any power law having spectral index $\alpha_1 \leq 5$. Note that for the normal distribution,

$$\sigma_s = \frac{\sigma}{\sqrt{2N}} \quad , \tag{10}$$

and evaluation of these two formulae yield σ_s=5 TeV for the simple power law and 0.229 for the normal distribution, which is roughly a factor of 22.

2.1 Estimation of the Spectral Parameter α_1

Of particular interest in the study of cosmic-rays is the estimation of the spectral parameter α_1 from a set of data. Even though in practice the actual incident GCR energies are never observed, but only a measure of their energy deposition from their passage through the detector, it is important to consider the concept of an ideal detector having zero resolution. Thus, such a detector would measure the GCR event energies exactly.

2.1.1 Method of Moments

The method of moments consists of equating the sample moments with the population moments, which in general leads to k simultaneous nonlinear algebraic equations in the k unknown population parameters. For the simple power law, there is only one parameter to be estimated, so the sample mean $\overline{E}$ is set to the population mean μ_E in eq. (5) and then this nonlinear equation is solved in terms of $\hat{\alpha}_1$, where

$$\overline{E} = \left(\frac{\hat{\alpha}_1 - 1}{\hat{\alpha}_1 - 2}\right) \frac{E_1^{2-\hat{\alpha}_1} - E_2^{2-\hat{\alpha}_1}}{E_1^{1-\hat{\alpha}_1} - E_2^{1-\hat{\alpha}_1}} \quad . \tag{11}$$

Thus, for a given sample of size N, this equation is solved in terms of $\hat{\alpha}_1$ by numerical methods to provide an estimate of α_1. This estimator, which is a function of the random variable $\overline{E}$, has its own associated pdf. Since the GCR incident energy E has mean μ_E and finite variance $\sigma_E{}^2$ (only because the upper energy E_2 is finite), it is known by the Central Limit Theorem that the distribution of the sample average $\overline{E}$ follows a normal distribution with mean μ_E and variance $\sigma_E{}^2/N$.

For example, when α_1=2.8, E_1=20 TeV, E_2=5,500 TeV, $\overline{E}$ is normally distributed with mean 44.5 TeV and standard deviation (74.1 TeV)/$N^{1/2}$. These results can be used to obtain the probability distribution of the estimator by solving the probability equation:

$$\Pr\left\{\frac{\left(\frac{\hat{\alpha}_1 - 1}{\hat{\alpha}_1 - 2}\right)\frac{E_1^{2-\hat{\alpha}_1} - E_2^{2-\hat{\alpha}_1}}{E_1^{1-\hat{\alpha}_1} - E_2^{1-\hat{\alpha}_1}} - 44.5}{\frac{74.1}{\sqrt{N}}} \le Z\right\} = \int_{-\infty}^{Z} \frac{1}{\sqrt{2\pi}} e^{-\frac{x^2}{2}}\, dx \tag{12}$$

in terms of $\hat{\alpha}_1$ for various values of Z. Letting Z vary from –4.7 to 4.7 and setting N=52,000 events gives the probability distribution of $\hat{\alpha}_1$ shown in figure 2. Also depicted in figure 2 is the relative frequency histogram of the estimates $\hat{\alpha}_1$, based on 5,000 simulated missions; where for each mission, 52,000 events, on average, are simulated and the estimate of α_1 obtained by solving eq. (11). Furthermore, even though an explicit mathematical form for the pdf is not readily available, its mean and standard deviation can be calculated by numerical methods. For the distribution shown here, a numerically evaluation reveals its mean to be 2.800 and standard deviation as 0.0115 when N=52,000, which compares to the mean and

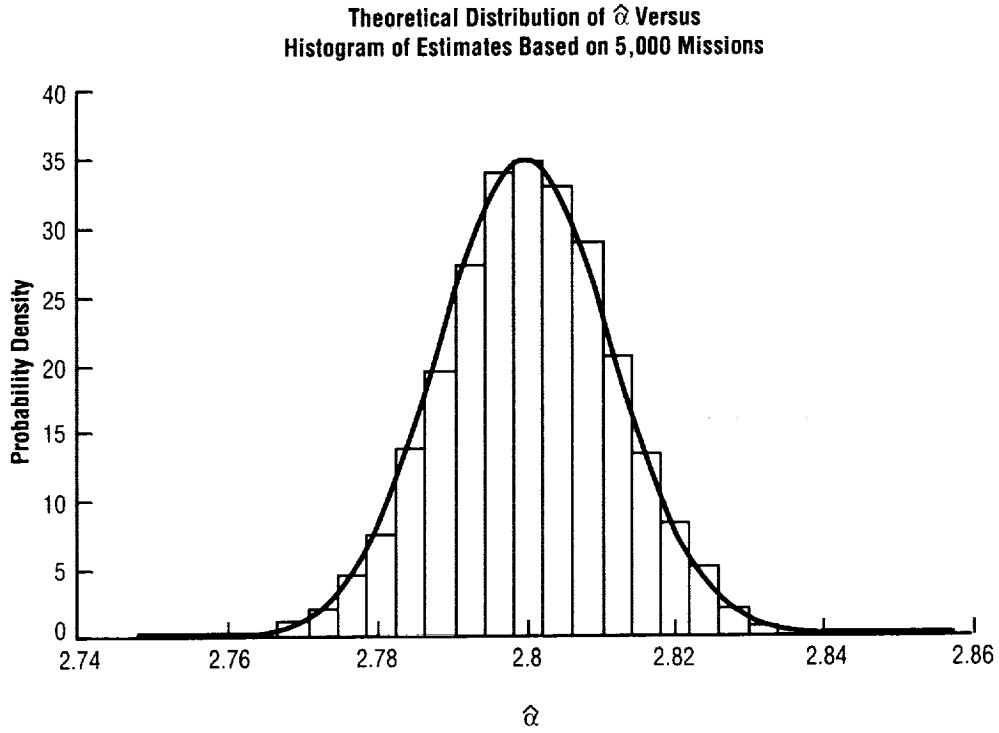

Figure 2. Probability distribution of method of moments estimate of α_1 with relative frequency histogram of spectral parameter estimates obtained from simulation.

standard deviation of the 5,000 simulated estimates with 2.800 and 0.0114, respectively. With the ability to numerically construct this estimator's pdf and moments, the important result is that its variance is inversely proportional to the sample size N, which is also true for many common estimators; e.g., the sample mean, standard deviation, and median. For example, if the number of events is doubled, then the variance is halved; and if the number of events is halved, then the variance doubles. Note that this relationship between sample size and the standard deviation of the estimator $\hat{\alpha}_1$ is based on keeping E_1 and E_2 fixed, so that in practice, the variance can be reduced by increasing the size and/or observing time.

2.1.2 Method of Maximum Likelihood

The likelihood function of a random sample from the simple power law, regarded as a function of the single unknown parameter α_1, is

$$L(\alpha_1) = \left(\frac{\alpha_1 - 1}{E_1^{1-\alpha_1} - E_2^{1-\alpha_1}} \right)^N \left(\prod_{i=1}^{N} E_i \right)^{-\alpha_1} \quad , \quad E_1 \le E_i \le E_2 \quad . \tag{13}$$

The method of maximum likelihood (ML) seeks as the estimate of α_1 that value (say, α_{ML}) which maximizes the likelihood function so that $L(\alpha_{ML}) \ge L(\alpha_1)$ for all α_1. Statistically speaking, this means that

the ML estimator leads us to a choice of α_1 that maximizes the probability of obtaining the observed data. In practice, it is often simpler to work with the logarithm of the likelihood function and seek solutions of $(\log L)'=0$ for which $(\log L)'' <0$ (indicating a maximum), where the prime and double prime indicate the first and second derivative, respectively. Thus, eq. (14) is numerically solved in terms of α_1 to obtain the ML estimate α_{ML}

$$\frac{\partial \log L}{\partial \alpha_1} = \frac{N}{\alpha_1 - 1} - N\left[\frac{(\log E_1)E_1^{1-\alpha_1} - (\log E_2)E_2^{1-\alpha_1}}{E_1^{1-\alpha_1} - E_2^{1-\alpha_1}}\right] - \sum_{i=1}^{N} \log E_i = 0 \quad . \tag{14}$$

The second derivative of the log-likelihood function is obtained next. Note that $(\log L)'' <0$ for all α_1, indicating that $\log L$ is concave; hence, there is a unique maximum, which was graphically observed by plotting $\log L$ as a function of α_1:

$$\frac{\partial^2 \log L}{\partial \alpha_1^2} = -N\left(\frac{1}{(\alpha_1 - 1)^2} + \left[\frac{E_2^{1+\alpha_1}E_1^{1+\alpha_1}(\log E_2 - \log E_1)^2}{(E_2E_1^{\alpha_1} - E_1E_2^{\alpha_1})^2}\right]\right) \quad . \tag{15}$$

By the Cramer-Rao inequality, the lower bound of the variance of any estimator $\tilde{\alpha}$ of α_1 is given by:[3]

$$Var(\tilde{\alpha}) \geq \frac{-1}{\dfrac{\partial^2 \log L}{\partial \alpha_1^2}} \quad , \tag{16}$$

which is asymptotically attained by the ML estimator. Also note that it is inversely proportional to the number of events N as was the variance of the estimator obtained using the method of moments. Other important properties of ML estimators are (1) asymptotically normally distributed and (2) consistency or asymptotically unbiased. Thus, a key question is, "For what values of N are these asymptotic properties achieved by the ML procedure?"

Based on the same 5,000 mission set discussed in the previous section, the mean and standard deviation of the 5,000 ML estimates are 2.800 and 0.00782, respectively. Using eqs. (15) and (16), the Cramer-Rao bound is computed to be 0.00786 when N=52,000 and α_{ML}=2.800, which compares very well with the simulation results. Furthermore, the frequency histogram of these 5,000 ML estimates resembled the normal distribution as stated in (1) of the above paragraph. A separate simulation study was conducted in which the sample size N was gradually reduced from 52,000 to 200, and the two asymptotic properties (1) attaining the Cramer-Rao bound and (2) consistency, were achieved by the ML estimates until around N=1,200. A bias on the high side of α_{ML} and failure to attain the Cramer-Rao bound became more and more evident as the number of events N diminished from 1,200 to 200.

Another very important comparison is the ratio of the standard deviation of α_{ML} to that of the estimator obtained using the method of moments. Direct calculation shows this ratio is roughly 1.45, implying that the ML procedure is significantly better than the method of moments when dealing with the

simple power law. This result is not too surprising, however, because ML estimators, in general, have better statistical properties than the estimators obtained by the method of moments.[4]

2.2 Detector Response Function

An original goal of this research was to create a Monte Carlo simulation in which various detector response functions describing the distribution of energy deposition in the detector as a function of incident GCR proton energy could be inserted. This desired flexibility led us to seek a numerical solution instead of a completely analytical approach.

Based on GEANT simulations of energy deposition for monoenergetic protons at specified energies at 0.1, 1, 10, 100, 1,000, and 5,000 TeV, the Gaussian distribution provided a reasonable description of the distribution of energy depositions at each of these incident energies.[5] Furthermore, the mean detector response was found to be well approximated by a linear function of incident energy in the range of interest for this study, which is typically between 10 and 5,500 TeV. Other detector response functions, such as a gamma distribution and another response function constructed from a combination of normal distributions having different parameters, have also been investigated and are presented in the broken power law section of this TP.

The random variable Y is introduced to represent the detector's response in terms of energy deposition of a GCR proton of incident energy E, and the conditional mean response and standard deviation of Y for a given event energy E modeled as $\mu_{Y|E} = (a + bE)$ and $\sigma_{Y|E} = (c + dE)$, respectively, where the four coefficients a, b, c, and d are estimated using linear regression on the GEANT simulation results. Thus, for each simulated incident GCR proton energy E_i, the detector response is simulated as

$$Y_i = \mu_{Y|E_i} + \sigma_{Y|E_i} Z_i \tag{17}$$

or

$$Y_i = (a + bE_i) + (c + dE_i) Z_i \ , \tag{18}$$

with the nonnegativity constraint $Y_i > 0$ and where Z_i is a standard normal random number having zero mean and unit standard deviation. Thus, the detector response function is defined as

$$g(y \mid E) = \frac{\eta_{y|E}}{\sqrt{2\pi\sigma^2_{y|E}}} e^{-\frac{(y-\mu_{y|E})^2}{2\sigma^2_{y|E}}} \ , \quad y > 0 \ , \tag{19}$$

where $\eta_{y|E}$ is a normalizing coefficient related to the truncation of the normal distribution resulting from the constraint $y>0$. It is worth noting for constant resolution studies in which a Gaussian response function is assumed and $\rho = \sigma/\mu$ is set to values 0.4 and 0.6, the corresponding detector energy resolution is 39 and 51 percent, respectively, and is rounded to 40 and 50 percent in the figures and tables in this TP.

Thus, $\eta_{y|E}$ is determined from

$$\frac{1}{\eta_{y|E}} = \int_{\frac{-1}{\rho_{y|E}}}^{\infty} \frac{1}{\sqrt{2\pi}} e^{-\frac{z^2}{2}} dz \ , \tag{20}$$

where the lower limit of integration is –1 divided by the resolution function given as

$$\rho_{y|E} = \sigma_{Y|E} / \mu_{Y|E} = (c + dE)/(a + bE) \ . \tag{21}$$

First, it is worthwhile to consider a detector having energy resolution $\rho_{y|E}=\sigma_{Y|E} / \mu_{Y|E}$ a constant ρ and independent of the cosmic-ray's energy (E) so that $\sigma_{Y|E} = \rho \, \mu_{Y|E}$, where typical values of interest for ρ are 0, 0.2, 0.3, 0.4, and 0.6. It should also be noted that the normalizing coefficient η in eq. (20) is constant whenever the detector resolution ρ is energy independent.

Second, a case where $\mu_{Y|E}$ and $\sigma_{Y|E}$ are linear but their ratio is not a constant so that the detector's resolution is a nonlinear function of incident energy E was investigated. For this second scenario, two studies were conducted in which the resolution is getting better from 40-percent resolution at 20 TeV to 30-percent resolution at 5,500 TeV and then getting worse from 30-percent resolution at 20 TeV to 40-percent resolution at 5,500 TeV. These two energy-dependent cases are presented in the broken power law section.

For detectors having constant energy resolution ρ, η is also a constant but depends on ρ, and is given in table 1 for several values of energy resolution.

Table 1. Normalizing coefficient η for Gaussian response function.

	Constant Resolution (ρ)					
	10%	20%	30%	40%	50%	60%
Truncated Probability	0	2.9E-07	0.00043	0.00621	0.02275	0.04779
η	1	1	1.00043	1.00625	1.02328	1.05019

2.3 Probability Distribution of the Detector Response

The probability distribution for the detector response in the presence of the simple power law energy spectrum over the energy range $[E_1,E_2]$ is:

$$g_0(y;\alpha_1) = \int_{E_1}^{E_2} g(y \mid E;\rho)\,\phi_0(E;\alpha_1)dE\,, \quad y>0\ . \tag{22}$$

The spectral parameter α_1 has been explicitly included in the argument list of both the simple power law pdf as $\phi_0(E;\alpha_1)$ and the detector response distribution $g_0(y;\alpha_1)$ in eq. (22) to indicate that this spectral index is inherited through the integral.

2.4 Ideal Detector

The concept of a zero-resolution or ideal detector is very useful because it sets an upper bound on the expected performance of any real detector. Furthermore, it allows quantifying the magnitude of the uncertainty in the estimate of the spectral parameter, measured in terms of the standard deviation of the estimator, attributable to event statistics (statistical fluctuation of incident GCR proton energies) relative to the uncertainty in measuring the spectral parameter estimate induced by the detector's nonzero energy resolution.

Thus, for an ideal detector, ρ=0 so that the standard deviation $\sigma_{Y|E}$=0 for all GCR event energies E. Hence, the detector response to a GCR of energy E is given by $Y=a+bE$ so that the incident energies may be directly obtained as $E_i=(Y_i-a)/b$; therefore, the estimation procedures developed in sections 2.1.1 and 2.1.2 apply.

2.4.1 Method of Moments for a "Real" Detector

The conditional expected value theorem, which says that the expected value of the conditional expected value is the unconditional expected value,[6] or in the notation of the mathematical expectation applied to the detector response Y,

$$\mu_Y = <Y> = <<Y \mid E>>\ , \tag{23}$$

to obtain the mean detector response μ_Y for a detector having constant resolution ρ:

$$\mu_Y = (a+b\mu_E)\left[1+\rho\eta(\rho)\int_{-1/\rho}^{\infty}\frac{x}{\sqrt{2\pi}}e^{-\frac{x^2}{2}}dx\right]\ , \tag{24}$$

where μ_Y is the mean detector response (energy deposit) and μ_E is the mean of the simple power law distribution. The term involving the integral can be thought of as a correction term to the mean for the truncation given in table 1 and can be ignored whenever ρ<0.30; i.e., 30-percent resolution or better. Using the method of moments, μ_Y is estimated with the sample average $\overline{Y}$ and when combined with eq. (5) for μ_E, yields eq. (25) that can then be solved in terms of $\hat{\alpha}_1$ by numerical methods:

$$\frac{\overline{Y}/b}{\left[1+\rho\eta(\rho)\int_{-1/\rho}^{\infty}\frac{x}{\sqrt{2\pi}}e^{-\frac{x^2}{2}}dx\right]}-\frac{a}{b}=\left(\frac{\hat{\alpha}_1-1}{\hat{\alpha}_1-2}\right)\frac{E_1^{2-\hat{\alpha}_1}-E_2^{2-\hat{\alpha}_1}}{E_1^{1-\hat{\alpha}_1}-E_2^{1-\hat{\alpha}_1}}\quad . \tag{25}$$

For example, when the resolution is a constant 40 percent (ρ=0.40), the point estimate of the spectral parameter α_1 based on the 5,000 missions is 2.801 using eq. (25) and 2.79 using the same equation but with the correction term set to zero in the denominator, resulting in a bias of ≈0.01 that can be removed by including this correction term. This effect is much more pronounced when ρ=0.60 and results in a bias of 0.1 in the point estimate of α_1 so that the correction term is critical.

When the detector response distribution is symmetric and truncation is negligible so that $\mu_Y=(a+b\mu_E)$, then α_1 can always be estimated using the mean of the detector responses $\overline{Y}$ to estimate μ_Y in eq. (24). This implies that knowledge of the variance of the detector distribution, and hence the resolution, is really not required in order to estimate α_1, provided knowing that the resolution is <30 percent so the effect of truncation can be ignored.

This is a useful result, because if the uncertainty regarding the true resolution is non-negligible, then the method of moments provides a way to proceed with the estimation of α_1; e.g., the detector's energy resolution is known to be <30 percent but nothing more. However, as already noted, the method of moments does not provide the minimum variance estimator that the ML method does which requires a complete specification of the detector parameters *a*, *b*, *c*, and *d* of this assumed Gaussian response function. Furthermore, the energy resolution of most real detectors is worse than 30 percent.

This estimator based on the method of moments is a function of the random variable *Y* and has its own associated pdf. Since *Y* has mean μ_Y and variance σ^2_Y, it is known by the Central Limit Theorem that the distribution of $\overline{Y}$ follows a normal distribution with mean μ_Y and variance σ^2_Y/N. Thus, the variance of the detector response *Y* is $\sigma_Y^2 = <Y^2> - \mu_Y^2$, where

$$<Y^2>=(a^2+2ab\mu_E+b^2\sigma_E^2+b^2\mu_E^2)\eta(\rho)\left[\int_{-1/\rho}^{\infty}\frac{(1+\rho x)^2}{\sqrt{2\pi}}e^{-\frac{x^2}{2}}dx\right]\quad . \tag{26}$$

For example, when α_1=2.8, E_1=20 TeV, E_2=5,500 TeV, and ρ=0.40, $\overline{Y}$ is normally distributed with mean 131.58 GeV and standard deviation (213.69 GeV)/$N^{1/2}$. The probability distribution of $\hat{\alpha}_1$, along with its mean and standard deviation, can be obtained by solving the probability equation in eq. (27) using the methods discussed with eq. (12):

$$\Pr\left\{\frac{\left[a+b\left(\frac{\hat{\alpha}_1-1}{\hat{\alpha}_1-2}\right)\frac{E_1^{2-\hat{\alpha}_1}-E_2^{2-\hat{\alpha}_1}}{E_1^{1-\hat{\alpha}_1}-E_2^{1-\hat{\alpha}_1}}\right]\left[1+\rho\eta(\rho)\int_{-1/\rho}^{\infty}\frac{x}{\sqrt{2\pi}}e^{-\frac{x^2}{2}}dx\right]-131.58}{\frac{213.69}{\sqrt{N}}}\le Z\right\}=\int_{-\infty}^{Z}\frac{1}{\sqrt{2\pi}}e^{-\frac{x^2}{2}}dx\ . \qquad (27)$$

If the truncation effect is assumed to be negligible in eq. (26), then the following succinct formula for the variance of the detector response as a function of detector parameters a, b, and ρ and the mean μ_E and variance σ_E^2 of the power law distribution is obtained:

$$\sigma_y^2 = b^2\sigma_E^2 + \rho^2\left[(a+b\mu_E)^2 + b^2\sigma_E^2\right]\ . \qquad (28)$$

In terms of the standard deviation of the detector response σ_y, the approximation in eq. (28) is seen to be actually quite good, for when ρ=0.40, this formula yields, σ_y=213.37 GeV as compared to the exact value of 213.69 GeV obtained from eq. (27) using the integral correction terms. When ρ=0.60, this approximation yields σ_y =237.31 GeV as compared to the actual value of 239.78 GeV. Thus, ignoring the truncation is not too serious when estimating the standard deviation but can be devastating for ρ>0.40 when estimating the mean μ_Y and hence α_1 when using the method of moments. Much insight into the estimation of the spectral parameter α_1 can be gleaned from eq. (28) because it shows the relationship between the variance σ_Y^2 of the detector response distribution, the variance σ_E^2 of the GCR proton energy spectrum, and the detector response function parameters a, b, and ρ.

The influence of the variance and other higher moments of the simple power law energy spectrum is visualized in figure 3 which shows the mean detector response (mean energy deposit) per mission for 30 simulated missions in comparison with the mean incident proton energy for 30 missions. Corresponding standard deviations per mission are plotted in figure 4. Note that the detector response mean and standard deviation per mission tend to track the mean and standard deviation of the incident energies for the 30 missions, illustrating the strong influence of the GCR energy mission-to-mission fluctuations on the detector response variation, even in the presence of the "smearing" induced by this detector having 40-percent energy resolution. As will be seen in section 2.4.2, the component of variation due to the GCR event statistics will be the dominating component of the total variation in the standard deviation of the estimator of the spectral index α_1.

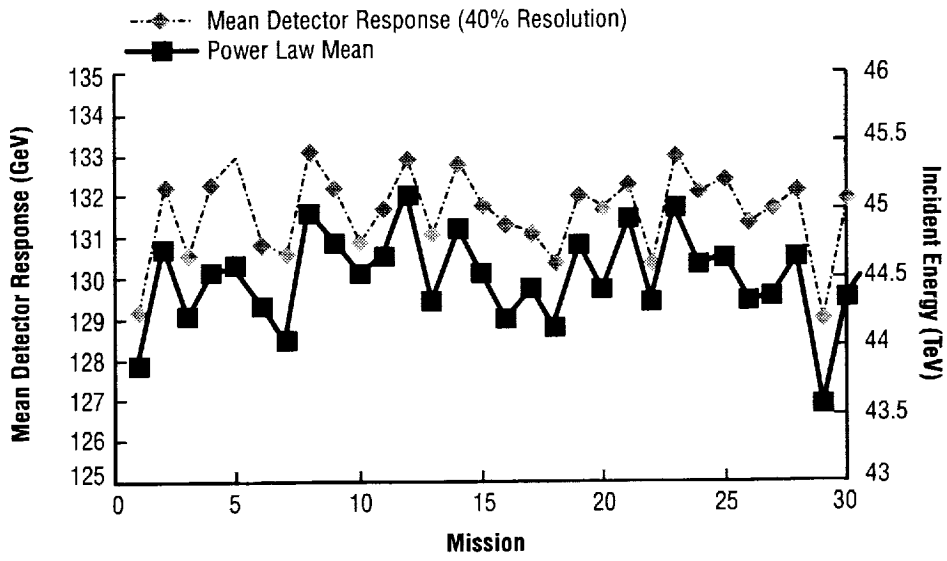

Figure 3. Comparing the mean incident energy with the mean of the detector responses for each of 30 missions.

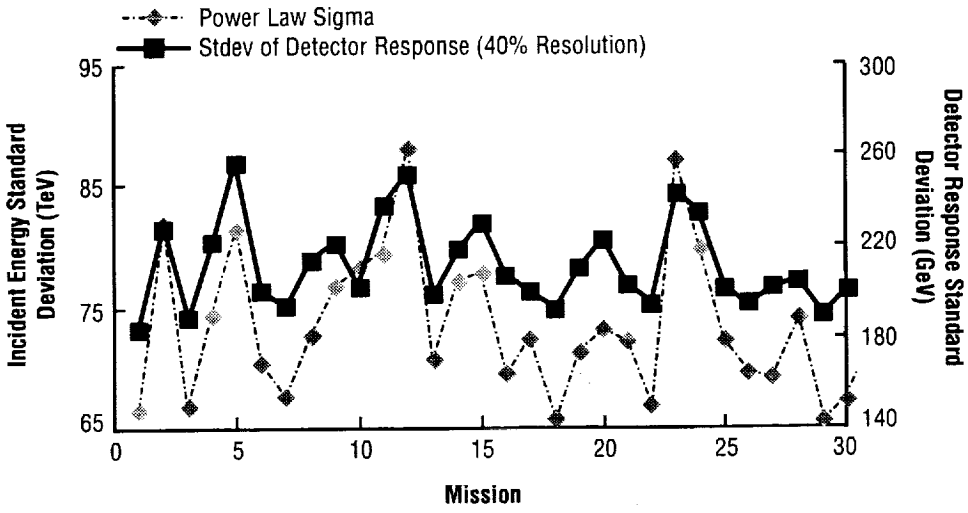

Figure 4. Comparing the standard deviation of the GCR incident energies with the standard deviation of the detector responses for each of 30 missions.

2.4.2 Maximum Likelihood for a "Real" Detector

As in section 2.1.2, the method of ML seeks α_{ML} which maximizes the log-likelihood function so that $\log L(\alpha_{ML}) \geq \log L(\alpha_1)$ for all α_1, where the likelihood function for the detector response in the presence of the simple power law energy spectrum of N incident GCR protons over the energy range $[E_1,E_2]$ is

$$\log L(\alpha_1) = \sum_{j=1}^{N} \log[g_0(y_j;\alpha_1)] = \sum_{j=1}^{N} \log\left[\int_{E_1}^{E_2} g(y_j \mid E)\, \phi_0(E;\alpha_1) dE\right] . \tag{29}$$

Because of the complexity of the integral and the desired capability to easily change the functional form of the detector response function g in eq. (29), a numerical approach for obtaining α_{ML} was chosen. Two optimization algorithms that do not require gradient information (derivatives) were selected for use; i.e., the multidimensional minimization algorithm called the Nelder-Mead downhill simplex method and Powell's direction set method.[7] While both methods provided matching results and were about the same in terms of computer run time, the Nelder-Mead downhill simplex method was easier to control and modify the termination criteria. Furthermore, the simplex method proved to be more robust with the emergence of multiple maxima in the likelihood function which occurred at the higher values of the knee location investigated in the broken power law section of this TP. Therefore, the discussion that follows is specific to the downhill simplex method. Since this is a minimization algorithm, the objective function is defined as

$$O(\alpha_1) = -\log L(\alpha_1) = -\sum_{j=1}^{N} \log\left[\int_{E_1}^{E_2} g(y_j \mid E)\, \phi_0(E;\alpha_1) dE\right] , \tag{30}$$

so that minimizing $O(\alpha_1)$ maximizes $\log L(\alpha_1)$ as desired, where the integral is numerically evaluated. The following two termination criteria are used to halt the search procedure for the ML estimate at the $(m+1)^{th}$ iteration:

$$\text{(i)}\ \ |\alpha_{1,m+1} - \alpha_{1,m}| < \varepsilon_1$$

and

$$\text{(ii)}\ \ |O(\alpha_{1,m+1}) - O(\alpha_{1,m})| < \varepsilon_2 \ . \tag{31}$$

The search procedure continues until the termination criteria are met, which in words are: (i) the movement in successive step sizes of α_1 is $<\varepsilon_1$ and (ii) the objective function is changing by an amount $<\varepsilon_2$. Typical values used for these two stopping tolerances are on the order of 10^{-5} and seem reasonable in light of the magnitude of the parameter being estimated ($\approx$2.8) and the value of the objective function in the vicinity of the ML solution, $O(\alpha_{ML})$ being of the order of magnitude 10^5 when E_1 is taken to be anywhere between 10 and 30 TeV, so the number of terms in the sum is between 182,000 to 26,000, respectively. Furthermore, changing ε_1 and/or ε_2 in either direction by an order of magnitude provided no noticeable change in results.

Figure 5 shows the ML estimates of α_1 for a zero-percent resolution detector obtained from eq. (14) in comparison with the ML estimates obtained from a 40-percent resolution detector and applying the downhill simplex algorithm to eq. (30) for 30 missions. This very close comparison suggests that the GCR event statistics are the dominating component of uncertainty in the estimation of the spectral parameter α_1.

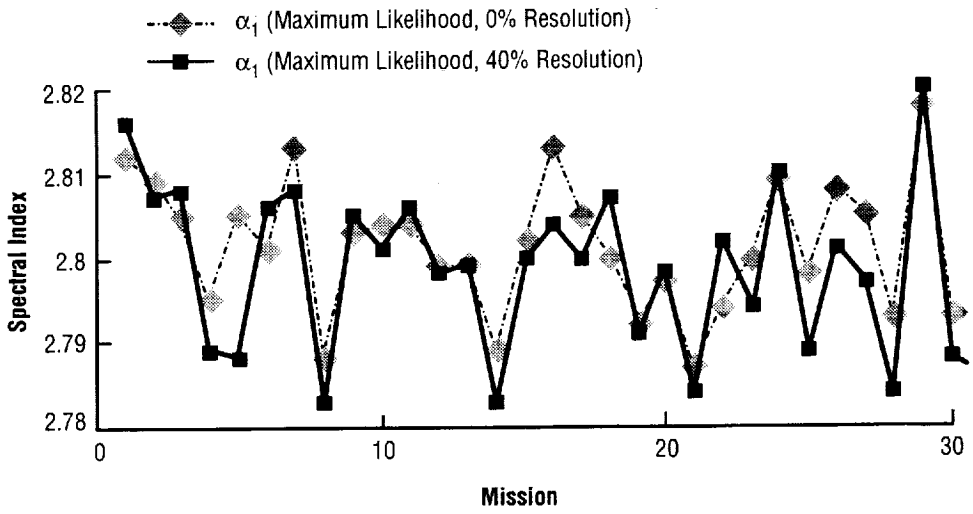

Figure 5. Maximum likelihood estimates for zero- and 40-percent resolution detector for 30 missions.

2.5 Summary Remarks and Conclusions for the Simple Power Law

Two methods for estimating the single spectral index (α_1) of a simple power law have been investigated. The first method—the method of moments—was found to be very useful in studying the general nature of the statistical estimation problem as well as yielding an analytical solution that could be compared with Monte Carlo simulation results. Furthermore, when the detector resolution is better than 30 percent so that the truncation of the detector response function is negligible, the method of moments provides an estimator of α_1 without requiring specific knowledge of the detector resolution ρ but only that it is better than 30 percent. This does not imply ρ is insignificant when it is <30 percent, but only that the correction terms previously discussed can be ignored and thus explicit knowledge is not needed of the value of ρ to estimate α_1. In fact, the standard deviation of the estimator increases as ρ increases as one would expect and results from the fact that whatever ρ happens to be, its impact is communicated to the estimate of α_1 through the variance of the detector mean response $\overline{Y}$ which is a function of ρ as indicated in eqs. (26)–(28).

Another interesting result is that when the resolution is <30 percent, it is not necessary to know the explicit functional form of the detector model, but only that it is symmetric. Unfortunately, most detector response functions are worse than 30-percent resolution and may be asymmetric as well.

The method of ML estimation clearly stands out as the method of choice for estimating α_1 in terms of minimum variance and consistency (asymptotically unbiased), as well as asymptotic normality which allows for probabilistic statements, such as confidence intervals for the unknown spectral parameter. These results as a function of detector resolution are shown in figure 6.

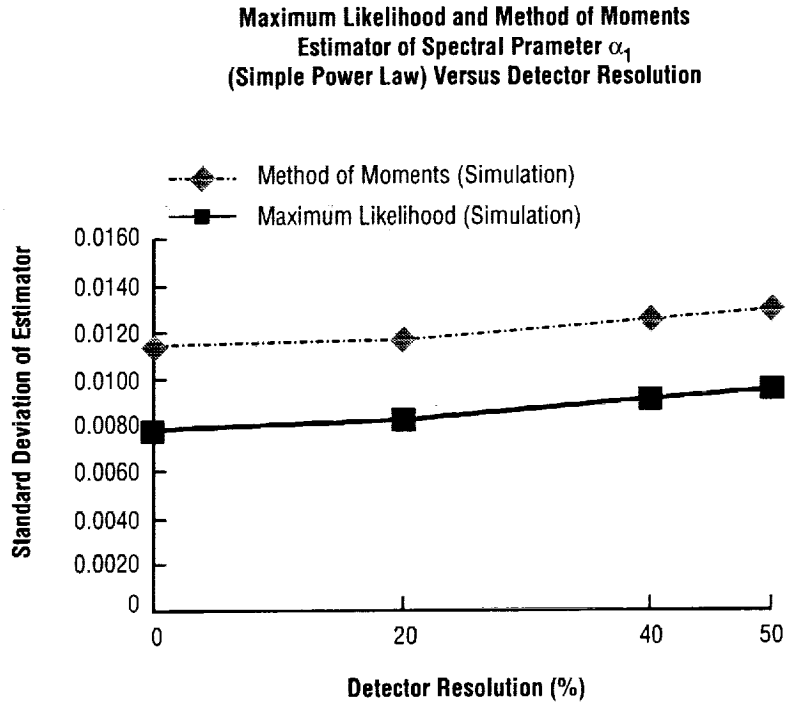

Figure 6. Comparison between method of moments and maximum likelihood as a function of detector resolution.

When compared to the standard deviation of the method of moments estimator, the ratio varies from 1.47 for the zero-percent resolution detector to 1.33 for the 50-percent resolution detector, which is roughly equivalent to giving away half of the detector's collecting power by choosing the inferior method of moments estimation technique.

Also shown was that the standard deviation of the estimate for both estimation procedures is inversely proportional to the square root of the sample size, so that halving the collecting power increases the standard deviation by a factor of $\sqrt{2}$. This holds true for the standard deviation of ML estimate as long as it attains the Cramer-Rao lower bound, which it does when the number of GCR events exceeds $\approx$1,200.

Another important result is the relationship between the collecting power and the energy resolution of the detector. A measure of the detector's ability to estimate the spectral parameter α_1 is its standard deviation and as seen in figures 6 and 7, the dominant component of the standard deviation of α_{ML} is attributable directly to the large fluctuations in GCR incident energies, being driven by the large variance and other higher moments of the simple power law distribution. This large component can only be reduced by increasing the number of events N that is controlled by the collection power of the dectector. A comparison of the standard deviation of α_{ML} for the generic detector discussed in this TP and when its collecting power is halved is given in figure 7. Table 2 provides the numerical results used to construct many of the figures in this section.

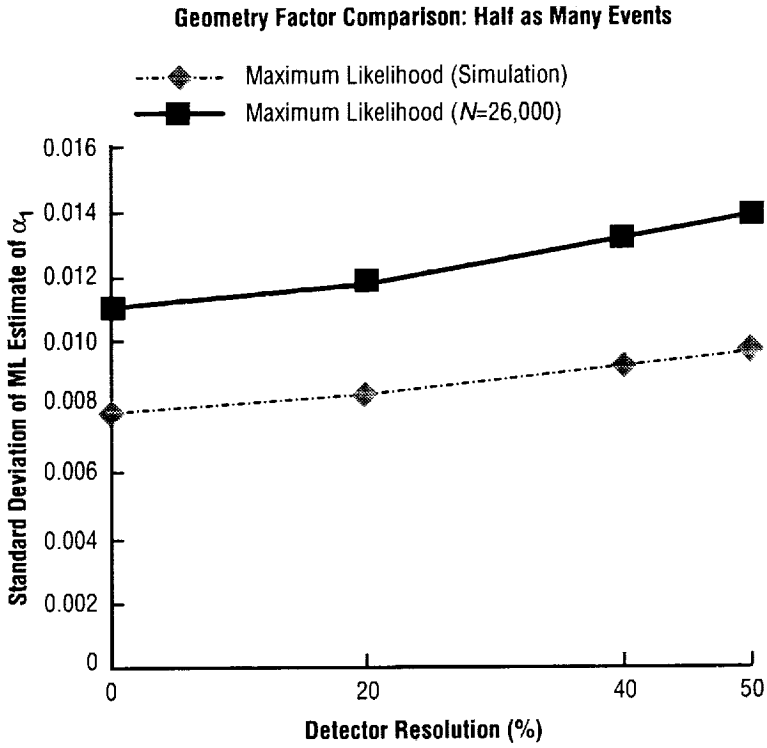

Figure 7. Comparing the effect of collecting power on the standard deviation of the maximum likelihood estimate of the spectral index α_1.

Table 2. Numerical values used to construct figures 6 and 7.

E_1=20 TeV, E_2=5,500 TeV, α_1=2.8, $N_{average}$=52,000 events. 5,000 mission averages for simulation results.	Detector Resolution			
	0%	**20%**	**40%**	**50%**
1. Method of moments (theory)	0.0115	0.0116	0.0128	0.0136
2. Method of moments (simulation)	0.0114	0.0117	0.0125	0.0133
3. Maximum likelihood (Cramer-Rao lower bound)	0.00786	Analytical solution not available		
4. Maximum likelihood (simulation)	0.0078	0.0083	0.0092	0.0100
5. Mean detector response (GeV) (theory)	130.66	130.66	131.58	138.85
6. Mean detector response (GeV) (simulation)	130.66	130.64	130.64	138.81
7. Standard deviation (theory)	192.07	197.61	213.69	239.77
8. Standard deviation (simulation)	191.47	196.86	213.33	238.82
9. Coefficient of variation V_Y (detector, %)	147	151	162	173
E_1=20 TeV, E_2=5,500 TeV, α_1=2.8, $N_{average}$=26,000 events. 5,000 mission averages for simulation results.				
10. Maximum likelihood	0.0110	0.0118	0.0132	0.0144
11. Ratio of line 4 to line 10, compare to sqrt(2)	1.41	1.42	1.43	1.44

3. BROKEN POWER LAW

This energy spectrum suggests a transition from spectral index α_1 below the knee location energy E_k to a steeper spectral index $\alpha_2 > \alpha_1$ above the knee. The broken power law predicts that the number of protons detected above an energy E is given by:[1]

$$N_1(>E) = \begin{cases} N_A\left(\frac{\alpha_1 - 1}{\alpha_2 - 1}\right)\left(\frac{E_k}{E_A}\right)^{-\alpha_1+1}\left(\frac{E}{E_A}\right)^{-\alpha_2+1} & \text{for } E \geq E_k \\ N_0(>E) - \left[N_0(>E_k) - N_1(>E_k)\right] & \text{for } E < E_k \end{cases}, \tag{32}$$

where E is in units TeV, N_A and E_A are 160 and 500 TeV as before, and currently available measurements suggest that α_1 is ≈2.8, α_2 is thought to be somewhere between 3.1 and 3.3, and E_k is parameterized in the range 100–300 TeV for this research. $N_0(>E)$ is the number of protons detected above an energy E as defined in eq. (1); and as in the simple power law section, these simulation studies assume the number of events for a given mission follow the Poisson probability distribution with mean determined by eq. (32). Writing $N_0(>E)$ in eq. (32) as

$$N_0(>E) = N_A\left(\frac{E_k}{E_A}\right)^{-\alpha_1+1}\left(\frac{E}{E_k}\right)^{-\alpha_1+1} \tag{33}$$

and constructing the cdf as in eq. (2), then differentiating, gives the pdf of the broken power law over energy range $[E_1, E_2]$ as

$$\phi_1(E;\alpha_1,\alpha_2,E_k) = \begin{cases} A\left(\frac{E}{E_k}\right)^{-\alpha_1} & \text{for} \quad E_1 \leq E < E_k \\ A\left(\frac{E}{E_k}\right)^{-\alpha_2} & \text{for} \quad E_k \leq E \leq E_2 \end{cases}, \tag{34}$$

where the normalizing coefficient A is given by

$$A = A(\alpha_1,\alpha_2,E_k) = \frac{(\alpha_1 - 1)(\alpha_2 - 1)}{E_k\left[\alpha_1 - \alpha_2 + (\alpha_2 - 1)\left(\frac{E_1}{E_k}\right)^{1-\alpha_1} - (\alpha_1 - 1)\left(\frac{E_2}{E_k}\right)^{1-\alpha_2}\right]}. \tag{35}$$

Note that ϕ_1 has "slope" α_1/α_2 below/above the knee location E_k and is continuous at E_k as required, and the single normalizing coefficient A in both mathematical terms of ϕ_1 in eq. (34) provides a succinct mathematical form, making calculation of the log-likelihood function in the ML search algorithm computationally more efficient than other equivalent mathematical representations of ϕ_1. The mean, variance, and other important moments of the broken power law distribution can be obtained from the general form of $<E^m>$ given as

$$< \mathrm{E}^{\mathrm{m}} >= \int_{E_1}^{E_2} E^m \phi_1(E) dE$$

$$= A E_k^{m+1} \left\{ \frac{1}{m+1-\alpha_1} \left[1 - \left(\frac{E_1}{E_k} \right)^{m+1-\alpha_1} \right] - \frac{1}{m+1-\alpha_2} \left[1 - \left(\frac{E_2}{E_k} \right)^{m+1-\alpha_2} \right] \right\} \tag{36}$$

which necessarily has dimension $(\mathrm{TeV})^m$ since A has dimension $(\mathrm{TeV})^{-1}$. A random sample of GCR proton event energies are obtained from the broken power law spectrum over the range $[E_1,E_2]$ as $E_i = \Phi_1^{-1}(u_i)$, where u_i is a random number from a standard uniform distibution and Φ_1^{-1} represents the inverse function of the broken power law cdf Φ_1.

Figure 8 shows $N_1(>E)$ with a histogram (the ragged curve in fig. 8) constructed from simulated events from the broken power law. $N_0(>E)$ is included in figure 8 for comparison with $N_1(>E)$ and clearly shows the transition from α_1 to α_2 at the knee E_k, with the plots cropped at 1,000 TeV to better illustrate this so-called knee region. Parameters used in this example are α_1=2.8, α_2=3.3, E_k=100 TeV, E_1=20 TeV, and E_2=5,500 TeV.

Note that at the knee, the difference between $N_0(>100$ TeV) and $N_1(>100$ TeV) is 626 events and reduces to 412 events when α_2 drops to 3.1. Another important observation is the significant reduction in the standard deviation of the incident energy when compared to the simple power law, which suggests that detector resolution will play a somewhat larger role in the overall contribution to the estimator's standard deviation than it did in the case of a simple power law. The mean μ_E, standard deviation σ_E, and coefficient of variation $V=\sigma_E/\mu_E$ are given in table 3 for selected parameters for comparison.

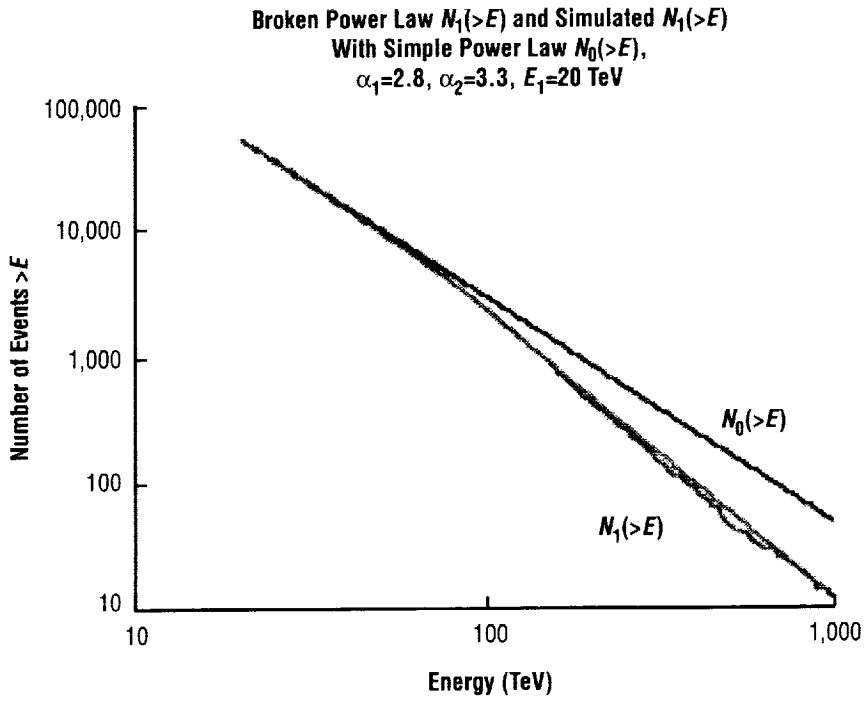

Figure 8. Comparison of $N_1(>E)$ with $N_0(>E)$. A histogram of simulated events from the broken power law are also included.

Table 3. Means, standard deviations, and coefficient of variation (mathematically the same as resolution) for the simple power law and broken power law.

Energy Range 20–5,500 TeV	Spectral Parameters	Mean (TeV)	Standard Deviation (TeV)	Coefficient of Variation (%)
Simple power law	α_1=2.8	44.50	74.1	166
Broken power law	α_1=2.8, α_2=3.1, E_k=100 TeV	41.83	54.17	129
Broken power law	α_1=2.8, α_2=3.3, E_k=100 TeV	40.67	45.54	101

3.1 Estimation of the Spectral Parameters α_1, α_2, and E_k

As suggested in the simple power law study in section 2, the ML procedure offers a superior approach for estimating the spectral parameters in terms of their known favorable statistical properties. Thus, concentration will be on obtaining the ML estimates of the three spectral indices of the broken power law distribution. For notational convenience, the vector $\boldsymbol{\theta}=(\alpha_1, \alpha_2, E_k)$ consisting of the three broken power law spectral indices is introduced.

The ML estimation procedure will be illustrated for a single mission by first estimating $\boldsymbol{\theta}$ directly from the incident energies E_i (equivalent to the so-called ideal detector having zero energy resolution), and then from their simulated detector responses Y_i using the same detector response function described in the simple power law section and for the case where α_1=2.8, α_2=3.3, E_k=100 TeV, E_1=20 TeV, and E_2=5,500 TeV. The results from many other parametric scenarios of interest will also be presented.

3.1.1 Method of Maximum Likelihood for the Ideal Detector

The likelihood function of a random sample of size N from the broken power law, regarded as a function of the unknown vector of parameters $\boldsymbol{\theta}=(\alpha_1, \alpha_2, E_k)$ is

$$L(\boldsymbol{\theta}) = A(\boldsymbol{\theta})^N \left(\prod_{E_i<E_k} \frac{E_i}{E_k} \right)^{-\alpha_1} \left(\prod_{E_j \geq E_k} \frac{E_j}{E_k} \right)^{-\alpha_2} , E_1 \leq E_i, E_j \leq E_2 \ , \tag{37}$$

where the first product is over the energies below the knee energy (E_k) and the second product is over those energies above E_k, and they total in number to N, and $A(\boldsymbol{\theta})$ is the coefficient given in eq. (35). The Nelder-Mead downhill simplex method is used to find the ML solution $\boldsymbol{\theta}_{ML}$ that minimizes the objective function (minus the log-likelihood) defined as

$$O(\boldsymbol{\theta}) = -L(\boldsymbol{\theta}) = -N \log A(\boldsymbol{\theta}) + \alpha_1 \left(\sum_{E_i<E_k} \log\left[\frac{E_i}{E_k}\right] \right) + \alpha_2 \left(\sum_{E_j \geq E_k} \log\left[\frac{E_j}{E_k}\right] \right) . \tag{38}$$

For the sample mission under consideration, the number of simulated events is N=51,259 and is a random number generated from a Poisson distribution with mean N_1(>20 TeV)=51,576 (recall N_0=52,200 for the simple power law). Note that 2,165 of these events are above the assumed knee location at 100 TeV. Also, the mean of these simulated incident energies is 40.28 TeV and standard deviation 40.79 TeV and can be compared with the bottom row of table 3.

To obtain a reasonable starting point for the search procedure, it is first assumed that α_1 will be largely influenced by those energies (E_i) thought to be well below the knee energy (E_k), even though the true value of E_k is unknown. For example, if all energies below 70 TeV (of which 49,094 are below 70 TeV, or 96 percent), with the assumption that a simple power law will dominate the statistical description of these event energies, then the ML estimate of α_1 is 2.81 using eq. (30). Next, keeping α_1 fixed at 2.81

and using the full set of simulated event energies, the other two parameters are fit using a two-dimensional simplex search for (α_2, E_k), which yields α_2=3.317 and E_k=95.44 TeV. The two-dimensional simplex search is illustrated in figure 9 and three things should be noted: (1) The knee energy (E_k) has been scaled by a factor of 0.1 so that it is fairly close in magnitude to the other two spectral parameters, (2) the simplex can leave the initial simplex region (but in this example, it returned), and (3) the simplex moves only one vertex per iteration.

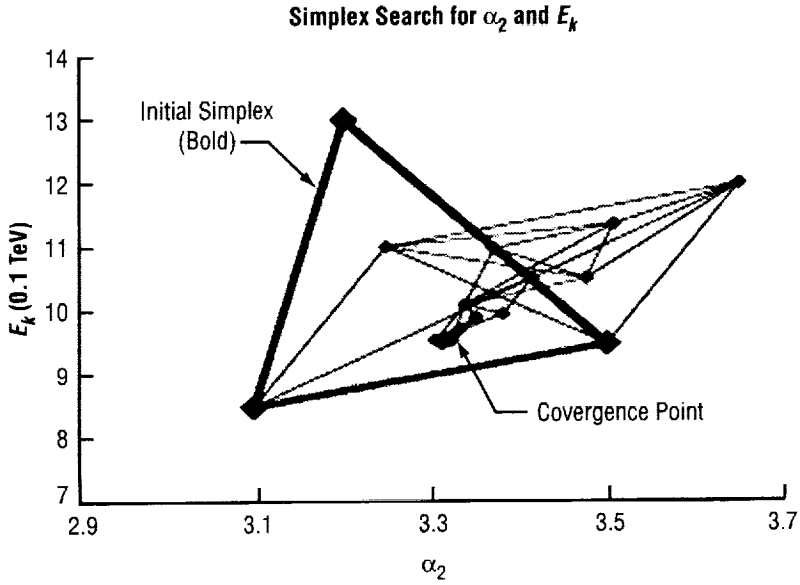

Figure 9. Two-dimensional simplex search for (a_2, E_k).

Next, $\boldsymbol{\theta}_{initial}$ =(2.810, 3.317, 95.44) is defined and used to construct the initial simplex for the three-dimensional search for $\boldsymbol{\theta}_{ML}$, where this simplex consists of the vertices of a tetrahedron centered at $\boldsymbol{\theta}_{initial}$ with edge lengths in each coordinate axis taken to be 20 percent of each component of $\boldsymbol{\theta}_{initial}$. For the two- and three-dimensional searches, slightly different termination criteria are used and the relative difference in magnitudes of the three spectral parameters are considered. The search halts when (1) the maximum of the greatest relative distance of each of the three spectral parameters is each smaller than ε_1 and (2) the maximum change in the objective function over each of the four vertices is $<\varepsilon_2$, so the simplex essentially shrinks to a very small, nonmoving tetrahedron at $\boldsymbol{\theta}_{ML}$. Setting the ε's to the values discussed in the simple power law section, $\boldsymbol{\theta}_{ML}$ =(2.801, 3.324, 94.95) is obtained. At this ML solution, note 2,434 of the 51,259 simulated GCR energies are above the estimated knee location at 94.95 TeV, whereas only 2,165 are above the "true" location at 100 TeV.

Also note that the two-stage approach for constructing a suitable initial simplex for the three-dimensional search produced in this example values of $\boldsymbol{\theta}_{initial}$ that are quite close to $\boldsymbol{\theta}_{ML}$, which of course is very desirable. However, in subsequent studies where the true knee location (E_k) is set to higher values such as 300 TeV, it was necessary to introduce a more sophisticated search because of the situation of multiple minima arising from the erosion of the asymptotic properties of the likelihood function as the number of events above the knee diminished.

Figure 10 shows a stereoscopic pair of the initial simplex tetrahedron and the first few steps, where only one vertex is moved per iteration. α_1, α_2, and E_k are along the xyz axis. The dot in the center is the tetrahedron at termination, and $\boldsymbol{\theta}_{ML}$ is obtained from the coordinates of the last step upon halting. Dimensions have been scaled according to the termination criteria and also to facilitate viewing.

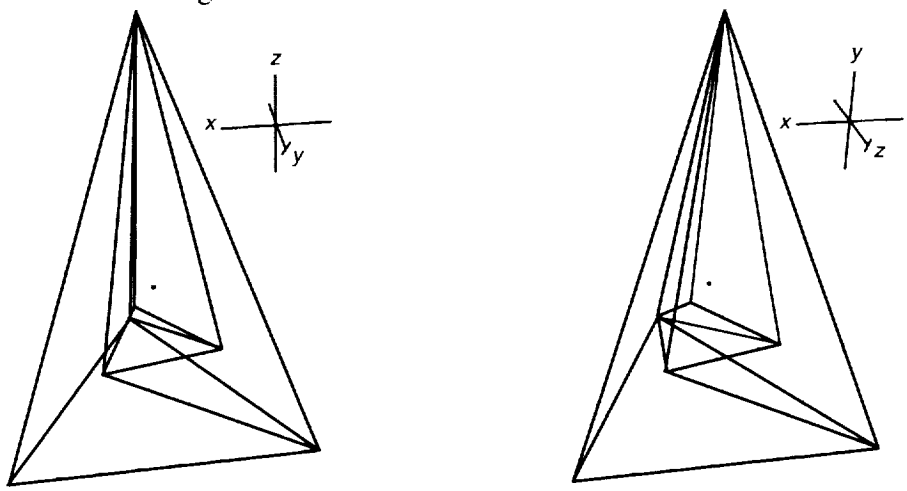

Figure 10. Stereoscopic view of the first few movements of the Nelder-Mead downhill simplex search (cross-eyed stereo).

As a check on the found solution, a coordinate frame is centered at $\boldsymbol{\theta}_{ML}$ and then the objective function evaluated along each axis by an amount of ±10 percent of each value to measure the behavior of $O(\boldsymbol{\theta})$ in the vicinity of $\boldsymbol{\theta}_{ML}$. The results are depicted in figure 11 and show that $O(\boldsymbol{\theta})$ is indeed a minimum at $\boldsymbol{\theta}_{ML}$. Note that variation in α_1 produces the greatest variation in the objective function, as one would expect, since it is a coefficient of 48,825 (95.2 percent) of the event energies below the estimated knee location at 94.95 TeV.

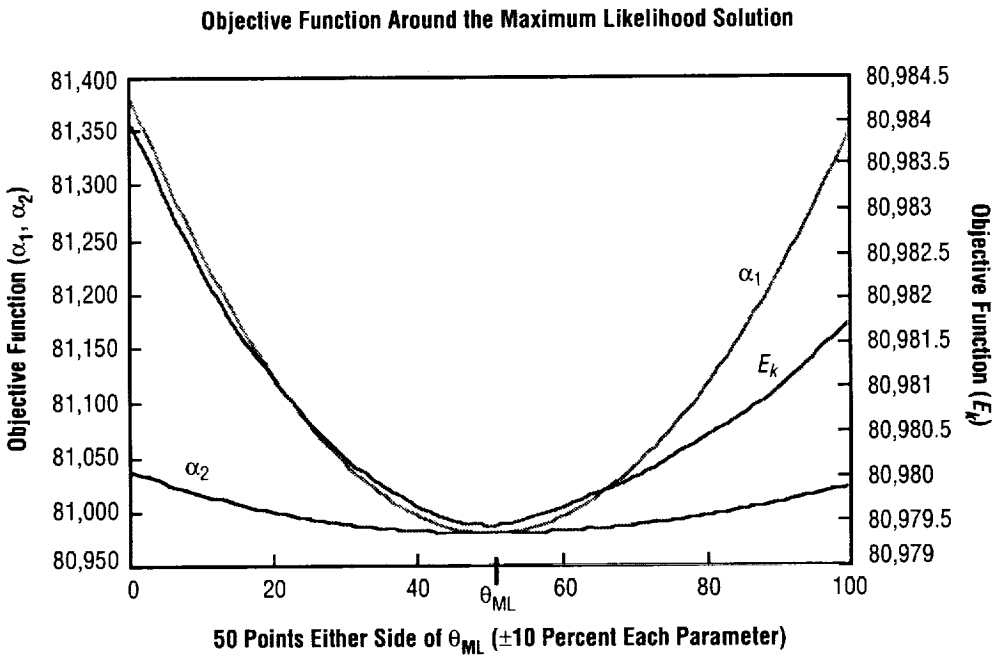

Figure 11. Objective function in the vicinity of the maximum likelihood solution $\boldsymbol{\theta}_{ML}$.

3.2 Estimation of the Spectral Indices With a "Real" Detector

For each simulated GCR event energy E_i from the broken power law spectrum, there is an associated simulated detector response Y_i according to the detector response function defined in eq. (19). The pdf of the detector response in the presence of the broken power law spectrum is thus given by

$$g_1(y;\alpha_1,\alpha_2,E_k) = \int_{E_1}^{E_2} g(y \mid E;\rho)\,\phi_1(E;\alpha_1,\alpha_2,E_k)dE, \qquad y>0\ , \tag{39}$$

where the integral limits $[E_1,E_2]$ must be split as $[E_1,E_k]$ and $[E_k,E_2]$ in the numerical integration. Figure 12 depicts this pdf for several different values of the detector energy resolution (ρ).

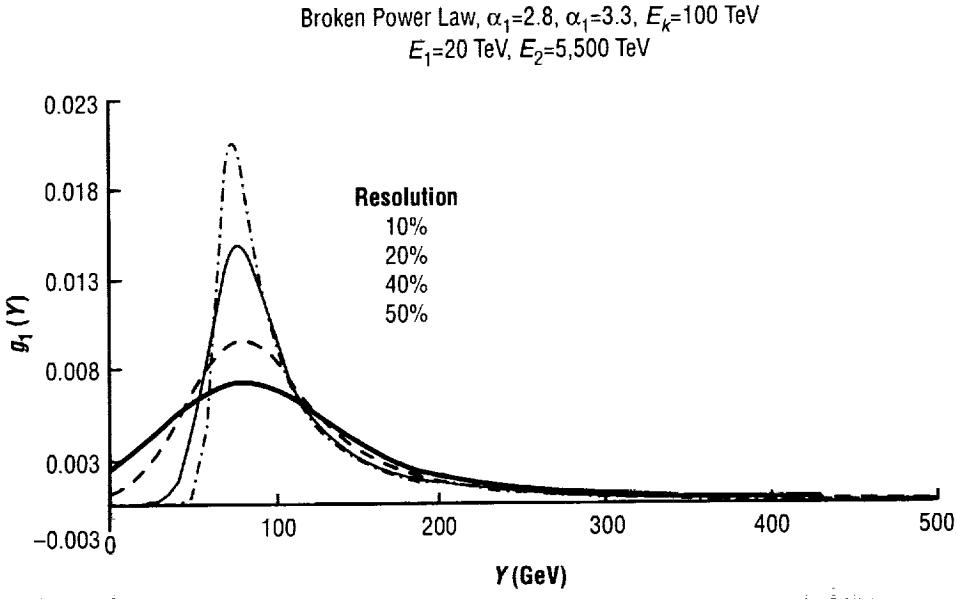

Figure 12. Detector response probability density function for resolutions 10, 20, 40, and 50 percent.

Detector responses Y_i for a detector with constant resolution ρ=0.40 are simulated and all other detector response function parameters are defined in the simple power law case, using the same set of 51,259 incident energies E_i from the broken power law spectrum considered in the zero-resolution case. The mean is calculated as 120.37 GeV and the standard deviation 123.99 GeV. Figure 13 compares probability curves (greater than) on a log-log scale for the detector response distributions in the presence of the broken power law ϕ_1 and the simple power law ϕ_0. A log-log scale helps illustrate the difference between detector response distributions to the two different GCR energy spectra ϕ_0 and ϕ_1. A frequency histogram of the simulated detector responses to a broken power law is also provided in figure 13 (lower curves), although it is virtually indistinguishable from the theoretical function.

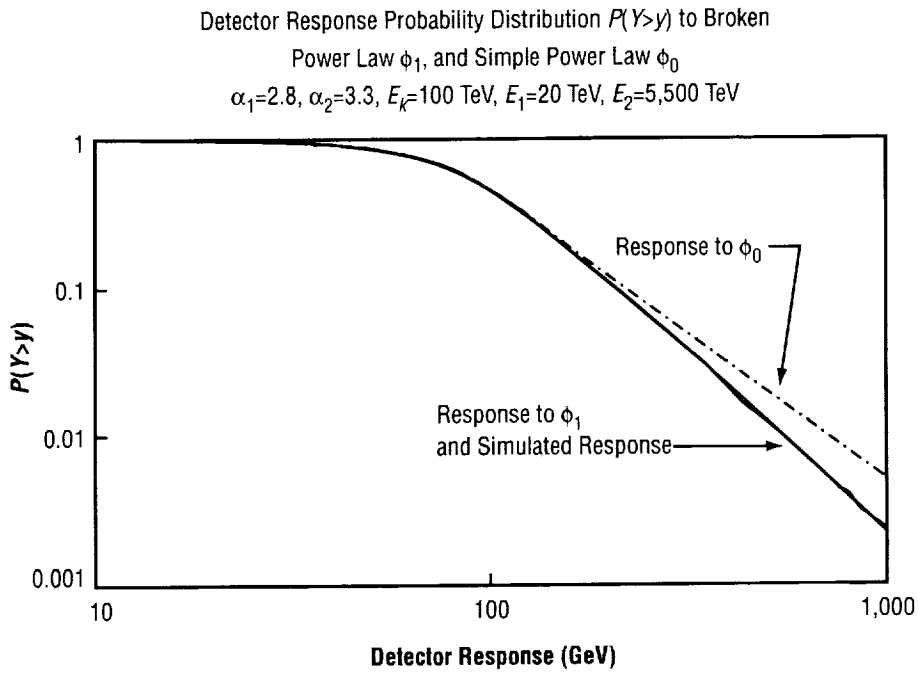

Figure 13. Detector response distributions $Pr(Y>y)$ in the presence of a simple power law and and broken power law. Histogram of simulated responses to broken power law is also included.

The simplex procedure is used to obtain the ML estimates $\boldsymbol{\theta}_{ML}$ for the three spectral indices that minimize the objective function (minus the log-likelihood):

$$O(\boldsymbol{\theta}) = -\sum_{i=1}^{N} Log\left[\int_{E_1}^{E_2} g(y_i \mid E;\rho)\,\phi_1(E;\boldsymbol{\theta})dE\right]. \tag{40}$$

Selection of a starting point for the three-dimensional search follows along similar lines to the zero-resolution energy case, but here only the detector responses Y_i are used. Again, assume the estimate of α_1 will be largely influenced by those detector responses Y_i thought to be below the detector's mean response to some GCR event believed to be below the knee E_k; e.g., a 70-TeV event. Thus, a simple power law is fit to those detector responses below 196.76 GeV (mean response to a 70 TeV GCR proton and accounts for 89 percent of all the detector responses in this simulated set), with the assumption that a simple power law will dominate the statistical description of these events. It is important to note that the present goal is to obtain a reasonable starting value of α_1. Even though some detector responses to incident energies below E_k will end up above the detector mean response to E_k and visa versa, the set of response energies below the mean detector response to a 70-TeV event given by μ(70 TeV)=196.76 GeV should be well represented by a simple power law. Thus, the conditional pdf $g_0(y,\alpha_1 \mid y< 196.76$ GeV) is used and its associated objective function minimized in terms of α_1 to obtain 2.8. In practical terms, the front end of the detector response pdf g_1 is approximated with the detector response pdf g_0 associated with a simple power law.

Figure 14 shows the fitted detector response distribution $1-G_0(Y \mid Y< 196.76\ \text{GeV})$ with the detector response histogram in the presence of the broken power law. Their difference is provided since the two curves are visually on top of each other.

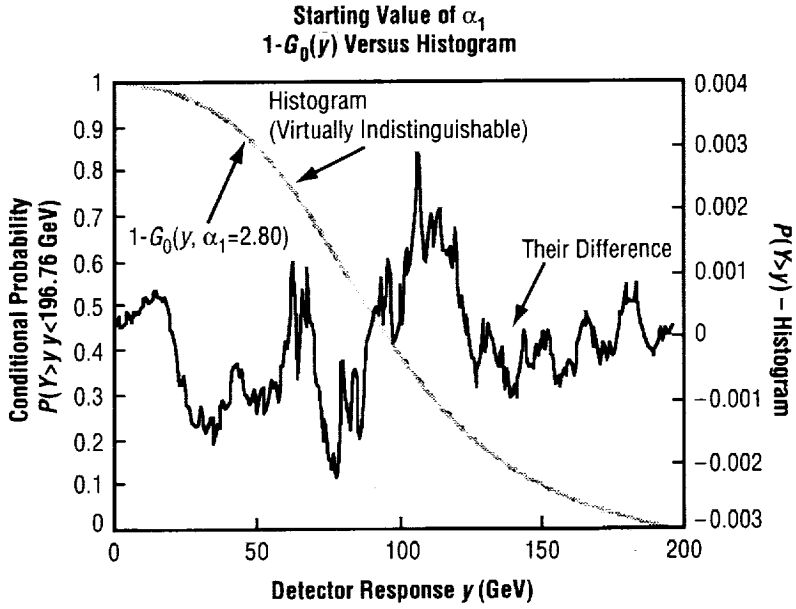

Figure 14. Approximating the front end of G_1 with G_0 (cumulative detector response distribution to simple power law).

Holding α_1 fixed at 2.8 and using the full set of detector responses, a two-dimensional search for (α_2, E_k) yields α_2=3.32 and E_k=96.8 TeV. Figure 15 shows the fitted distribution making the transition along the two parts of the broken power law distribution joined at the knee E_k, and tracks the histogram of simulated detector responses. A simple power law response distribution given by $Pr(Y>y)=1-G_0(y)$ is provided for comparison. As before, a tetrahedron about $\boldsymbol{\theta}_{\text{initial}} = (2.80, 3.32, 96.8)$ provides the initial simplex and then a three-dimensional search using all the detector responses yields $\boldsymbol{\theta}_{\text{ML}} = (2.81, 3.38, 102.9)$.

To check the ML solution, a coordinate frame is centered at $\boldsymbol{\theta}_{\text{ML}}$ and the objective function evaluated along each axis by an amount of ±10 percent of each value to measure the behavior of $O(\boldsymbol{\theta})$ in the vicinity of $\boldsymbol{\theta}_{\text{ML}}$. The results are depicted in figure 16 and indicate that the objective function is indeed a minimum at $\boldsymbol{\theta}_{\text{ML}}$. A slightly more rigorous check was also performed in which the objective function was evaluated at each point of a random cloud consisting of 1,000 points surrounding $\boldsymbol{\theta}_{\text{ML}}$ and for which $O(\boldsymbol{\theta}_{\text{ML}})$ was observed to be the smallest.

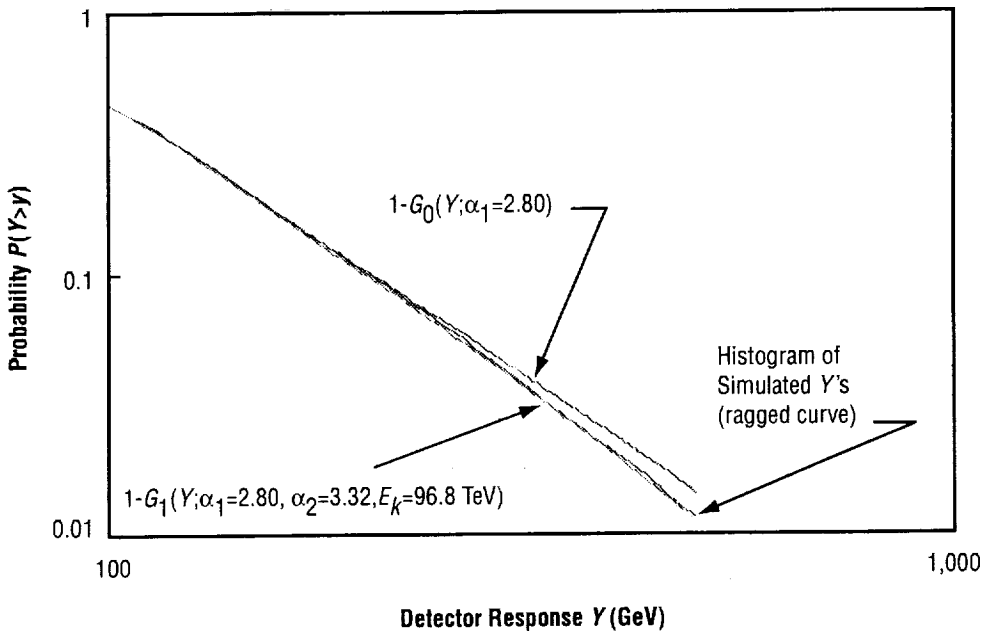

Figure 15. Results of the two-dimensional fit of (a_2, E_k).

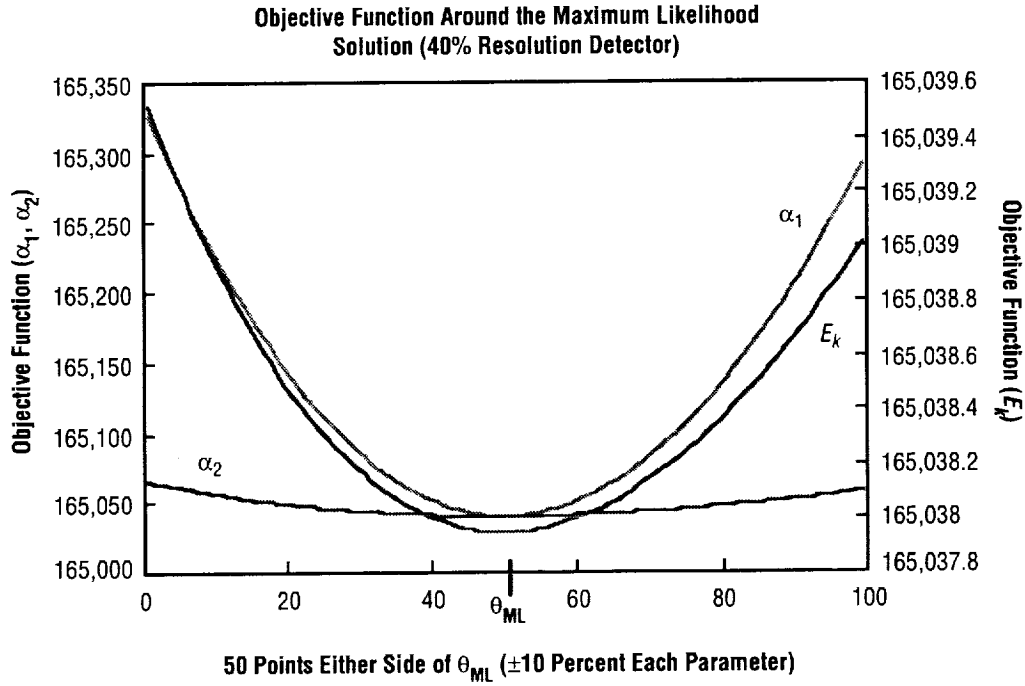

Figure 16. Objective function in the vicinity of the maximum likelihood solution $\boldsymbol{\theta}_{ML}$.

4. RESULTS

Methods for obtaining the ML estimates of the three spectral parameters of the broken power law distribution from simulated detector responses have been developed, thereby enabling us to study various calorimeter design parameters and their impacts on the statistical properties of these ML estimates. The following studies are of particular interest and are included: (1) Statistical properties of the ML estimates and variation of the knee location and spectral break size, (2) data analysis range, (3) energy-dependent resolution, (4) non-Gaussian detector response functions, (5) collecting power versus energy resolution, and (6) implications of detector response model uncertainties.

4.1 Statistical Properties of the Maximum Likelihood Estimates and Variation of the Knee Location and Spectral Break Size

In this section, the statistical behavior of the ML estimates of the three spectral parameters based on simulating many missions is explored. Figure 17 shows relative frequency histograms of these estimates based on 1,000 simulated missions in which the spectral parameters were set to α_1=2.8, α_2=3.3, and E_k=100 TeV for the data analysis range 20–5,500 TeV and a detector having a Gaussian response function with 40-percent constant energy resolution. Note that the histograms are roughly Gaussian in shape but with a slight skewness to the right, exhibited for α_2 and E_k but not α_1.

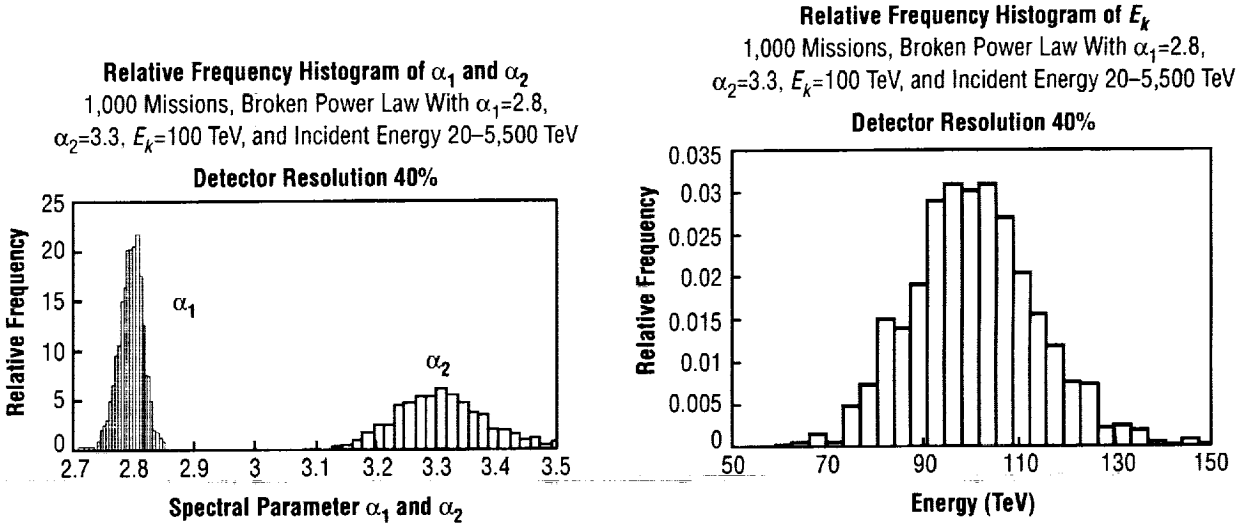

Figure 17. Relative frequency histograms of the maximum likelihood estimates of the spectral parameters α_1, α_2, and E_k of the broken power law energy spectrum.

These observations lead to a more general investigation of the asymptotic behavior of ML estimates. Table 4 provides a summary of these findings. The first column lists the Gaussian response function resolution (zero and 40 percent) for the studies presented in table 4, and the second column gives the average number of events above E_1=20 TeV used in each simulated mission, along with the average number of events above the knee location E_k given in parentheses for values of E_k=100, 200, and 300 TeV. For example, the entry 51,576 (2,255) appearing in the first row indicates there are 51,576 events on average above 20 TeV for the baseline detector of which 2,255 of them would be above the knee location, E_k=100 TeV. The next three columns give the mean of each spectral parameter based on the simulation results, followed by the last three columns that give their respective standard deviations. The rows labeled as "Theoretical Limits" provide the input parameters for these simulation studies along with the Cramer-Rao bound which is the bound below which the variance of an estimator cannot fall[2] and is thus very important when comparing different estimation techniques.

First, note in table 4 that as the true knee location (E_k) is set at 100, 200, and 300 TeV in the simulations, an ever-increasing amount of bias is observed in the mean estimate of α_2 and E_k due to the erosion of consistency (asymptotically unbiased) and is a direct consequence of the diminishing number of events above the knee, whereas the ML estimate of α_1 continues to enjoy this favorable statistical property.

The Cramer-Rao lower bound is provided for comparison with the standard deviations of the ML estimates obtained from the simulations. Note that while this theoretical minimum variance bound is nearly attained when the true knee location (E_k) is 100 TeV and the number of events above E_k is over 2,000, the ability to achieve this lower bound gradually declines as the true knee location E_k increases to 200 TeV, and then even more so when E_k=300 TeV. The gradual growth in bias and inability to achieve the Cramer-Rao lower bound, coupled with a growing skewness in the frequency histograms of the estimates for α_2 and E_k that indicate the asymptotic normality property is slipping away too, are symptoms of the increasing difficulty in estimating the spectral parameters when the true knee location (E_k) is too high for this baseline detector. Furthermore, an investigation of the behavior of the objective function defined in eqs. (38) and (40) shows the emergence of multiple minima at these higher values of E_k and is a condition that is observed to worsen with increasing E_k.

Table 4. Asymptotic behavior of the maximum likelihood estimates for E_k= 100, 200, 300 TeV, collecting power 1× (baseline) and 5×, with a special 6.4× detector only for the E_k=300 TeV case.

Detector Resolution (%)	E_k (TeV) N_1(>20 TeV) (N_1(>E_k))	Mean			Standard Deviation			
		α_1	α_2	E_k	α_1	α_2	E_k	
0	100 51,576	2.80	3.30	100	0.012	0.049	6.6	1X Theoretical Limit (unbiased, Cramer-Rao LB)
0	(2,255)	2.80	3.31	101	0.012	0.053	7.6	Simulation (3,000 missions)
40		2.80	3.31	102	0.020	0.076	14.0	Simulation (3,000 missions)
0	100 257,880	2.80	3.30	100	0.0052	0.022	3.0	5X Theoretical Limit (unbiased, Cramer-Rao LB)
0	(11,275)	2.80	3.30	100	0.0052	0.022	3.2	Simulation (3,000 missions)
40		2.80	3.30	101	0.0088	0.033	6.2	Simulation (3,000 missions)
0	200 52,022	2.80	3.30	200	0.0094	0.092	23.4	1X Theoretical Limit (unbiased, Cramer-Rao LB)
0	(647)	2.80	3.32	202	0.0096	0.11	30.3	Simulation (2,000 missions)
40		2.80	3.33	205	0.013	0.16	47.7	Simulation (2,000 missions)
0	200 260,110	2.80	3.30	200	0.0042	0.041	10.5	5X Theoretical Limit (unbiased, Cramer-Rao LB)
0	(3,235)	2.80	3.30	200	0.0042	0.043	11.8	Simulation (2,000 missions)
40		2.80	3.31	201	0.0059	0.063	20.3	Simulation (2,000 missions)
0	300 52,116	2.80	3.30	300	0.0088	0.13	50.0	1X Theoretical Limit (unbiased, Cramer-Rao LB)
0	(312)	2.80	3.34	310	0.0087	0.18	71.0	Simulation (3,000 missions)
40	Further Study Required							Simulation (3,000 missions)
0	300 260,580	2.80	3.30	300	0.0039	0.060	22.3	5X Theoretical Limit (unbiased, Cramer-Rao LB)
0	(1,560)	2.80	3.31	302	0.0040	0.067	26.3	Simulation (3,000 missions)
40		2.80	3.31	304	0.0053	0.092	39.8	Simulation (3,000 missions)
0	300 333,542	2.80	3.30	300	0.0035	0.053	19.7	6.4X Theoretical Limit (unbiased, Cramer-Rao LB)
0	(2,000)	2.80	3.30	300	0.0036	0.056	22.4	Simulation (1,500 missions)
40		2.80	3.31	301	0.0046	0.078	35.3	Simulation (1,500 missions)

As noted in table 4, the case where E_k=300 TeV and the detector's energy resolution is 40 percent resulted in several errant estimates of α_2 and E_k, which is perhaps an indication that a simple power law would provide an adequate explanation of these particular simulated "missions." However, as indicated in table 4, these favorable statistical properties are largely restored when the collecting power is increased by a factor of 5 and reinforces the importance of collecting power. Furthermore, no errant estimates were observed. Figure 18 shows the effect of collecting power on the histograms of the estimate of the knee location when E_k=200 TeV and compares the baseline (outer curve) with a 2× (middle) and 5× (inner) detector.

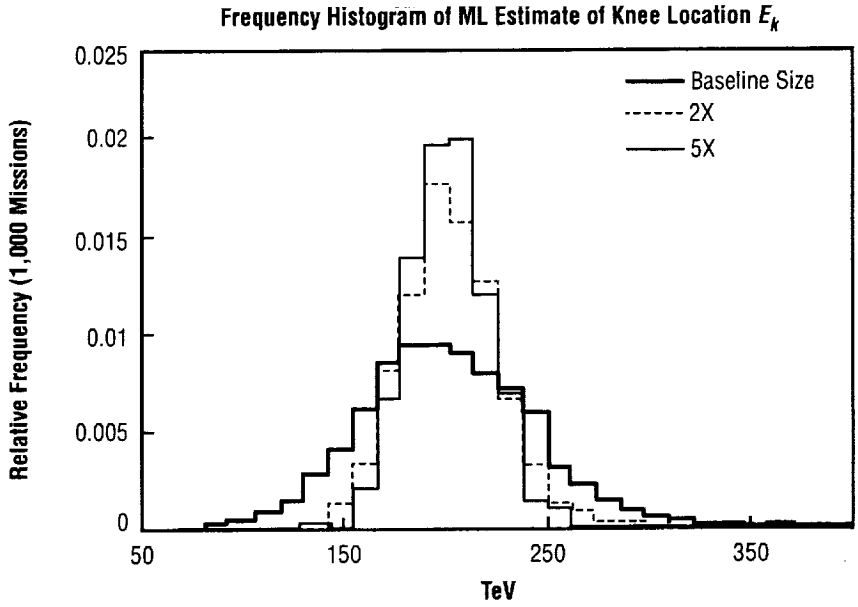

Figure 18. Effect of collecting power on histogram of knee location estimates.

It should be noted that the Cramer-Rao bound was derived for the ideal detector having zero energy resolution and shows those values of the knee location E_k where one begins to see an erosion of the asymptotic properties of ML estimates and the difficulties encountered with the multiple minima of the objective function. Attempts to derive the Cramer-Rao bound for a "real" detector having a nonzero resolution and involve the convolution integral in eq. (39) were found to be mathematically intractable. However, they can readily be numerically constructed using record-order difference equations.

Also of interest is the correlation between the ML estimates of the three spectral parameters, a direct consequence of the mathematical definition of the broken power law in which the knee E_k acts as a "hinge," connecting the lower part of the distribution controlled by α_1 with the upper part controlled by α_2. Thus, one can easily visualize a correlation between α_1 and E_k and α_2 and E_k, while α_1 and α_2 appear to be only slightly correlated according to the simulation results.

For example, when α_1=2.8, α_2=3.2, E_k=125 TeV, E_1=20 TeV, E_2=5,500 TeV, and the detector resolution is zero, the correlation matrix given in table 5 is based on 25,000 simulated missions. When the detector resolution is 40 percent and a Gaussian response function used, the correlation was seen to be slightly greater among the estimates of the three spectral parameters.

Table 5. Correlation matrix based on 25,000 simulated missions.

	Correlation Matrix		
	α_1	α_2	E_k
α_1	1.00	0.08	0.42
α_2	0.08	1.00	0.72
E_k	0.42	0.72	1.00

4.1.1 Spectral Break Size of 0.3

The case where α_2 is set to 3.1 in the simulations and the so-called spectral break size is reduced to 0.3 when α_1 remains fixed at 2.8 is of particular interest. Figure 19 shows relative frequency histograms of three estimates $(\alpha_1, \alpha_2, E_k)_{ML}$ based on 1,000 simulated missions in which the GCR events were simulated from the broken power spectrum with α_1=2.8, α_2=3.1, and E_k=100 TeV over the range 20–5,500 TeV for which the average number of events above 20 TeV is 51,800 and of which 2,500 are above the assumed knee location at 100 TeV. The detector is assumed to have a constant 40-percent energy resolution with a Gaussian response function.

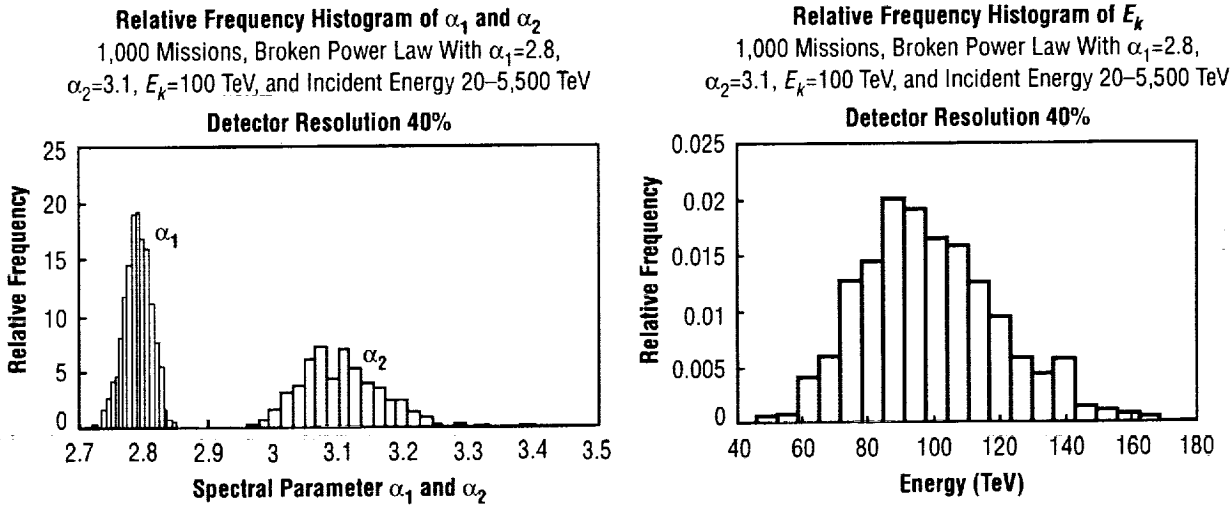

Figure 19. Relative frequency histograms of the maximum likelihood estimates of the three spectral parameters α_1, α_2, E_k of the broken power law energy spectrum. Detector response function is Gaussian having 40-percent constant energy resolution.

Also note that the mean and standard deviation of the incident GCR energies are μ_E=42 TeV and σ_E=54 TeV, respectively, for this simulation scenario. Comparing to the case where α_2=3.3 and the other parameters the same shows an average of 51,600 events above 20 TeV of which 2,250 are above the assumed knee location at 100 TeV and with μ_E=41 TeV and σ_E=46 TeV. Thus, the standard deviation is considerably larger for the α_2=3.1 case but also has ≈10 percent more events above the knee E_k.

Figures 20a and 20b compare standard deviations of the ML estimate of α_1 and α_2, respectively, for the α_2=3.1 with α_2=3.3 case as a function of detector energy resolution. A somewhat surprising result is observed in figure 20b where the standard deviation of the α_2 estimate actually decreases when the spectral break size decreases from 0.5 to 0.3 and is attributable to the 10-percent increase in events above the knee, despite the increase in GCR incident energy variance (σ_E increases as the break size decreases, and hence so does the standard deviation of the detector responses σ_Y which would tend to increase the standard deviation of the estimate of α_2). Thus, as seen in figure 20b, the increase in events above the knee slightly outweighs the increase in variance associated with the decrease in spectral break size. Note in figure 20c the standard deviation of the E_k estimate almost doubles when the spectral break size decreases from 0.5 to 0.3, a more intuitive result.

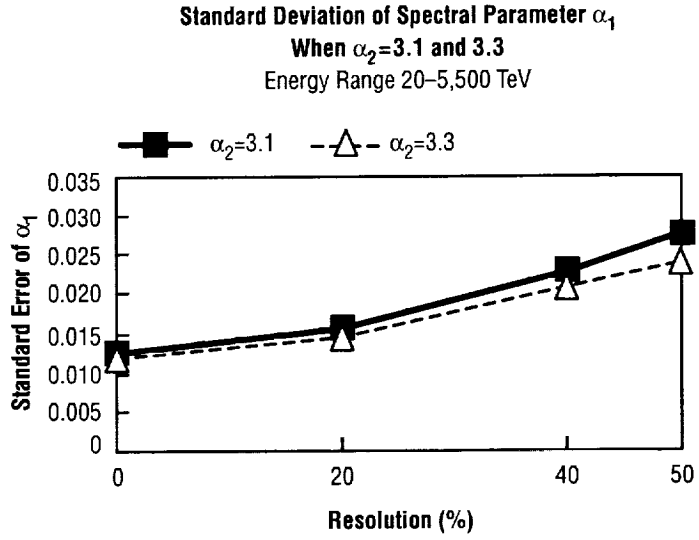

Figure 20a. Standard deviation of the maximum likelihood estimate of α_1 for the α_2=3.1 and α_2=3.3 case as a function of detector (assumed Gaussian) resolution.

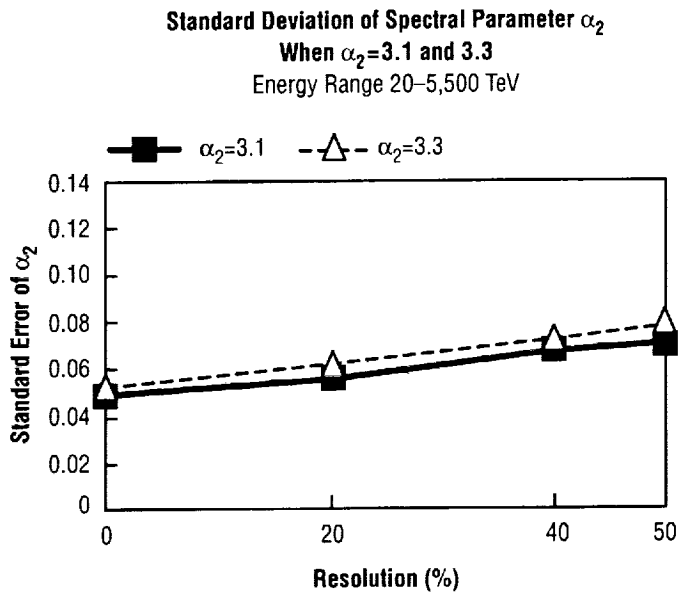

Figure 20b. Standard deviation of the maximum likelihood estimate of α_2 for the α_2=3.1 and α_2=3.3 case as a function of detector (assumed Gaussian) resolution.

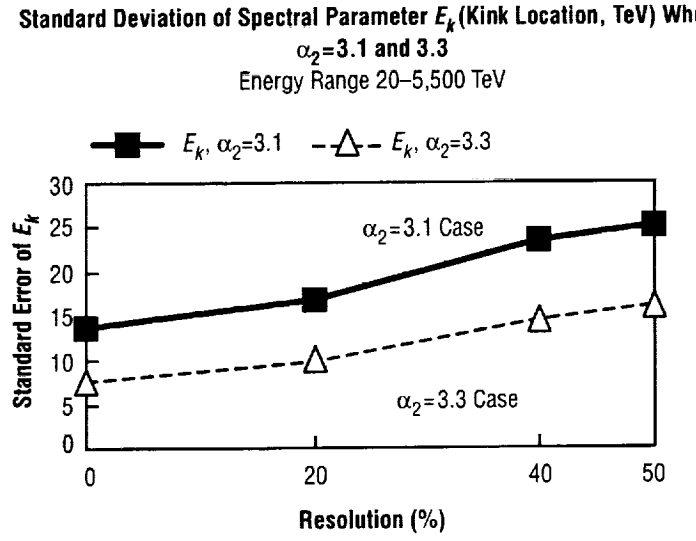

Figure 20c. Standard deviation of the maximum likelihood estimate of E_k for the α_2=3.1 and α_2=3.3 case as a function of detector (assumed Gaussian) resolution.

Last, the asymptotic properties and correlation among the estimates is explored by simulating 100,000 missions from the broken power distribution with α_1=2.8, α_2=3.1, and E_k=100 TeV over the range of 20–5,500 TeV. This is accomplished using a detector having twice the collecting power of the baseline detector and thus providing 103,600 events on average above 20 TeV, of which ≈5,000 are above the assumed knee location at 100 TeV. The ideal or zero-resolution detector is also used for comparison with the Cramer-Rao bound which has only been derived for zero-resolution detectors. Table 6 gives the means, standard deviations, and Cramer-Rao bound for this scenario and table 7 gives the correlation matrix based on these 100,000 simulated missions.

Table 6. Means, standard deviations, and Cramer-Rao bounds.

	Mean	Standard Deviation	Cramer-Rao Bound
α_1	2.80	0.0084	0.0083
α_2	3.10	0.032	0.031
E_k	100.5 TeV	8.6 TeV	7.6 TeV

Table 7. Correlation matrix.

	α_1	α_2	E_k
α_1	1.00	0.06	0.47
α_2	0.06	1.00	0.68
E_k	0.47	0.68	1.00

4.2 Data Analysis Range Study

The energy range $[E_1,E_2]$ from which GCR proton events are simulated has a significant impact on the statistical properties of the ML estimates. While increasing E_2 beyond 5,500 TeV has no noticeable effect since events of energy exceeding 5,500 TeV are very unlikely, lowering E_1 does have a significant impact on the standard deviation of the estimates of α_1 and E_k. By lowering E_1, many more events representative of that part of the broken power law below the knee and controlled by α_1 will be detected, along with the extension of the estimation range or "moment arm" for α_1, the combination thereby providing greater precision in the estimation of α_1. Furthermore, as α_1 is estimated with greater precision, E_k can be measured with somewhat greater precision too since reducing the variation in α_1 removes additional variation in the "hinge" E_k. Hence, lowering the data analysis range results in a reduction in uncertainty of α_1 and E_k and thus reduces the total uncertainty so that very slight gains in variance reduction in the estimate of α_2 is also realized. These results are depicted in figures 21a–21c for α_1, α_2, and E_k, when E_1=30, 20, 15, and 10 TeV and for which there were on average 24,500, 51,500, 87,000, and 181,000 events, respectively, with ≈2,250 above the knee for each. Other parameters are α_1=2.8, α_2=3.3, E_k=100 TeV, E_2=5,500 TeV, and the response function is assumed Gaussian.

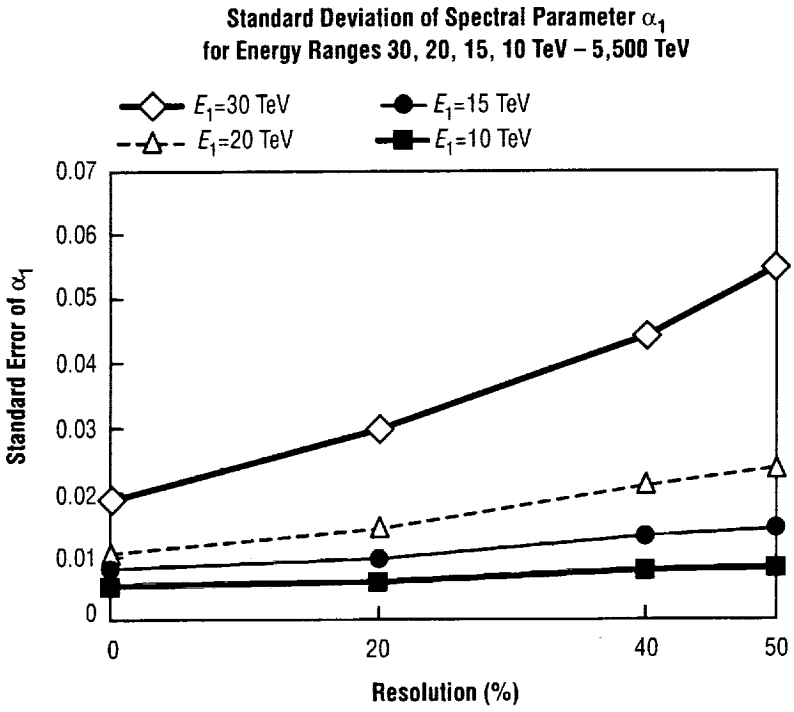

Figure 21a. Effects of lowering E_1 on the standard deviation of the estimate of α_1.

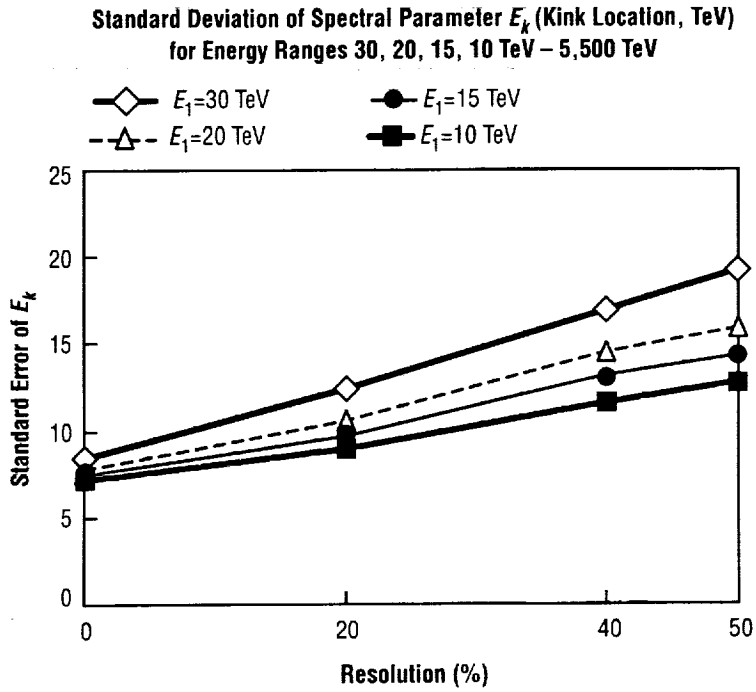

Figure 21b. Effects of lowering E_1 on the standard deviation of the estimate of E_k.

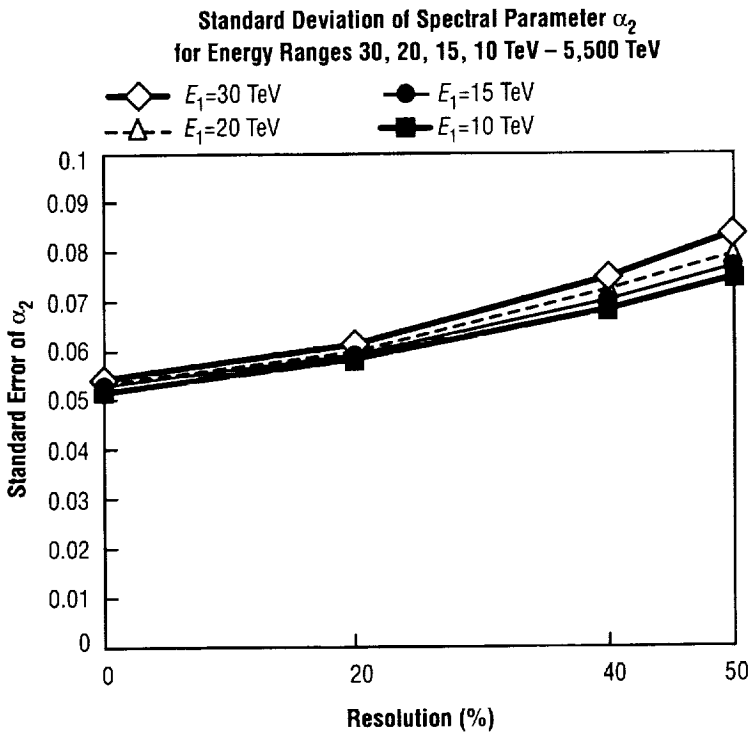

Figure 21c. Effects of lowering E_1 on the standard deviation of the estimate of α_2.

4.3 Energy-Dependent Resolution Study

The situation in which the detector response function is assumed to be Gaussian but the detector energy resolution varies with incident GCR event energy is of particular interest to designers of cosmic-ray detectors. In previous studies presented so far in this TP, the detector response function is assumed to be Gaussian with a linear mean response (energy deposit) of the form $(a + bE)$ and with constant detector energy resolution ρ so that the parameter σ in the Gaussian response function is defined as $\sigma(E)=\rho(a + bE)$. Two cases of interest are (1) energy resolution is "getting better" from 40-percent resolution at E_1=20 TeV to 30 percent at E_2=5,500 TeV and (2) "getting worse" from 30-percent resolution at E_1=20 TeV to 40 percent at E_2=5,500 TeV. These two cases are modeled by assuming that $\sigma(E)$ is a linear function of incident GCR energy of the form $(c + dE)$ and then the coefficients c and d are determined by matching the conditions for each of the two cases. Doing so yields the energy-dependent resolution curves depicted in figure 22.

Table 8 shows the results based on 100 simulated missions using the same incident GCR energies for both cases and the mean estimates shown are essentially unbiased, with standard deviations having expected comparisons; e.g., standard deviations slightly larger for the "getting worse" case. The constant 40-percent case is included for comparison.

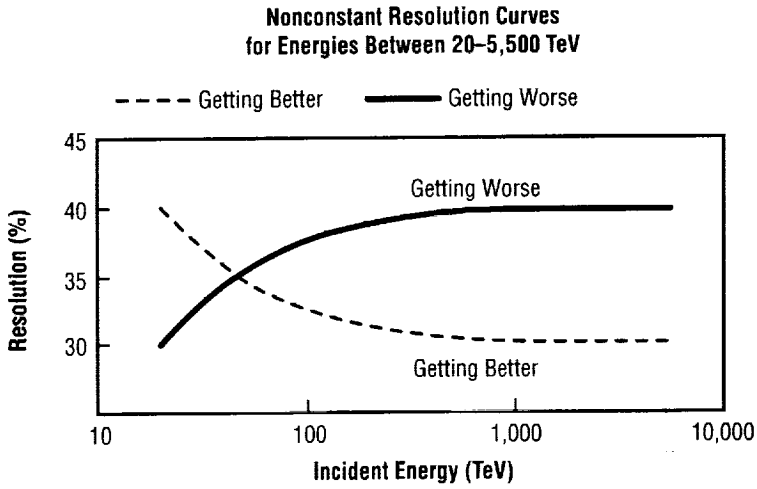

Figure 22. Energy-dependent resolution curves.

Table 8. Nonconstant energy resolution results.

Mean and Standard Deviation of the Estimates Based on 100 Missions						
	Resolution					
	Constant 40%		Nonconstant (Getting Better)		Nonconstant (Getting Worse)	
Spectral Parameter	Mean	Standard Deviation	Mean	Standard Deviation	Mean	Standard Deviation
α_1	2.80	0.02	2.794	0.018	2.794	0.018
α_2	3.33	0.072	3.309	0.067	3.312	0.073
E_k	100.7	14.4	99.63	12.6	99.93	13.5

4.4 Non-Gaussian Detector Response Functions

The simulation studies presented so far have assumed a Gaussian detector response function. While reference 5 suggests that a Gaussian function is reasonable, there is concern that perhaps the response function is skewed slightly to the right and that this "tail" will contribute to greater difficulties in estimating the broken power law spectral parameters. The gamma response function, capable of describing a wide variety of shapes with right-hand skewness (outer curve from the right in fig. 23) and the broken-Gaussian consisting of two blended normal distributions (middle curve from right) suggested by reference 8 for its closeness to the Gaussian response function but with the tail region, as desired, were introduced to address this concern. Both were used as detector response functions in 1,000 simulated missions using the baseline detector collecting power and simulating GCR events from the broken power law with parameters α_1=2.8, α_2=3.3, E_k=100 TeV, from the range 20–5,500 TeV. The results are shown in table 9. Note that the gamma response function produces a slight bias in the estimate of the knee location that was removed in a subsequent run with the collecting power doubled. Also note that the standard deviation of the estimate of α_2 increases by ≈13 percent for both response models relative to the Gaussian response function having 40-percent resolution. It should also be noted that while the gamma response function has a constant energy resolution of 40 percent, the broken Gaussian has a 41-percent resolution because of the added skewness while keeping the rest of the distribution matching the Gaussian.

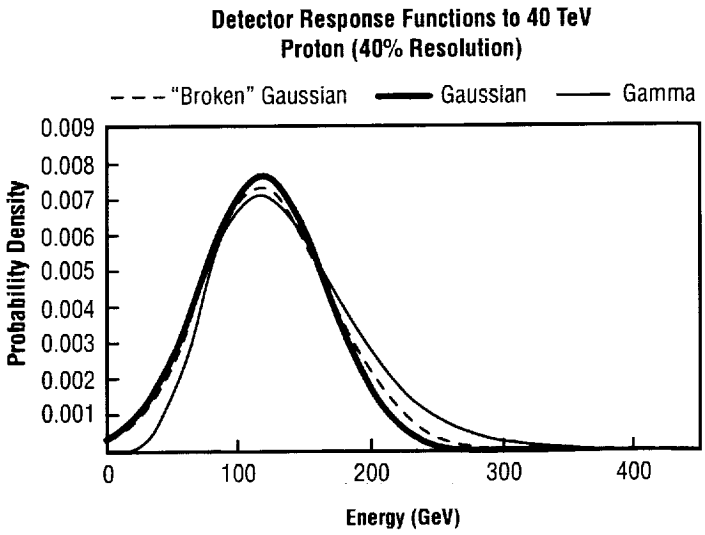

Figure 23. Gamma, broken Gaussian, and Gaussian response functions.

Table 9. Gaussian, broken Gaussian, and gamma response function study.

Mean and Standard Deviation of Maximum Likelihood Estimates of Spectral Parameters (1,000 Missions)						
Response Model (40% Resolution)	α_1		α_2		E_k	
	Mean	Standard Deviation	Mean	Standard Deviation	Mean	Standard Deviation
Gaussian	2.80	0.020	3.31	0.072	100.7	14.4
Broken Gaussian	2.80	0.021	3.31	0.082	100.8	14.9
Gamma	2.80	0.023	3.31	0.082	102.3	16.1

4.5 Collecting Power Versus Resolution Study

Cosmic-ray instrument developers must often make trade studies in design parameters as a function of the science objectives, which is very important for space-based detectors where physical parameters, such as dimension and weight, impose rigorous practical limits to the design envelope. Particularly important is the comparison between detector energy resolution and collecting power (combination of detector size and observing time) two parameters often played against each other in the design phase of a new detector program. As seen in the simple power law section, the ability to measure the spectral parameter α_1, measured in terms of the standard deviation as its estimator, depends rather weakly on resolution and strongly on collecting power as is evidenced in figure 7. Also observed was that the standard deviation is inversely proportional to the square root of the number of events, so that halving or doubling the collecting power scales the standard deviation by a factor of $\sqrt{2}$ for the ML estimate when the number of events exceeds around 2,000. As noted in table 3, the variance of the broken power law distribution (and its higher moments too, although not shown in table 3) is somewhat smaller than the variance of the simple power

law, implying the detector's energy resolution will play a somewhat stronger role in the estimation of the three spectral parameters. Figures 24a–24c illustrate the relationship between collecting power and detector energy resolution by showing the impact on the standard deviation of the three spectral parameters when the collecting power of the baseline detector is halved and then doubled. In this study, GCR events were simulated from the broken power law with parameters α_1=2.8, α_2=3.3, E_k=100 TeV, from the energy range 20–5,500 TeV, and the baseline number of events is 51,600 above 20 TeV of which 2,250 are above the assumed knee at 100 TeV. In approximate terms, note that doubling the collecting power compares with about a 20-percent trade in resolution for α_1 and E_k but also note that a 40-percent resolution detector is better than a zero-resolution detector of half its size relative for the event-starved α_2 parameter.

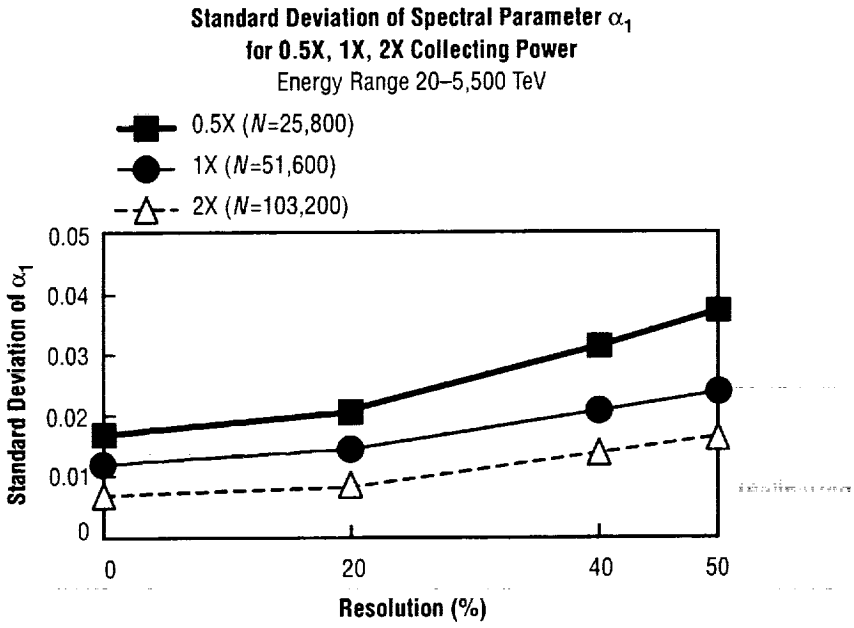

Figure 24a. Relationship between collecting power and energy resolution measured in terms of the standard deviation of the maximum likelihood estimate of α_1.

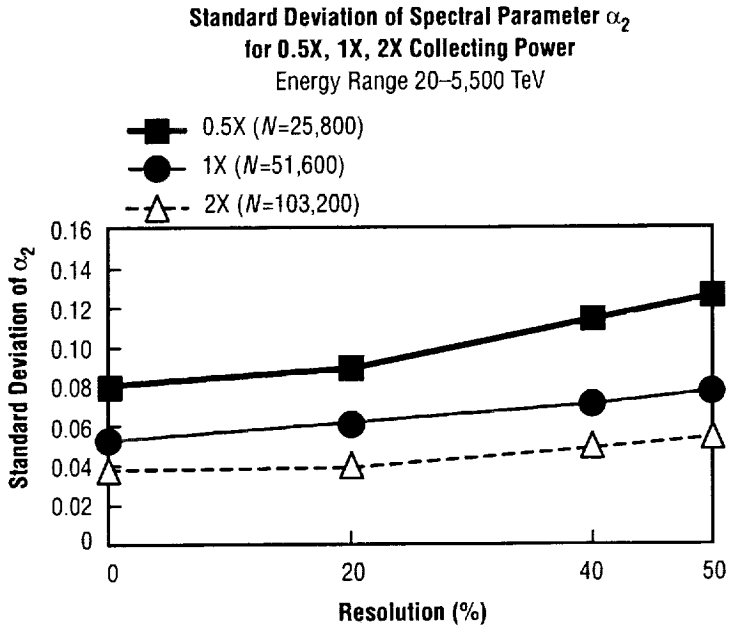

Figure 24b. Relationship between collecting power and energy resolution measured in terms of the standard deviation of the maximum likelihood estimate of α_2.

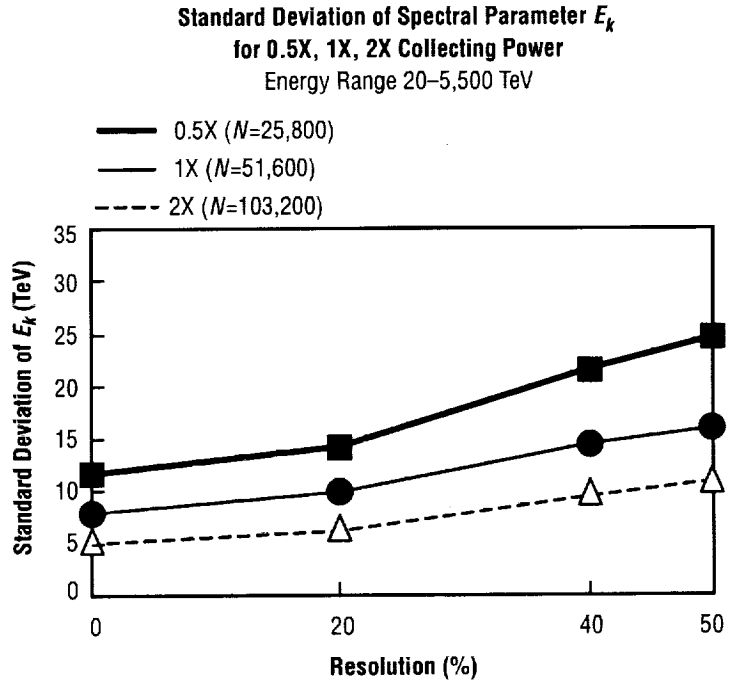

Figure 24c. Relationship between collecting power and energy resolution measured in terms of the standard deviation of the maximum likelihood estimate of E_k.

It is important to note that the relationships illustrated in figures 24a–24c are independent of the energy range as similar comparisons were observed when E_1 was lowered to 15 TeV and to 10 TeV. Raising E_2 has no effect since the number of events above E_2=5,500 TeV is negligible for detectors with this collecting power.

Because the Cramer-Rao lower bound always scales by $\sqrt{N}$ for each of the three spectral parameters and, as noted in table 4, the asymptotic properties (including attainment of the Cramer-Rao bound) of the ML estimates of α_2 and E_k are nearly met whenever the number of events above the knee exceeds 2,500, which is about the situation for the baseline detector collecting power when E_k=100 TeV, it can be seen that doubling the collecting power means the standard deviation of the α_2 and E_k estimators scales by $\sqrt{2}$, but halving results in a factor of around 1.5 instead of 1.41, as attainment of the Cramer-Rao bound is slipping away faster for the smaller detector. Obviously, as E_k increases to 200 and 300 TeV as in table 4, the number of events above the knee diminishes too so that the bound is not attained, so scaling will not go by the $\sqrt{N}$ until the collecting power is such that the number of events above E_k is ≈2,500 or more. This latter result is the rationale for selecting the hypothetical 5× detector in table 4 so that the number of events above E_k=200 is 3,235. Of course since the number of events representative of α_1 is always quite large and is on the order of 50,000 or greater when the lower limit of the data analysis range is 20 TeV or less for the baseline detector, scaling by $\sqrt{N}$ will hold for the standard deviation of the ML estimate of α_1.

4.6 Implications of Detector Response Model Uncertainties

Maximum likelihood estimation of cosmic-ray spectral parameters as presented in this TP requires the complete specificity of all detector response model parameters. The reality of actually knowing these parameters with little or no surrounding uncertainty depends largely on designers being able to calibrate the detector at different incident energies at a particle accelerator facility. However, because space-based detectors will be exposed to GCR events having energy much greater than those energies available at accelerator facilities, it becomes essential to gain an understanding of the detector's response function using Monte Carlo simulations of the detector's response (energy deposit) to those energies that cannot be attained at accelerator facilities. These simulations, coupled with a favorable comparison between simulation results and accelerator results at energies available in a test facility, will provide a better understanding of the detector response function.

By way of example, the impacts on spectral parameter estimation when certain detector response function parameters are incorrectly known are investigated next. This state of ignorance will manifest itself as a bias in the mean or point estimate of the spectral parameters. This situation is modeled by simulating detector responses according to one set of detector response function parameters and then using a different set of parameters in the detector response function g in eq. (40) of the ML estimation procedure.

Since detector resolution is an important design parameter, the case is first considered where the detector has a constant energy resolution; however, a different resolution value was used in an assumed state of misunderstanding in eq. (40). For example, suppose the real detector resolution is a constant 35 percent, but in the simplex search the resolution parameter (ρ) is set to different constant values in eq. (40) corresponding to resolutions ranging from 31 to 39 percent. This situation is modeled by simulating the detector responses Y_i as

$$Y_i = (a + bE_i)(1 + 0.35\, Z_i) \tag{41}$$

according to eq. (18) and for GCR event energy E_i from an assumed broken power law with parameters α_1=2.8, α_2=3.3, and E_k=100 TeV, from the energy range 20–5,500 TeV and for an assumed Gaussian response model having 35-percent energy resolution. Z_i is a Gaussian random number having zero mean and unit variance, along with the nonnegativity constaint $Y_i > 0$. Next, in the ML procedure, ρ is set to the different values in eq. (40) to obtain the ML estimates of the three spectral parameters. Table 10 at the end of this section shows the mean for each of ML spectral parameter estimates based on 100 simulated missions, each where ρ is set to 0.31, 0.32, ... , 0.39 in eq. (40).

Table 10. Implications of detector response model uncertainties.

	Assumed Resolution	α_1	α_2	E_k (TeV)
Constant resolution versus assumed constant 35%	31%	2.76	3.29	96.6
	32%	2.76	3.29	96.8
	33%	2.77	3.30	97.4
	34%	2.79	3.30	98.2
	35%	2.80	3.30	99.4
	36%	2.81	3.31	101
	37%	2.83	3.31	103
	38%	2.84	3.32	106
	39%	2.86	3.32	109
Nonconstant resolution versus assumed constant 35%	Getting worse: 30% to 40% over 20–5,500 TeV	2.88	3.34	145
	Getting better: 40% to 30% over 20–5,500 TeV	2.65	3.25	67
Gaussian versus assumed Broken Gaussian	Method 1	2.98	3.38	171
Broken Gaussian versus assumed Gaussian	Method 1	2.53	3.21	67
Broken Gaussian versus assumed Gaussian	Method 2	2.85	3.32	115

Note that the mean estimates exhibit a bias as a result of using incorrect values of ρ in eq. (40). Also see in table 10 that when ρ=0.35 in eq. (40) and matches the "correct" resolution as used in eq. (41) to simulate the detector responses, the means of the ML estimates match the assumed spectral parameters used in the simulation, and thus there is no bias in the estimates. It was also noted that their variances were essentially unaffected and this example is akin to a misaligned riflescope that results in the rifle shooting off-axis from the line of sight but the shot group size remains unaffected.

Next, consider the situation where the real detector resolution is energy dependent, but a constant resolution of 35 percent is used in eq. (40). For example, if the real detector resolution is "getting better" over the simulated GCR energy range 20–5,500 TeV as shown in figure 22 but instead a constant ρ=0.35 is used in eq. (40) in the simplex search for $\boldsymbol{\theta}_{ML}$ and 100 simulated missions, very large biases result (given in table 10). Another case where the real resolution was "getting worse," depicted in figure 22, was when a constant of 35-percent resolution was again used in eq. (40), resulting in the other large biases given in table 10. Based on these studies, one concludes that the real key is to understand what the true energy-resolution relationship is and not so much a matter that it has a particular mathematical form. However, as these studies indicate, designs having a constant resolution are more forgiving as long as the error amount is a constant.

Another important study regards the so-called tails of the response function. The response functions depicted in figure 23 were used to address this concern. The results from these simulations are presented in table 9 and indicate that while a "smaller tail" is desirable, having a larger tail is not as bad as perhaps feared. Of particular interest is the situation in which the real detector response function is Gaussian but in a state of ignorance, the broken Gaussian function is inserted as the detector response function g in eq. (40) in the ML search for $\boldsymbol{\theta}$. Based on 1,000 mission averages, a large bias in the mean estimates of the spectral parameters is noted in table 10. In the case where the real detector response function is the broken Gaussian function, the Gaussian function was incorrectly used in eq. (40) and is also included in table 10, and again large biases are seen. These two cases are labeled as method 1 and will be compared to a revised technique labeled method 2.

It should be noted that in method 1, as well as in all simulation studies presented so far in this TP, GCR events are simulated from an energy range E_1 to E_2, where typically E_2=5,500 TeV and E_1 is a value between 10 and 25 TeV. The choice of E_2 is based on the collecting power of the detector and is chosen such that there will only be a negligible number of events above E_2. The selection of E_1 is largely dictated by the practical number of events that can be handled in the simulation and for a thousand or more missions. Setting E_1 to ≈20 TeV proved to be a good working value since 50,000 events on average are generated for the baseline-sized detector that are representative of α_1 and hence provides a robust estimate of α_1 for the unconstrained multistage approach of estimating the three spectral parameters; i.e., first fitting α_1, then keeping α_1 fixed at this value and fitting α_2 and E_k, followed by the three-dimensional search for $(\alpha_1, \alpha_2, E_k)_{ML}$ on the full set of energy deposits. The adequacy of this working value of E_1=20 TeV is further reinforced by noting in figure 21c that the critical parameter α_2 is essentially independent of lowering E_1 below 20 TeV when the knee location is 100 TeV or greater.

Next, for each of these simulated GCR events, a detector response is simulated according to the assumed detector response function and then the full set of simulated responses are used to estimate the spectral parameters. However, because no energies below E_1 are simulated, frequency histograms of the simulated detector responses, which resemble the appropriate detector pdf shown in figure 12, do not match the front-end portion of a real cosmic-ray energy spectrum which does look like those depicted in figure 8. This difference or mismatch is an artifact of not generating events from below E_1 that would have otherwise had the effect of filling in this front-end portion of the histogram and consequently resembling a real cosmic-ray energy spectrum.

This difference is not critical when making relative comparisons of the effects of design parameters or energy spectrum parameters when detector response function parameters used to generated the simulated responses match those detector response function parameters used in eq. (40) in the simplex search for $\boldsymbol{\theta}_{ML}$; i.e., implies a perfect understanding of the response function. However, when the impacts of response function uncertainties are studied, it is more important that the simulation techniques produce results that are closer to a real cosmic-ray energy response spectrum. To illustrate this point, suppose E_1 is set to 5 TeV in the simulation and the baseline detector collecting power is used, along with a broken power law energy spectrum with parameters α_1=2.8, α_2=3.3, and E_k=100 TeV, and E_2=5,500 TeV so that there will be around 634,000 events above 5 TeV. Next, if detector responses assuming a Gaussian response function with a constant 40-percent energy resolution are simulated, then there will be 477,400 responses on average <50 GeV, whereas there will be 459,400 responses <50 GeV if the broken-Gaussian response function depicted in figure 23 is used, or a difference of 18,000 events. This region of energy deposits <50 GeV results in that portion of the histograms that are of the greatest mismatch between the Gaussian and broken-Gaussian detector response histograms and is an artifact of not having any events <5 TeV in the simulation, and it is also the same region that does not match a real cosmic-ray response spectrum. Thus, it is this large mismatch that is driving the large biases seen in table 10 for α_1 and E_k when responses according to one of these response functions are simulated and then the other response function is used in eq. (40) of the simplex search for $\boldsymbol{\theta}_{ML}$ to study the impact of incorrectly understanding the "tail" of the detector response function.

The goal of method 2 is to make the histogram of the simulated detector responses match a real cosmic-ray energy spectrum when studying the effects of incorrectly known detector response function parameters so that a better estimate of their impact on the spectral parameter estimates is gained. This is achieved by placing a cut y_c in the simulated detector responses and then dropping all responses $<y_c$. In the simulation, the choice of y_c dictates the value of E_1 because E_1 must be chosen so that the probability of events having energy $<E_1$ but producing detector responses $>y_c$ is negligible, which obviously depends on the detector's energy resolution. For example, if y_c=60 GeV and a Gaussian response function having a 40-percent energy resolution and a mean response $(a + bE)$ is considered, as used for the baseline detector and defined in eq. (18), then E_1 can be any value ≤7 TeV, since only a negligible number of events from below 7 TeV will deposit more than 60 GeV. Selecting E_1=5 TeV provides ≈634,000 GCR events and setting y_c=60 GeV and dropping all simulated detector responses smaller than y_c produces a simulated response spectrum that does indeed look like a real response spectrum. Estimating the spectral parameters using only the simulated detector responses that are $>y_c$ as described here and for the case where the real detector response function is the broken Gaussian but a Gaussian function is inserted in eq. (40) in the simplex search for $\boldsymbol{\theta}_{ML}$ which results in the much more modest and intuitive biases shown as method 2 in the last row of table 10. Varying the cut y_c between 60 and 100 GeV produced similar results for all three spectral parameters, while lowering y_c below 55 GeV resulted in the more severe bias obtained using method 1 and associated with the large front-end mismatch of the histograms.

A very important practical benefit realized by introducing the cut y_c is that the lower limit of integration in eq. (40) can be any value $E_L<E_1$, which means that the ML procedure can be made independent of the range of integration, as long as E_L is chosen wisely. Thus, the ML estimation procedure herein developed can now be applied to real cosmic-ray detector response data. It should be mentioned that cuts on the high end are not required, since any value $E_H \geq E_2$ is suitable because the probability of events $>E_2$

are essentially zero. However, setting E_H unnecessarily high would result in many unnecessary calculations in the numerical integration of eq. (40).

Introducing the cut y_c requires a modification to the objective function in eq. (40) to handle the conditional detector response distribution. Thus, the objective function for method 2 becomes

$$O(\alpha_1,\alpha_2,E_k) = -\log L = -\sum_{j=1}^{N} \log[g_1(y_j \mid y_j > y_c;\alpha_1,\alpha_2,E_k)] \ , \tag{42}$$

where

$$g_1(y_j \mid y_j > y_c;\alpha_1,\alpha_2,E_k) = \frac{\int_{E_L}^{E_H} g(y_j \mid E;\rho)\,\phi_1(E;\alpha_1,\alpha_2,E_k)dE}{1-\int_0^{y_c} g_1(y\ ;\alpha_1,\alpha_2,E_k)dy}, \quad y_j > y_c \ . \tag{43}$$

From a simulation point of view, E_1=5 TeV is about the lowest value that was used because of the vast number of generated events and the requirement to handle thousands of simulated missions which are needed to make meaningful inferences. Consequently, cuts much less than 60 GeV are generally not feasible in simulations designed to study detector response function uncertainties. However, cuts in real cosmic-ray data can be taken to be much lower since the spectrum is already filled in from events having energies much less than 5 TeV.

5. CONCLUSIONS

Methods for estimating cosmic-ray spectral parameters from simulated detector responses with implications for detector design are presented in this TP. The method of ML estimation is seen to be the method of choice for estimating the single spectral parameter α_1 of a simple power law spectrum in terms of minimum variance and other important statistical properties and was thus selected as the estimation procedure for the broken power law spectrum. Again, the ML estimates attained these favorable statistical properties when the true knee location was around 100 TeV, but then these properties gradually slipped away for knee locations of 200 TeV and greater. The case of a spectral break size of 0.3 was also investigated and the results compared with the 0.5 break-size case in figures 20a–20c. A data analysis range study was conducted and showed that significant improvements in the precision in estimating the slope α_1 below the knee and the location E_k (but to a lesser degree) can be realized by lowering the lower limit of the simulation range E_1 but had essentially no impact on the estimation of the slope parameter α_2 above the knee.

The effects of detector energy resolution, collecting power, as well as various functional forms for the detector response function and energy-dependent resolution functions have also been studied and these results presented in this TP. While the energy resolution observed plays a somewhat stronger role in the estimation of the spectral parameters of a broken power law energy spectrum relative to a simple power law, the ability to estimate these spectral parameters, measured in terms of their standard deviations, still depends rather weakly on resolution and strongly on collecting power.

While increasing the size of the right-hand tail of the detector response function did indeed cause a slight rise in the standard deviation of the estimates of the three spectral parameters (greatest for α_2), the ML estimation procedure yielded estimates that, from a practical point of view, are unbiased. Similar results were gleaned from the studies using energy-dependent resolution functions. The implications of detector response model uncertainties were also investigated and the magnitude of such induced biases for various uncertainties presented. Cuts in the detector response data were introduced to simulate a more realistic cosmic-ray response spectrum and thereby provide a better description of the induced biases in the spectral parameter estimates when detector parameters are incorrectly known. Introduction of these cuts yielded the additional benefit of freeing the integral used in the ML procedure of requiring unique integration limits, thereby making this ML estimation procedure applicable to real cosmic-ray data.

APPENDIX A—SALIENT RESULTS AND THEIR APPLICATION TO DESIGN OF SPACE-BASED COSMIC-RAY DETECTORS

A number of the salient results from this research and their application to the design of space-based cosmic ray deterctors are presented in appendix A.

NASA/MSFC

Spectral De-Convolution

Estimating Cosmic Ray Spectral Parameters from Simulated Detector Responses

Energy Spectrum *assumed*
- Broken Power Law ϕ_1
  α_1, α_2, E_k (knee location)
- *Simple Power Law ϕ_0 also*

E

Number of Events
- Size, Time
  Baseline: 1 m^2, 3 yr
- Poisson

N

Detector Response Model GEANT
Normally incident protons
-linear mean response*(ED)* $\mu_{y|E}=a+bE$
- Gaussian uncertainty $g(y|E; \rho)$
  (function of resolution, ρ)
- *also gamma and "broken" Gaussian*

Y

Estimate the Spectral Parameters from Detector Responses Y_i

Maximum Likelihood estimates* - Multi-dimensional minimization algorithm (Nelder-Mead Downhill Simplex), to find $(\alpha_1, \alpha_2, E_k)_{ML}$ that minimizes the objective function (minus log-likelihood)

$$(\alpha_1, \alpha_2, E_k)_{ML} = \underset{\{\alpha_1, \alpha_2, E_k\}}{Min} O(\alpha_1, \alpha_2, E_k) = -\log L = -\sum_{j=1}^{N} \log[g(y_j; \alpha_1, \alpha_2, E_k)]$$

where

$$g(y_j; \alpha_1, \alpha_2, E_k) = \int g(y_j \mid E; \rho)\, \phi_1(E; \alpha_1, \alpha_2, E_k)\, dE$$

- **Study the statistical behavior of $(\alpha_1, \alpha_2, E_k)_{ML}$ over many missions**
- **Vary calorimeter size, resolution, response function, and spectral parameters, etc.**

* asymptotically minimum variance, consistent (unbiased for large samples), and normal. Kendall & Stuart, Advanced Theory of Statistics

Estimation of the Three Spectral Parameters: 0% and 40% Resolution

Events from ϕ_1 with α_1, =2.8, α_2 =3.3, E_k = 100 TeV over the range

20 TeV < E_i < 5,500 TeV, for which $N_{Average}$ 51,600 (2,250 > 100 TeV) – *baseline detector*

α_2

α_1

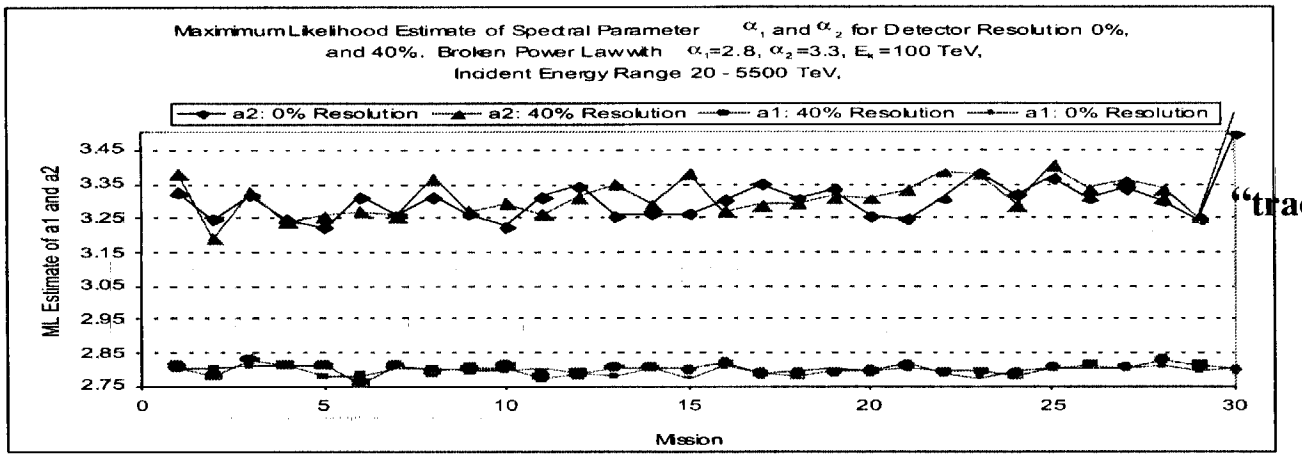

"tracking"

E_k

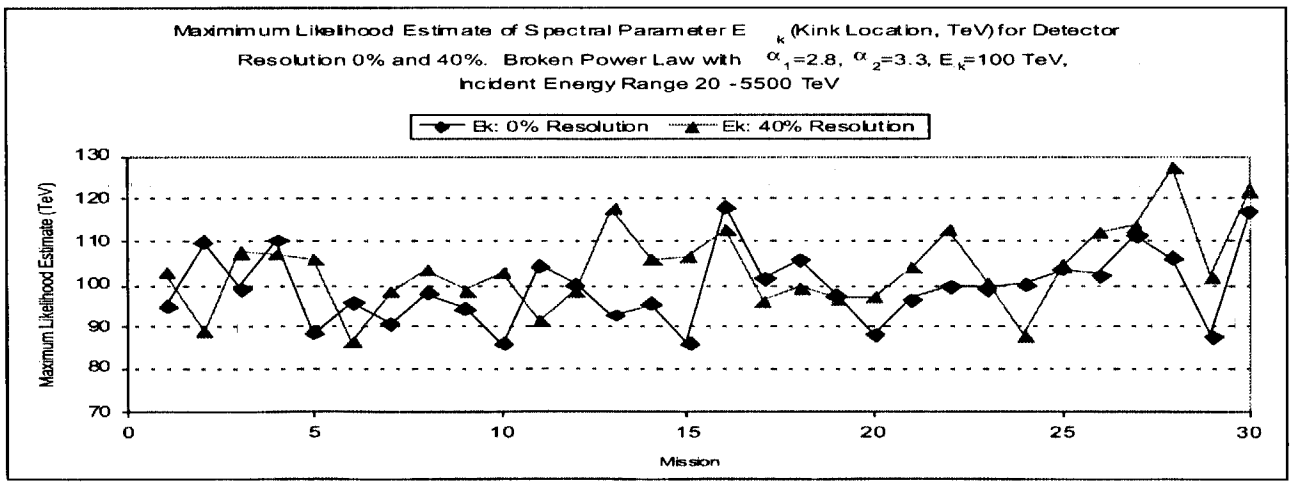

NASA MSFC

Relative Frequency Histograms of $(\alpha_1, \alpha_2, E_k)_{ML}$ for 1000 Missions

Events were simulated from ϕ_1 with $\alpha_1 = 2.8$, $\alpha_2 = 3.3$, $E_k = 100$ TeV over the range $20 \text{ TeV} < E_i < 5{,}500$ TeV, for which $N_{\text{Average}} = 51{,}600$ (2,250 > 100 TeV)

Gaussian Response Function, 40% Resolution

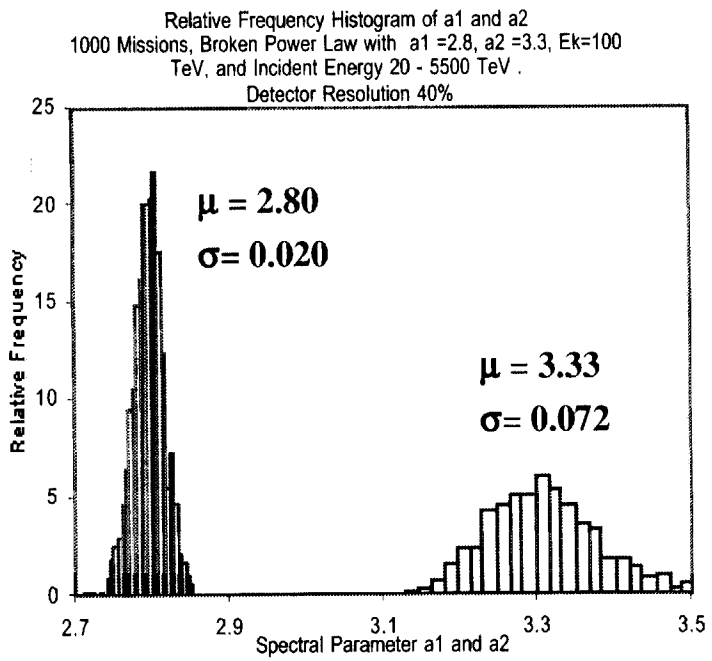

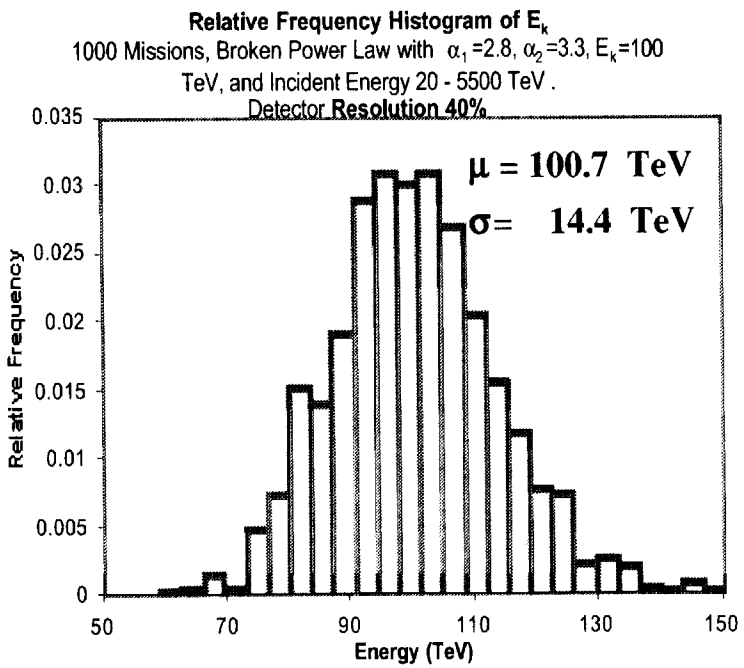

Standard Error of the ML Estimates $(\alpha_1, \alpha_2, E_k)_{ML}$ vs Detector Resolution

Events simulated from ϕ_1 with α_1=2.8, α_2=3.3, E_k=100 TeV, 1000 Missions

Gaussian Response Function

1. Energy Range: 20 TeV < E_i < 5,500 TeV, $N_{average}$ = 51,600, (2,250 > 100 TeV)

2. Detector Resolution ρ: 0%, 20%, 40%, & 50% **Note:** we define $\sigma(Y|E) = \rho\,\mu(Y|E)$ for ρ = 0.2, 0.4, and 0.6 in the Gaussian Response function. However, due to truncation (negative responses are re-sampled until a positive response is obtained), when ρ =0 .40, **RMS/Mean=0.39** and when ρ =0.60, **RMS/Mean = 0.51.**

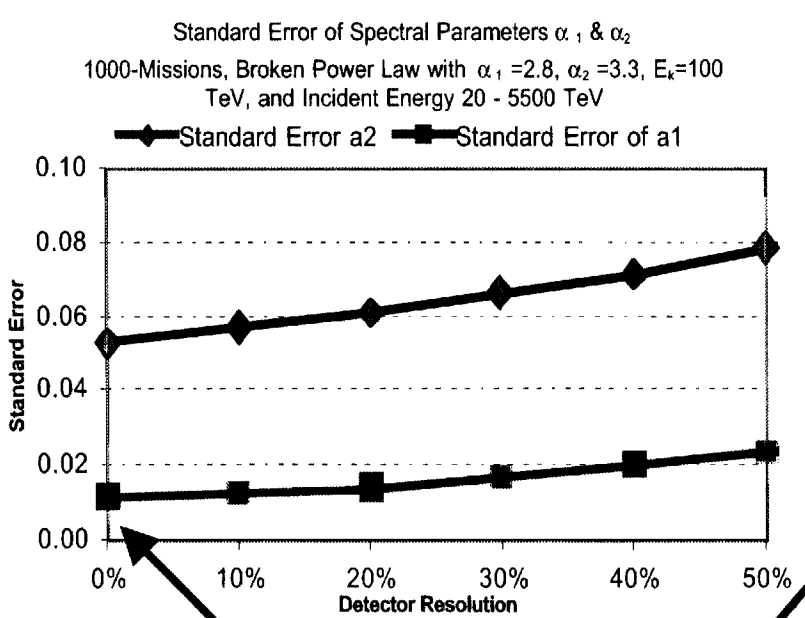

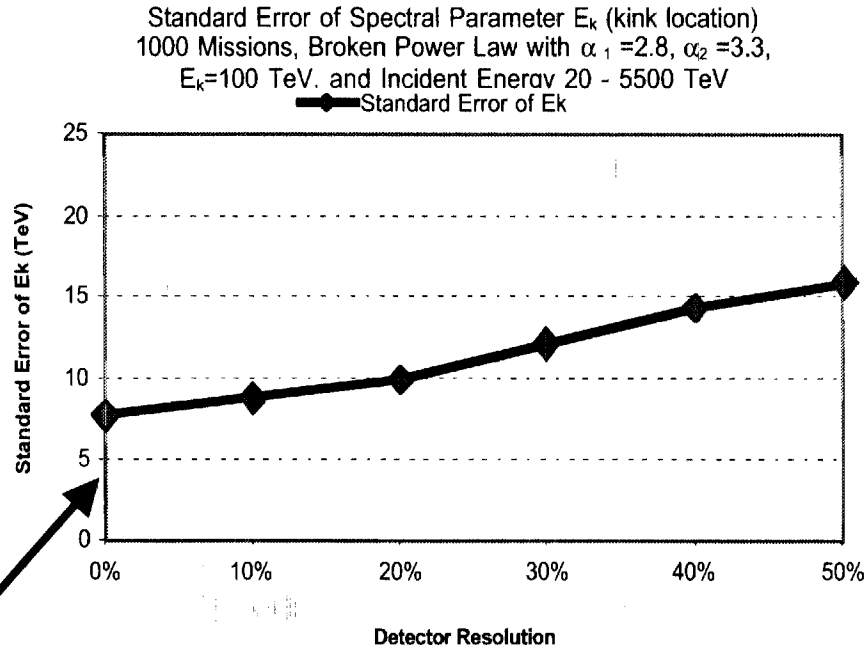

Component due to Event Statistics
(independent of detector response model)

NASA/MSFC

Data Analysis Range Study: Lowering E_1

Events from ϕ_1 with α_1 =2.8, α_2 =3.3, E_k = 100 TeV, Gaussian Response Function 150 Missions

Energy Ranges:

30, 20, 15, 10 - 5,500 TeV,

$N_{average}$ = 24,500, 51,500, 87,000, 181,000, respectively,

and (~2,250 > 100 TeV for each)

α_1

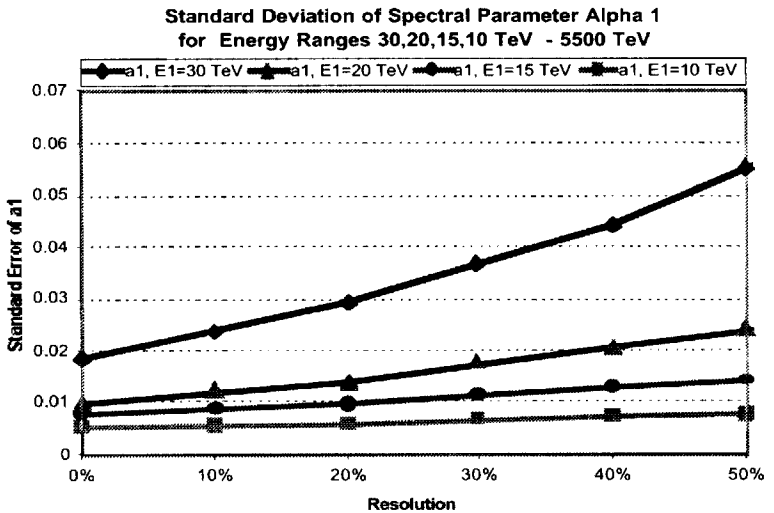

E_k

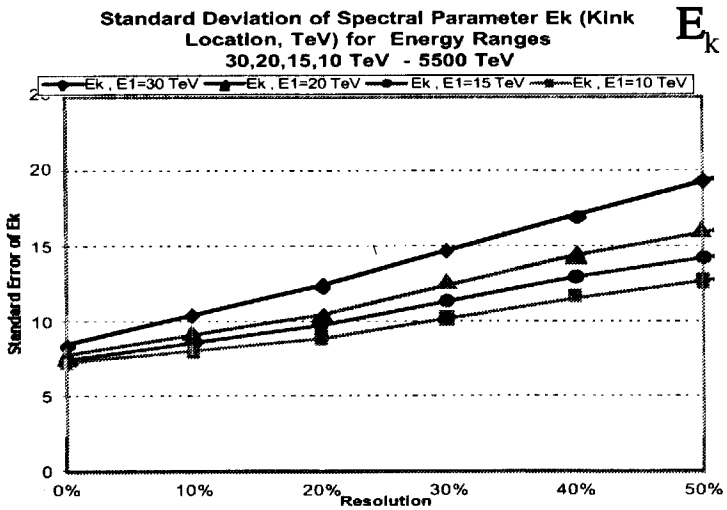

α_2

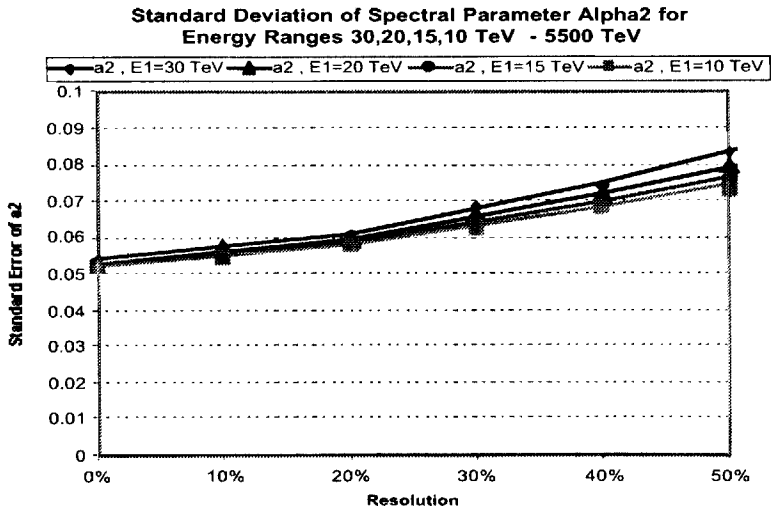

Calorimeter Size and Resolution Study: $20 < E_i < 5{,}500$ TeV

ϕ_1 with $\alpha_{1,} = 2.8$, $\alpha_2 = 3.3$, $E_k = 100$ TeV, Gaussian Response Function 1000 Missions

1. Baseline: ~ $1m^2$, 3 yr (middle curve)
   $N_{average} = 51{,}600$ (~$2{,}250 > E_k$)
2. Half-size (top curve)
   $N_{average} = 25{,}800$ (~$1{,}125 > E_k$)
3. Double-size (bottom curve)
   $N_{average} = 103{,}200$ (~$4{,}500 > E_k$)

α_1

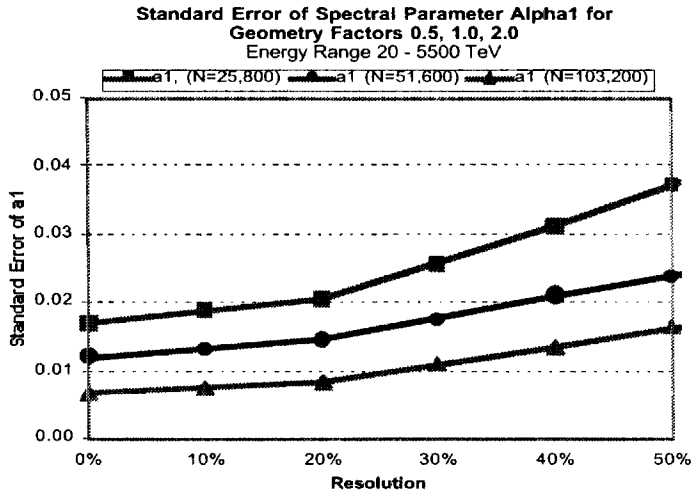

E_k

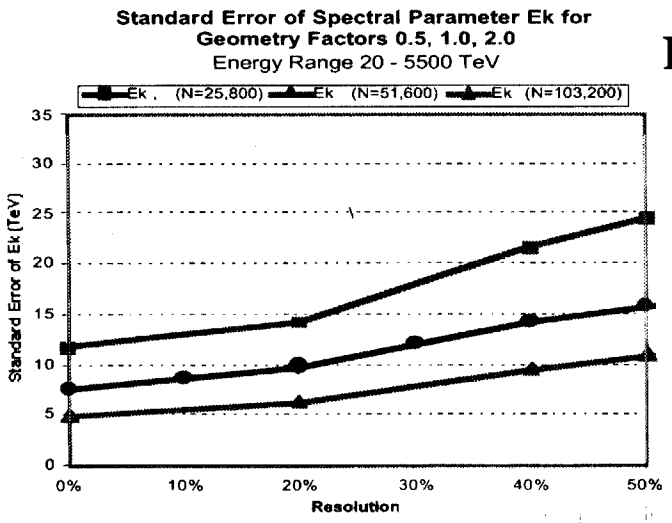

α_2

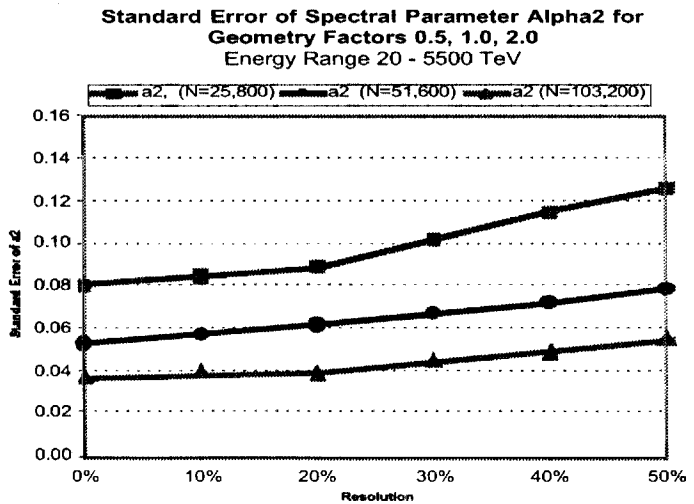

NASA/MSFC

Calorimeter Size and Resolution Study: $20 < E_i < 5{,}500$ TeV

ϕ_1 with $\alpha_1 = 2.8$, $\alpha_2 = 3.3$, $E_k = 100$ TeV, Gaussian Response Function 1000 Missions

1. Baseline: ~ $1m^2$, 3 yr (middle curve)
   $N_{average} = 51{,}600$ (~$2{,}250 > E_k$)
2. Half-size (top curve)
   $N_{average} = 25{,}800$ (~$1{,}125 > E_k$)
3. Double-size (bottom curve)
   $N_{average} = 103{,}200$ (~$4{,}500 > E_k$)

α_1

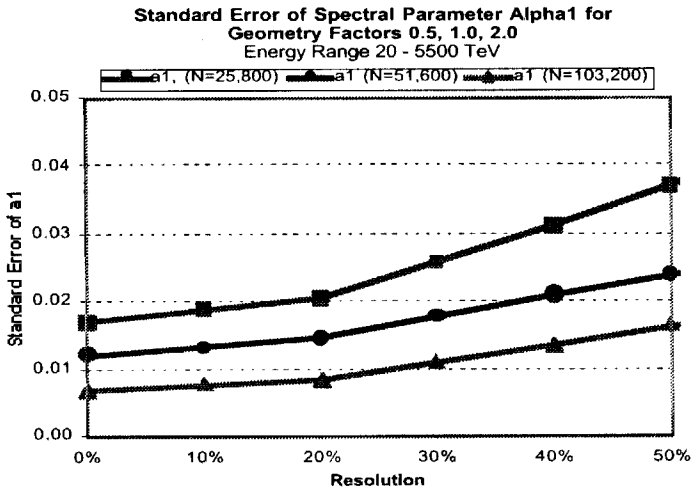

E_k

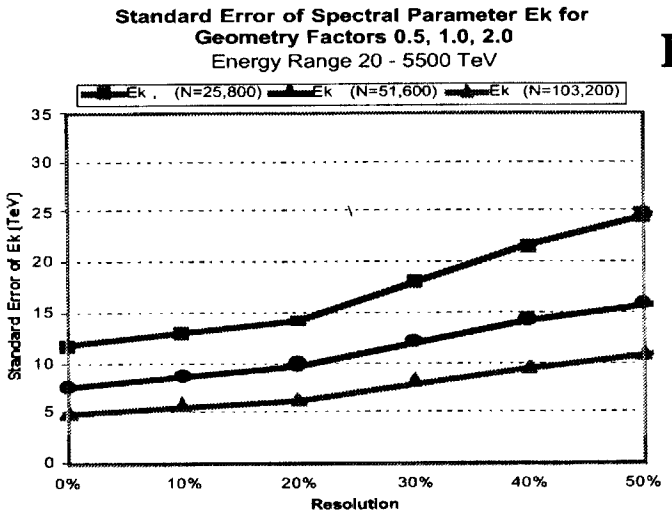

α_2

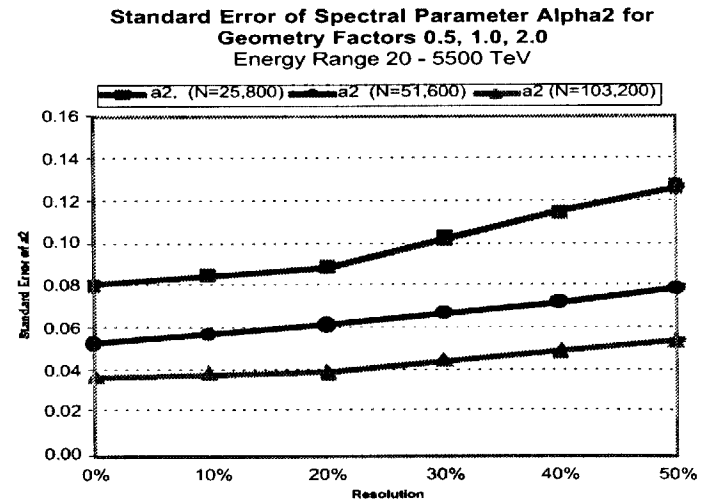

Estimation of the Three Spectral Parameters: 0% and 40% Resolution, α_2 =3.1

Events from ϕ_1 with α_1 =2.8, α_2 =3.1, E_k = 100 TeV 20 TeV < E_i < 5,500 TeV,

$N_{Average}$ = 51,800 (~2,500 > 100 TeV)

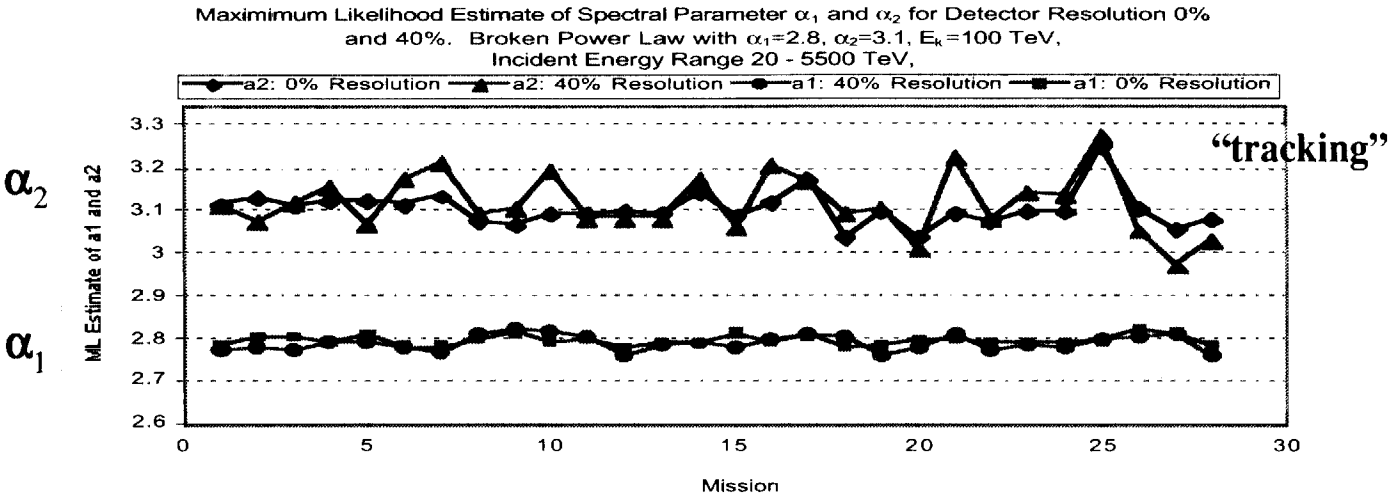

α_2

α_1

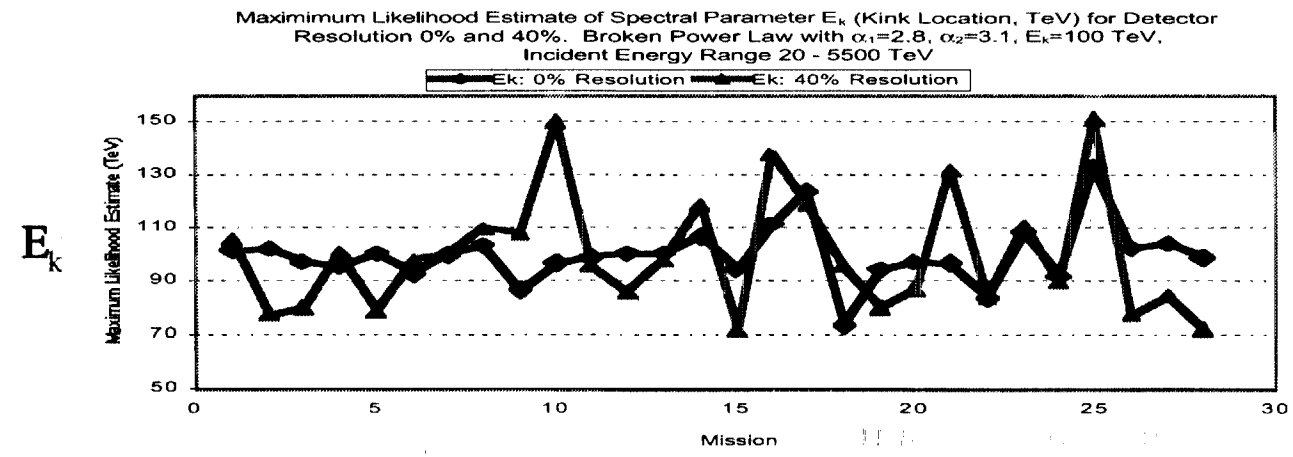

E_k

NASA/MSFC

Relative Frequency Histograms of $(\alpha_1, \alpha_2, E_k)_{ML}$ for 1000 Missions when $\alpha_2 = 3.1$

Events were simulated from ϕ_1 with $\alpha_1 = 2.8$, $\alpha_2 = 3.1$, $E_k = 100$ TeV over the range $20 \text{ TeV} < E_i < 5{,}500$ TeV, for which $N_{\text{Average}} = 51{,}800$ (2,500 > 100 TeV)

Detector Resolution - 40%

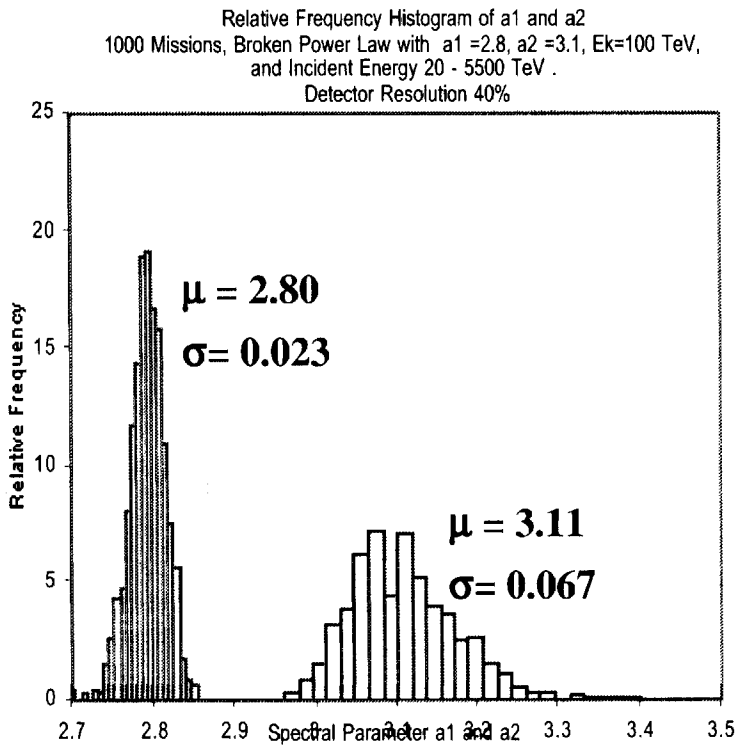

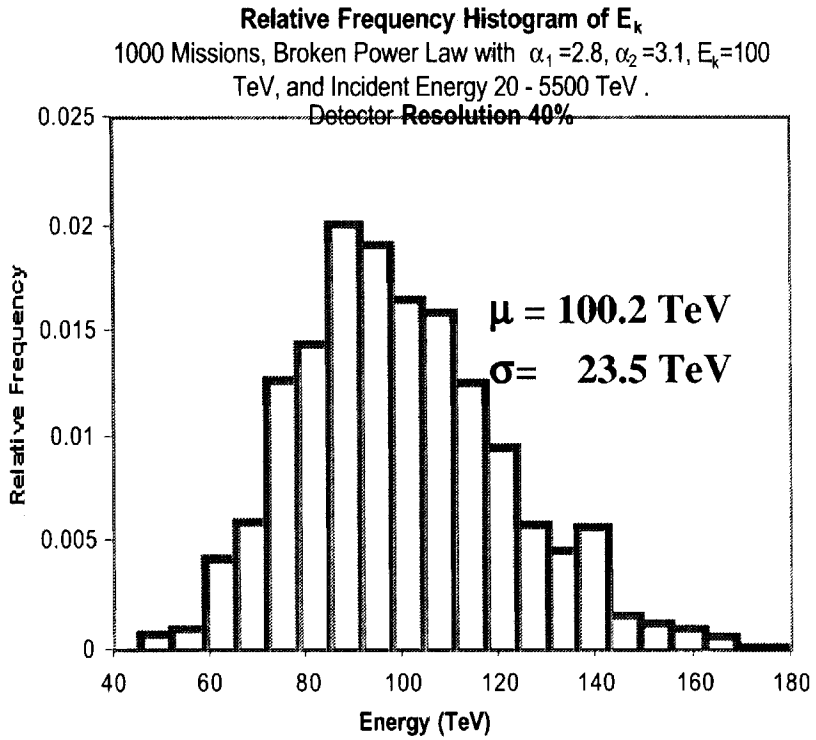

Comparing Standard Error of $(\alpha_1, \alpha_2, E_k)_{ML}$ when α_2=3.1 and α_2=3.3

with α_1 =2.8, E_k = 100 TeV, Energy Range 20- 5,500 TeV

When α_2=3.1, N= 51,800 (~2,500>100 TeV), the incident energy mean, standard deviation, and resolution (not the detector response resolution) are μ_E=42 TeV, σ_E=54 TeV, ρ_E=130% .
When α_2=3.3, N= 51,600 (~2,250>100 TeV)
μ_E=41 TeV, σ_E=46 TeV, ρ_E=112%

~10% difference above knee, but as σ_E goes up, so does σ_Y *(standard deviation of detector response)* and therefore $\sigma(\alpha_2)$ would increase. However, the increase in events above knee slight outweighs the increase in variance.

α_1

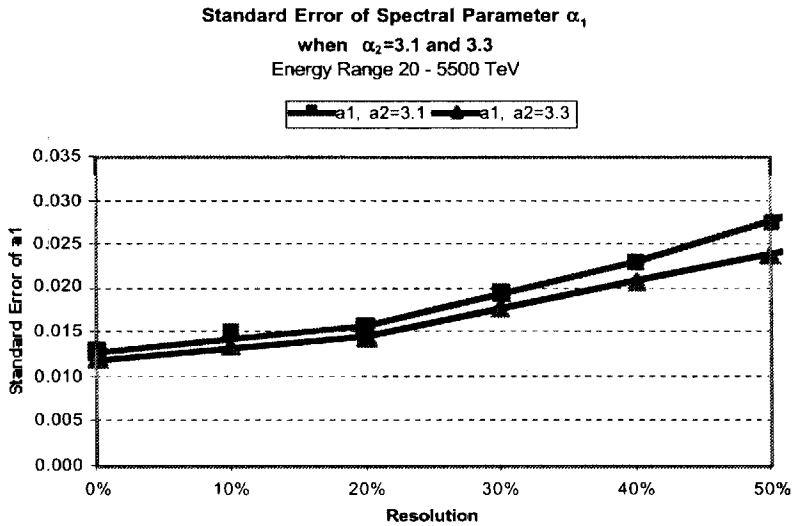

E_k

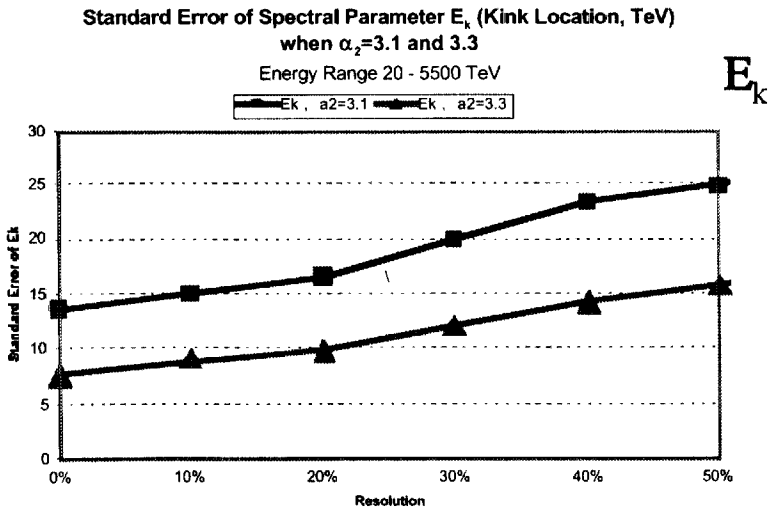

α_2

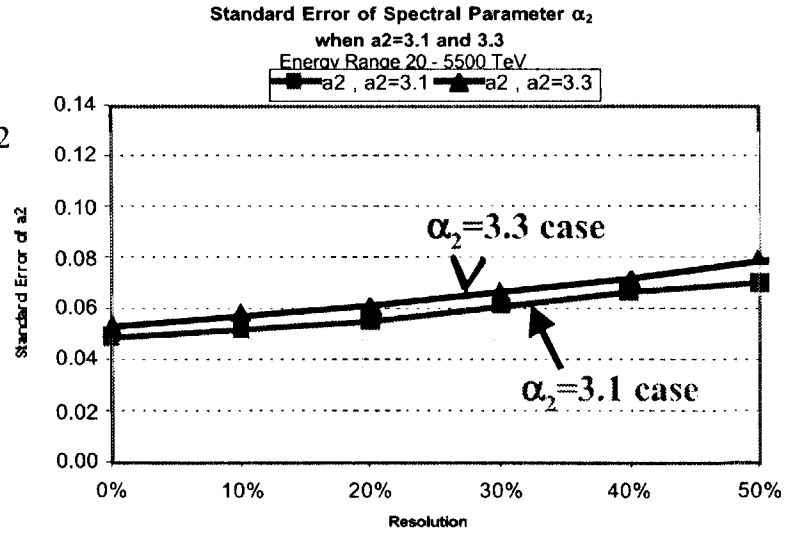

2-D Histogram of $(\alpha_1, \alpha_2)_{ML}$

Events from ϕ_1 with $\alpha_1 = 2.8$, $\alpha_2 = 3.2$, $E_k = 125$ TeV over the range

$20 \text{ TeV} < E_i < 5{,}500 \text{ TeV}$, for which N_{Average} 51,900 (1,600 > 125 TeV) – *baseline detector*

Gaussian Response Function, 40% Resolution - *25,000 Simulated Missions*

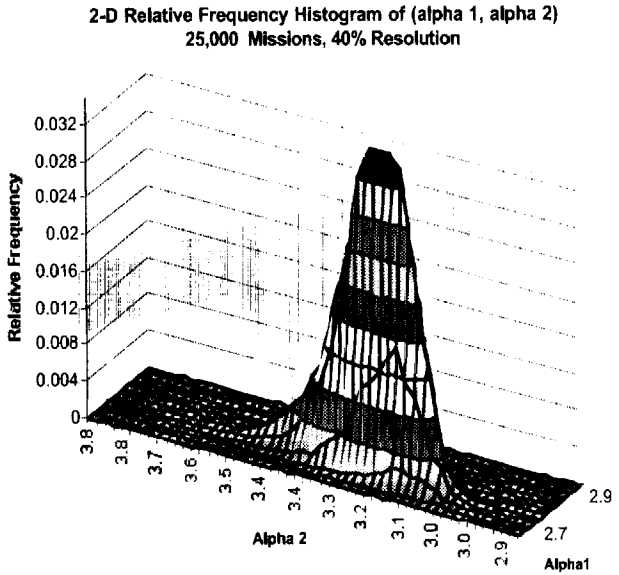

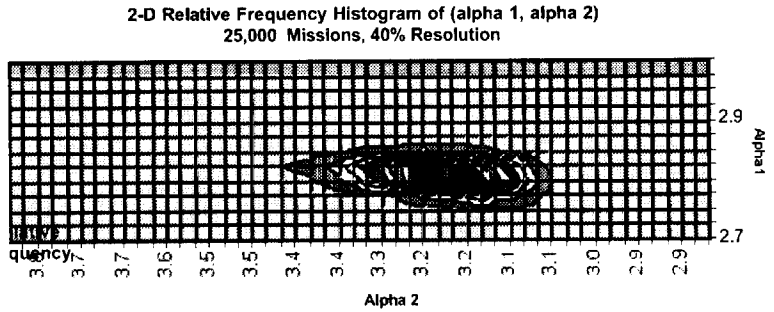

	Mean	Standard Deviation
α_1	2.80	0.017
α_2	3.21	0.088
E_k	128 TeV	25.1 TeV

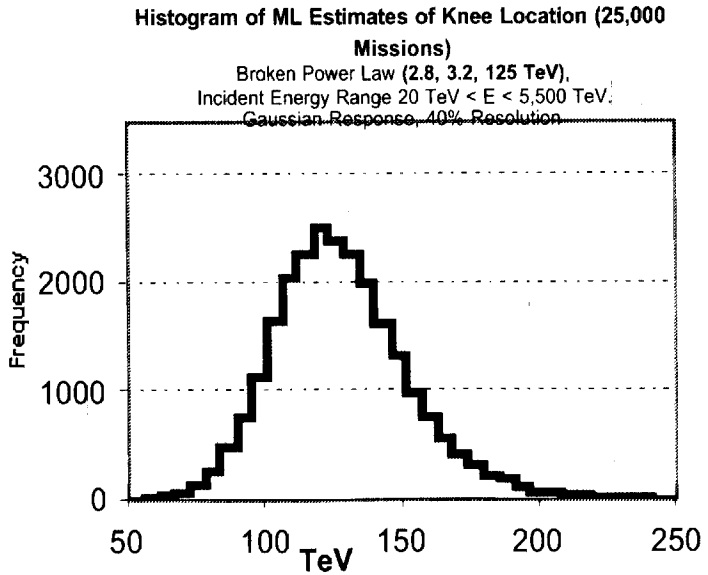

NASA/MSFC

2-D Histogram of $(\alpha_1, \alpha_2)_{ML}$ - Zero Resolution

Events from ϕ_1 with α_1 =2.8, α_2 =3.2, E_k = **125 TeV** over the range

20 TeV < E_i < 5,500 TeV, for which $N_{Average}$ 51,900 (1,600 > 125TeV) – *baseline size*

25,000 Simulated Missions

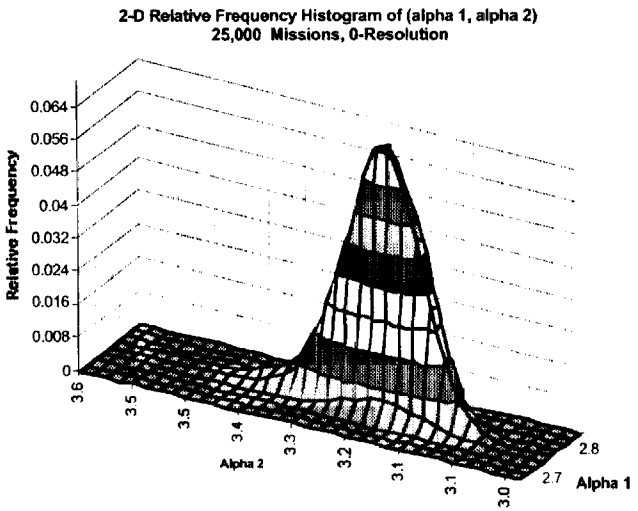

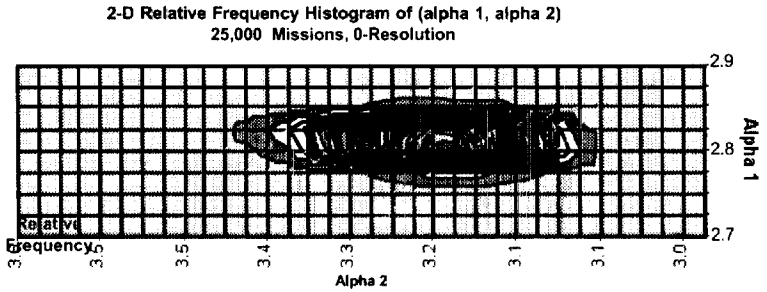

	Mean	Standard Deviation
α_1	2.80	0.011
α_2	3.21	0.062
E_k	126 TeV	15.1 TeV

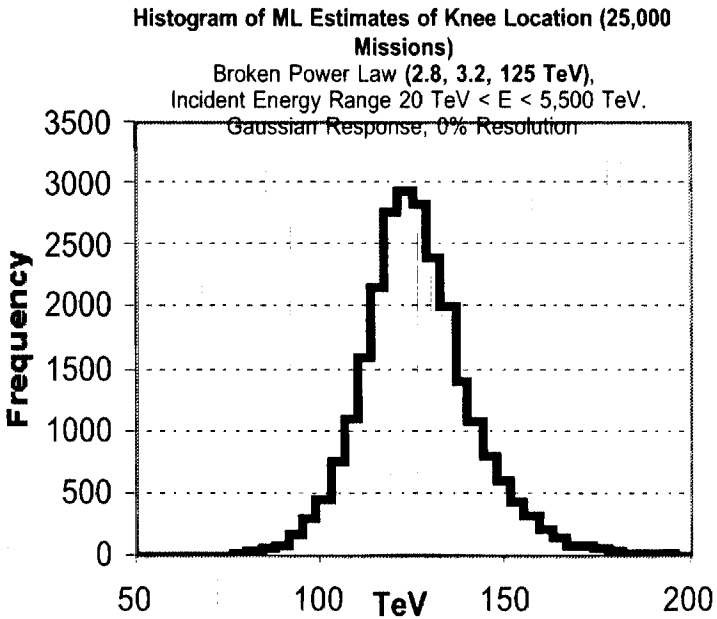

NASA/MSFC

2-D Histogram of Standardized $(\alpha_1, E_k)_{ML}$ and $(\alpha_2, E_k)_{ML}$ - Zero Resolution

Events from ϕ_1 with $\alpha_1 = 2.8, \alpha_2 = 3.2, E_k = \mathbf{125\ TeV}$ over the range

$20\ \text{TeV} < E_i < 5{,}500\ \text{TeV}$, for which N_{Average} 51,900 (1,600 > 125TeV) – *baseline size*

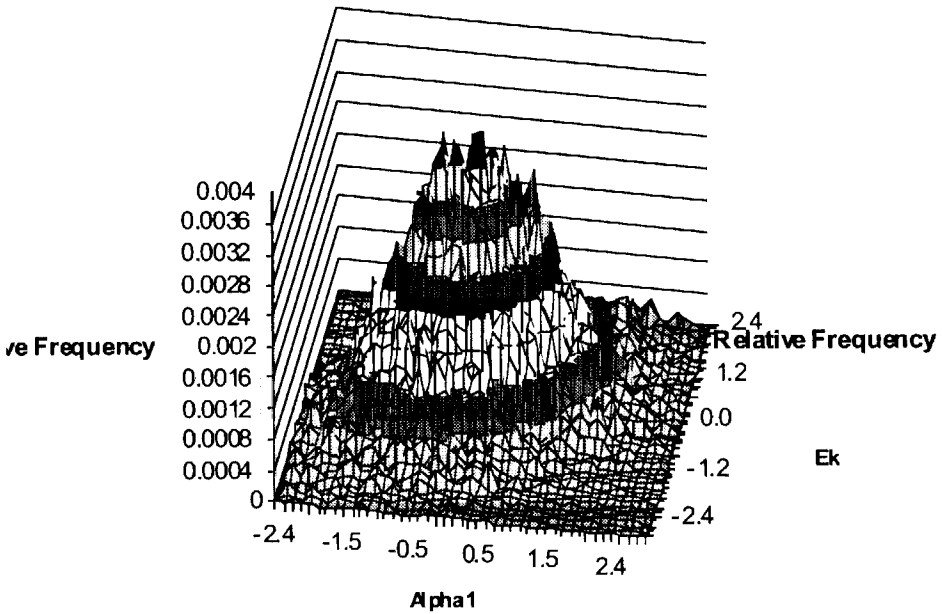

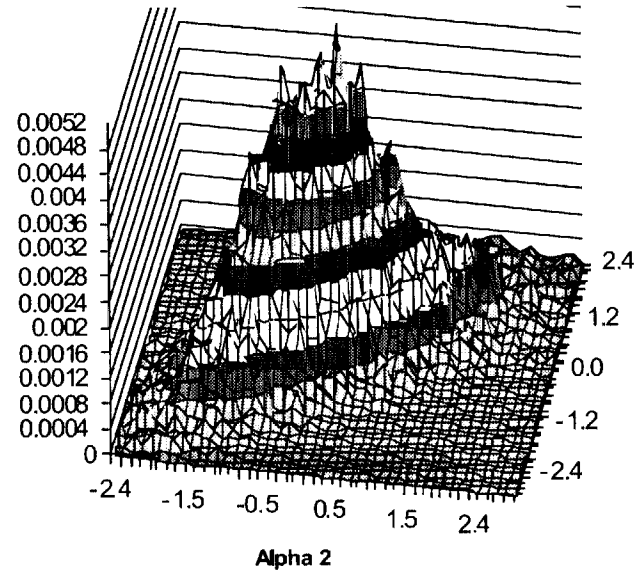

Correlation Matrix			
	α_1	α_2	E_k
α_1	1.00	0.08	0.42
α_2	0.08	1.00	0.72
E_k	0.42	0.72	1.00

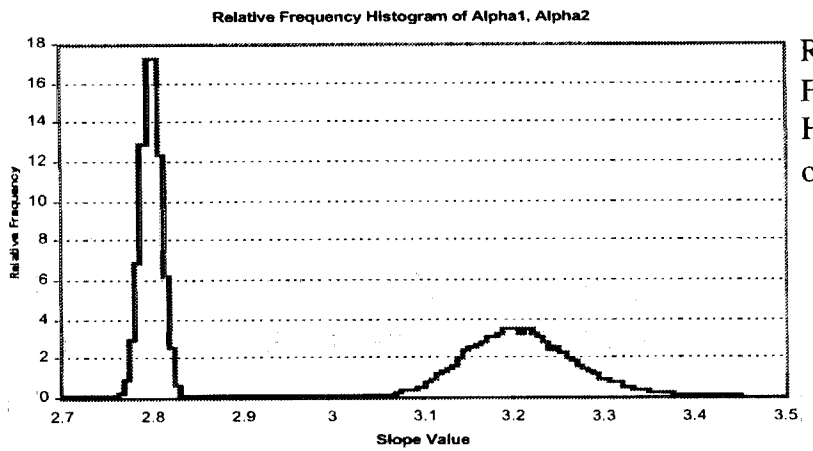

Relative Frequency Histogram of α_1 and α_2

NASA/MSFC

2-D Histogram of Standardized $(\alpha_1, E_k)_{ML}$ and $(\alpha_2, E_k)_{ML}$ - Zero Resolution

Events from h_1 with $a_1 = 2.8, a_2 = 3.1, E_k = 100$ TeV over the range

20 TeV < E_i < 5,500 TeV, for which $N_{Average}$ = 103,600 (5,000>100 TeV) – 2X baseline size

100,000 Missions

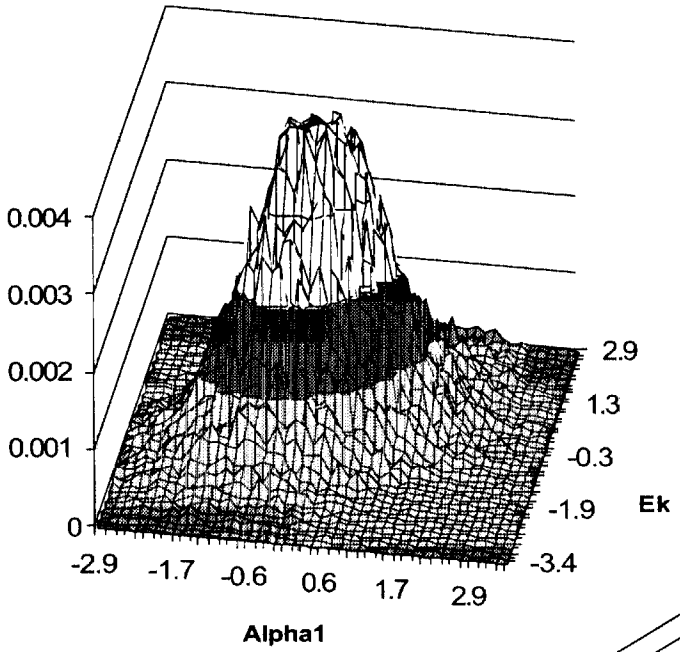

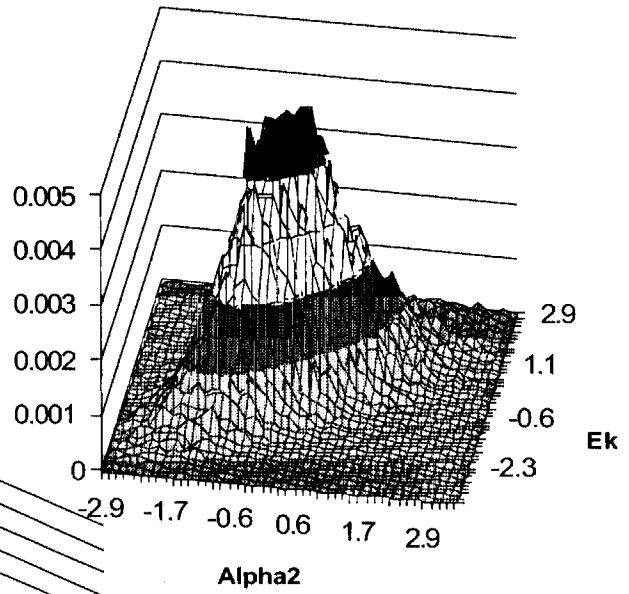

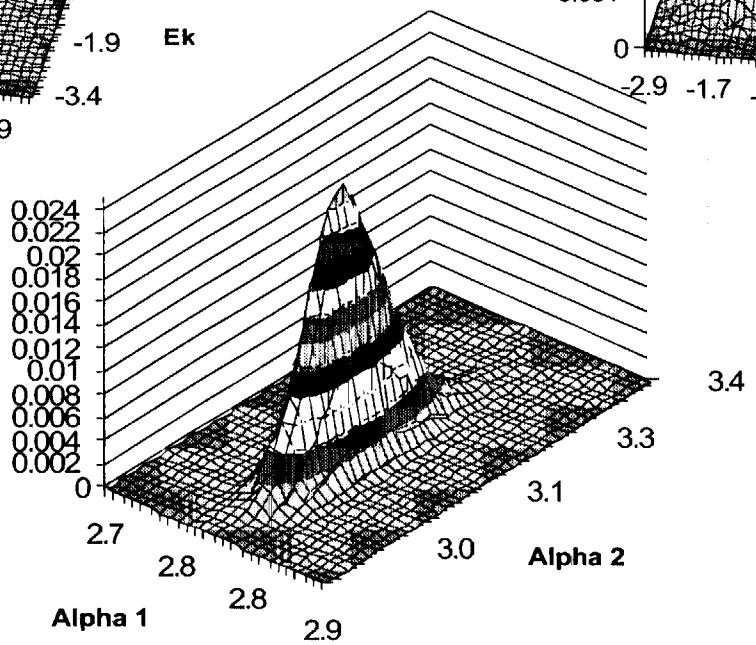

	Mean	Standard Deviation
α_1	2.80	0.0084
α_2	3.10	0.032
E_k		8.6 TeV

	Correlation Matrix		
	α_1	α_2	E_k
α_1	1.00	0.06	0.47
α_2	0.06	1.00	0.68
E_k	0.47	0.68	1.00

NASA/MSFC

Non-constant Energy Resolution Study (Gaussian Response Function)

Events from ϕ_1 with α_1,=2.8, α_2 =3.3, E_k= 100 TeV

20 TeV< E_i < 5,500TeV, $N_{Average}$ = 51,600 (2,250 > 100 TeV); 100 Missions

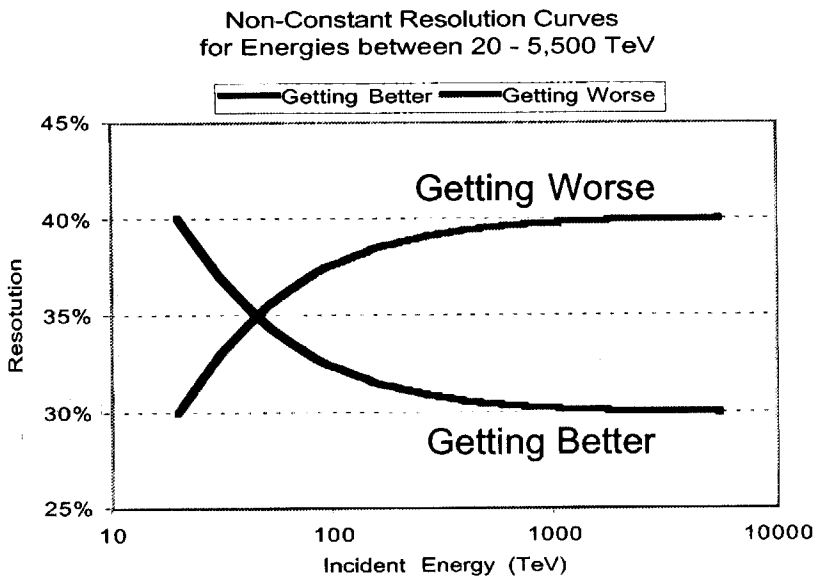

Spectral Parameter	Mean and Standard Deviation of the Estimates based on 100 Missions					
	Resolution					
	Constant 40%		Non-Constant (getting better)		Non-Constant (getting worse)	
	Mean	Std. Dev.	Mean	Std. Dev.	Mean	Std. Dev.
α_1,E1=20	2.800	0.020	2.794	0.018	2.794	0.018
α_2, E1=20	3.330	0.072	3.309	0.067	3.312	0.073
E_k, E1=20	100.70	14.40	99.63	12.6	99.93	13.5

Asymptotic Properties of the Maximum Likelihood Estimates as Knee Location Varies

α_1, =2.8,α_2 =3.3,E_k = 100, 200, 300** TeV,

Data Analysis Range 20 – 5,500TeV *Baseline Detector*

Gaussian Response function (40%)

Note : Cramer-Rao minimum variance bound* begins to slip away for the ML estimates of α_2 and E_k as the true knee location E_k increases and hence the number of events above the knee diminish. The ML estimator ofα_1 continues to achieve the CR Bound.

***A few spurious results occurred for the (E_k=300 TeV,40% Resolution) case , and a simple power law might have provided a better fit to the "data" thus suggesting the need for hypothesis testing.*

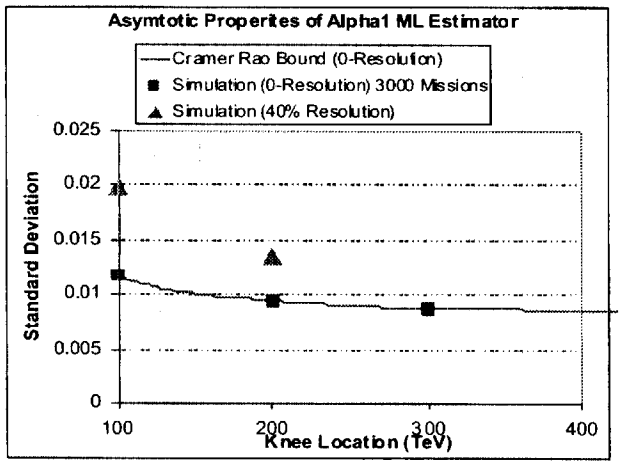

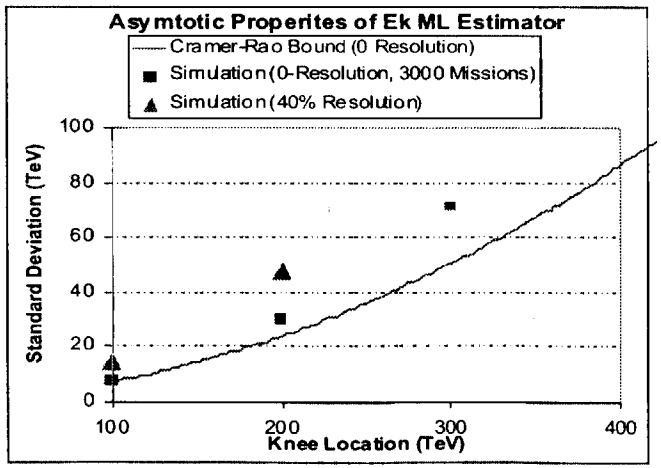

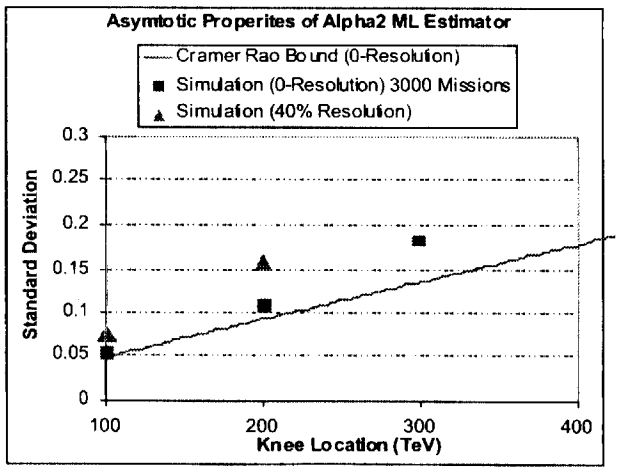

Rule of thumb: need about 2000 events or more above E_k to achieve CR Bound

NASA/MSFC

*Bound below which the variance of an estimator cannot fall.
Kendall and Stewart, Advanced Theory of Statistics

Asymptotic Properties of the Maximum Likelihood Estimates as Knee Location Varies

α_1, =2.8, α_2 =3.3, E_k = 100, 200, 300 TeV,

Data Analysis Range 20 – 5,500 TeV *5X Detector*

Gaussian Response function (40%)

Note : Cramer-Rao minimum variance bound* for the ML estimates of α_2 and E_k is largely recovered by the 5X detector when E_k=300 TeV.

Also, no spurious results occurred for the Ek=300 TeV case using the 5X-40% resolution detector.

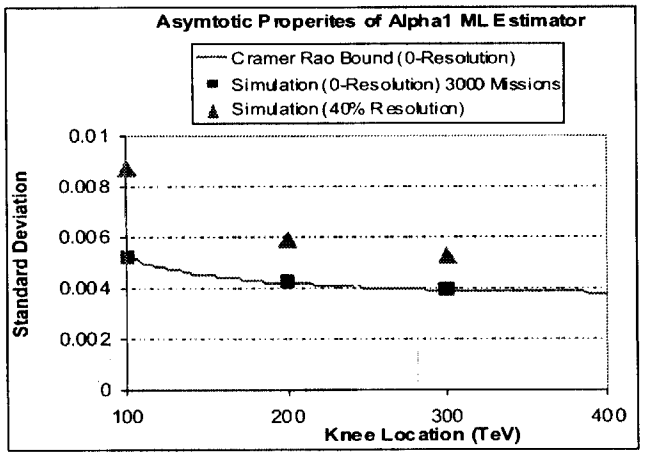

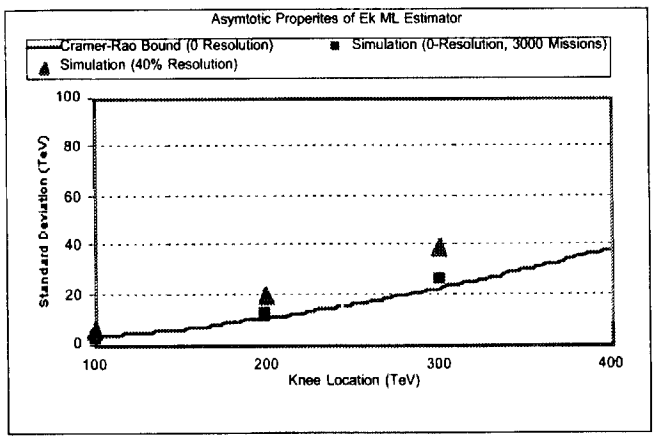

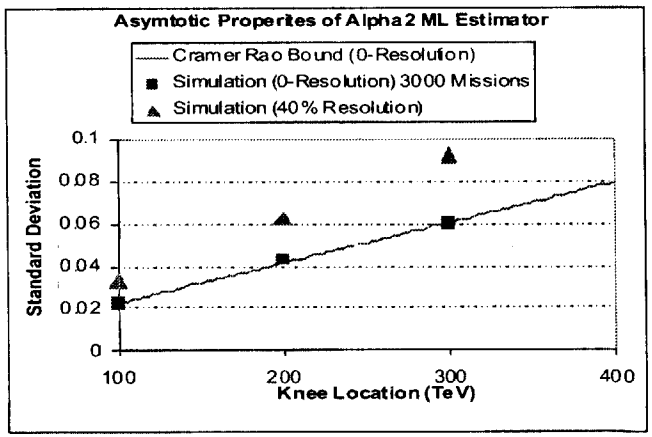

Study of Kink Location and Asymptotic Properties of the Maximum Likelihood Estimates

α_1 =2.8, α_2 =3.3, E_k = 100, 200, 300 TeV, Data Analysis Range 20 – 5,500 TeV

Note how the properties of unbiasedness and achieving the Cramer-Rao minimum variance bound begin to slip away for the ML estimates of α_2 and E_k as the true knee location E_k increases and hence the number of events above the knee diminish, but are largely recovered by the hypothetical 5X detector. The ML estimator of α_1 will always enjoy these favorable statistical properties.

Recall that RMS/Mean is 51% when σ/μ =0.6 for Gaussian response function

		Mean			Standard Error			
Resolution	E_k (TeV) N_1(>20 TeV) (N_1(>E_k))	α_1	α_2	E_k	α_1	α_2	E_k	
0%	**100** 51,576 (2,255)	2.80	3.30	100	0.012	0.049	6.6	Theoretical Limit (unbiased, Cramer-Rao LB
0%		2.80	3.31	100.7	0.012	0.053	7.6	Simulation (3000 Missions)
40%		2.80	3.31	101.7	0.020	0.076	14.0	Simulation (3000 Missions)
0%	**100** 257,880 (11,275)	2.80	3.30	100	0.0052	0.022	3.0	5X Theoretical Limit (unbiased, Cramer-Rao LB
0%		2.80	3.30	100.1	0.0052	0.022	3.2	Simulation (3000 Missions)
40%		2.80	3.30	100.9	0.0088	0.033	6.2	Simulation (3000 Missions)
0%	**200** 52,022 (647)	2.80	3.30	200	0.0094	0.092	23.4	Theoretical Limit (unbiased, Cramer-Rao LB
0%		2.80	3.32	202.0	0.0096	0.11	30.3	Simulation (2000 Missions)
40%		2.80	3.33	205.1	0.0135	0.16	47.7	Simulation (2000 Missions)
0%	**200** 260,110 (3,235)	2.80	3.30	200	0.0042	0.041	10.5	5X Theoretical Limit (unbiased, Cramer-Rao LB
0%		2.80	3.30	200.2	0.0042	0.043	11.8	Simulation (2000 Missions)
40%		2.80	3.31	201.4	0.0059	0.063	20.3	Simulation (2000 Missions)
0%	**300** 52,116 (312)	2.80	3.30	300	0.0088	0.13	50.0	Theoretical Limit (unbiased, Cramer-Rao LB
0%		2.80	3.34	309.9	0.0087	0.18	71.0	Simulation (3000 Missions)
40%		Further Study Required *						Simulation (3000 Missions)
0%	**300** 260,580 (1,560)	2.80	3.30	300	0.0039	0.060	22.3	5X Theoretical Limit (unbiased, Cramer-Rao LB
0%		2.80	3.31	301.8	0.0040	0.067	26.3	Simulation (3000 Missions)
40%		2.80	3.31	303.7	0.0053	0.092	39.8	
0%	**300** 333,542 (2,000)	2.80	3.30	300	0.0035	0.053	19.7	6.4X Theoretical Limit (unbiased, Cramer-Rao LB
0%		2.80	3.30	300.3	0.0036	0.056	22.4	Simulation (1500 Missions)
40%		2.80	3.31	301	0.0046	0.078	35.3	
60%		**2.80**	**3.31**	**301**	**0.0052**	**0.091**	**41.4**	**KLEM (6.4 X)**

- A few spurious results occurred for this case, and a simple power law might have provided a better fit to the "data" thus suggesting the need for hypothesis testing

NASA/MSFC

Calorimeter Size and Resolution Study

Histogram of ML Estimates of Knee Location for Baseline, 2X, 5X Detector

Events from ϕ_1 with α_1 =2.8, α_2 =3.3, E_k = 200 TeV, **20 < E_i <5,500 TeV** , 1000 Missions

(Gaussian Response Function, 40% Resolution)

ML Estimate of Knee Location (1000 Missions)

	Mean (TeV)	Standard Deviation (TeV)
Baseline (N=52,025)	209	53
Double (2X)	204	31
5X (500 Missions)	202	19

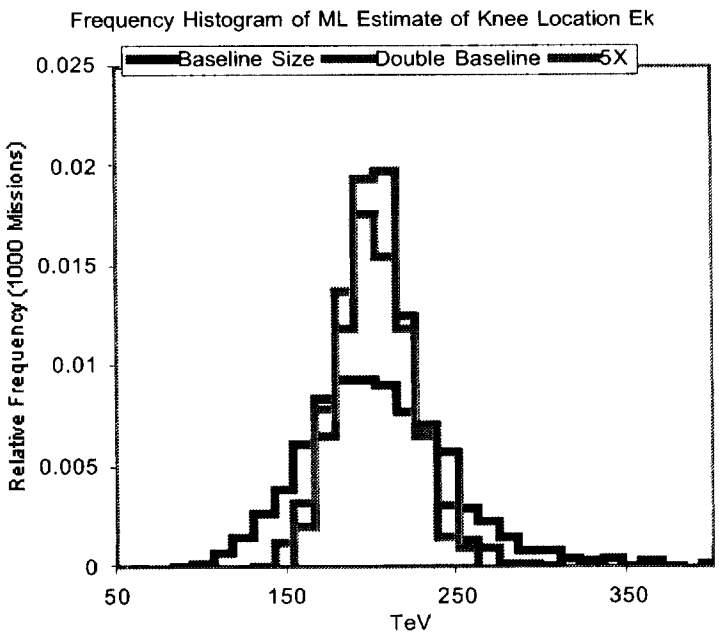

Calorimeter Size and Resolution Study
Histogram of ML Estimates of Knee Location for Baseline, 5X, and KLEM

Events from ϕ_1 with α_1 =2.8, α_2 =3.3, E_k = **300** TeV, **20** < E_i <**5,500** **TeV** , 1000 Missions

GaussianResponse Function, 40% Resolution for Baseline* and 5X Detector, 60% for KLEM (6.4X)**

ML Estimate of Knee Location (500 Missions)

Detector Size (# of events,events above Ek)	Mean (TeV)	Standard Deviation (TeV)
5X (260580, 1560)	302	40
KLEM ** (333540, 2000)	302	42

*** Recall that RMS/Mean is 51% when σ/μ =0.6 for Gaussian response function*

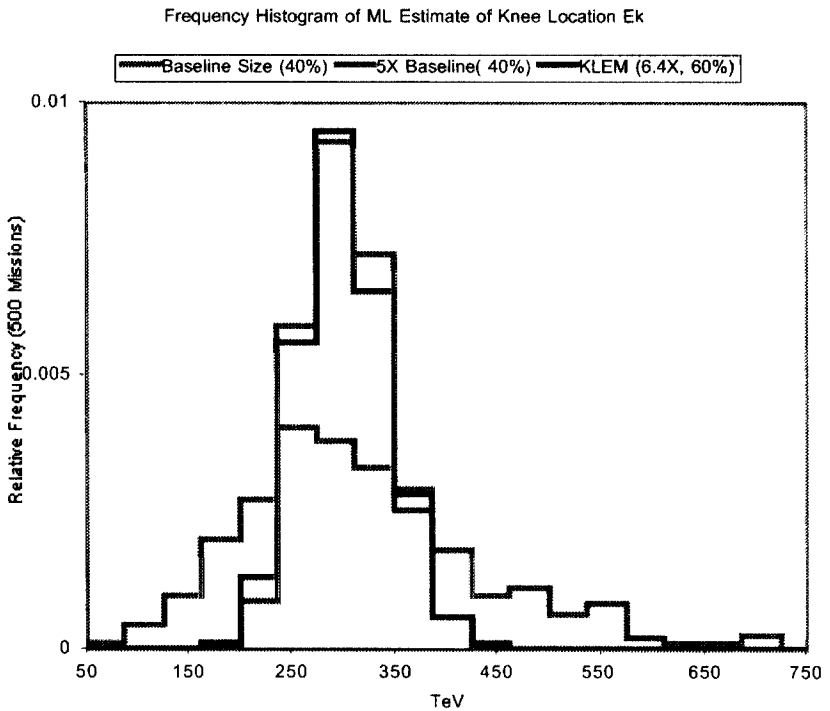

* A few spurious results occurred for the baseline case, and a simple power law might have provided a better fit to the "data" thus suggesting the need for hypothesis testing.

NASA/MSFC

How Well do We Need to Know our Detector Response Function?

Uncertainties in Gaussian Response Model Parameters

What if the true resolution is 35%, but we think it is ....

Simulating Detector Response

we use $\rho = 0.35$

$Y_i = \mu_{Y|E} + \sigma_{Y|E} Z_i$ ($\sigma = \rho\mu$, so $\sigma_{Y|E} = 0.35\ \mu_{Y|E}$)

$Y_i = (a + bE_i)(1+0.35Z_i)$, a, b from GEANT sim's

Spectral De-Convolution

we use $\rho = 0.31, \ldots, 0.39$

$$Min\ O(\alpha_1, \alpha_2, E_k) = -\log L = -\sum_{j=1}^{N} \log[g(y_j; \alpha_1, \alpha_2, E_k)]$$

$$g(y_j; \alpha_1, \alpha_2, E_k) = \int g(y_j \mid E; \rho)\, \phi_1(E; \alpha_1, \alpha_2, E_k)\, dE$$

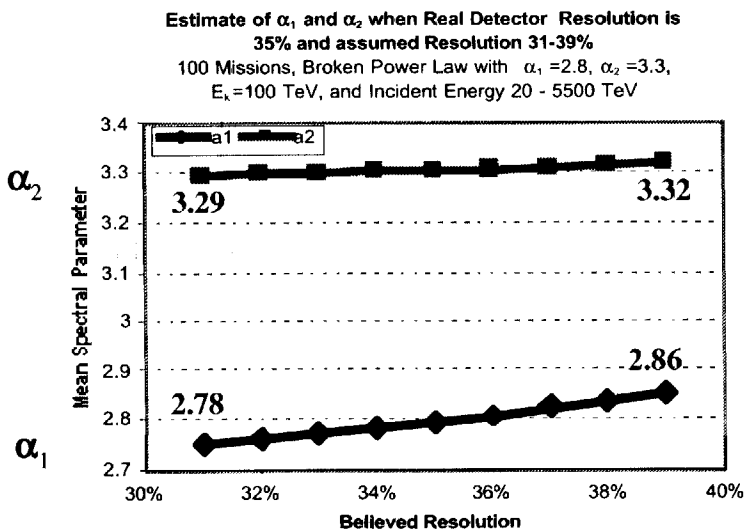

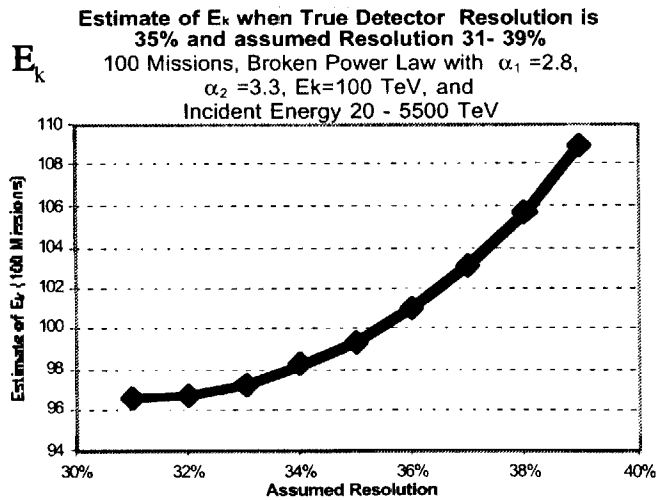

Uncertainties in Gaussian Response Model Parameters

True Resolution is Non-Constant, but we assume it is a constant (35%)

Case 1: Resolution is Getting Better (40% to 30% over 20 – 5,500 TeV, as previously)
α_1=2.65, α_2=3.25, E_k=67 TeV, indicated by ● in figures. *100 Missions average*

Case 2: Resolution is Getting Worse (30% to 40% over 20–5,500 TeV)
α_1=2.88, α_2=3.34, E_k=145 TeV, indicated by ▮ in figures. *100 Mission average*

Case 1&2 added to Figures on previous chart, with different scale

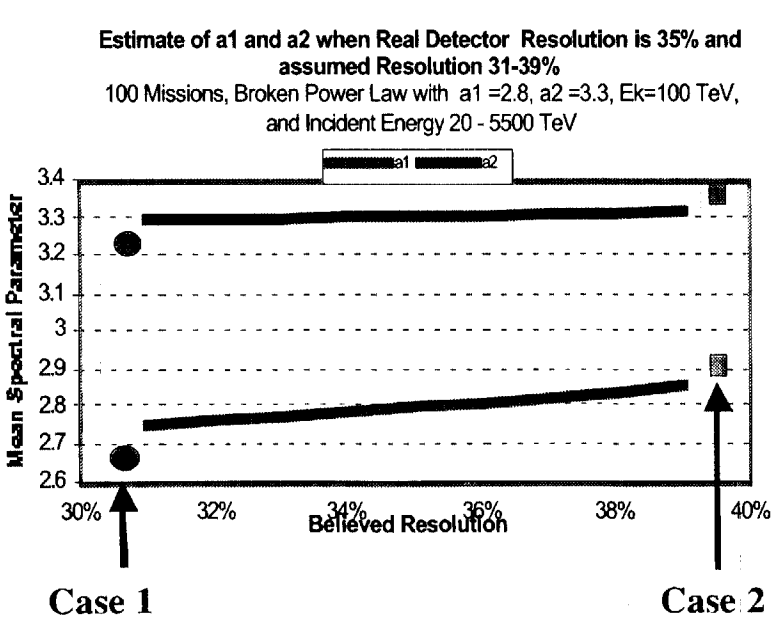

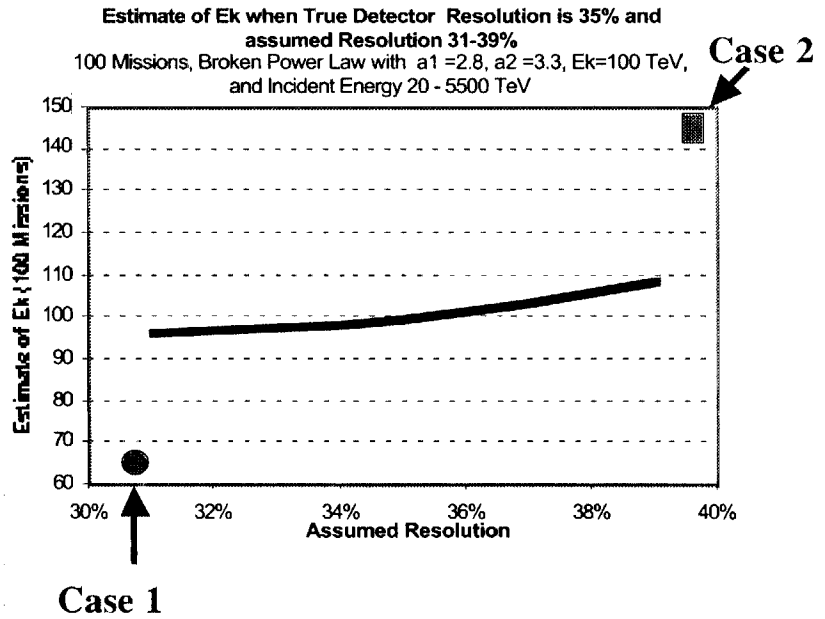

NASA/MSFC

Gaussian (40%) vs "Broken" Gaussian – *Method 1*

ϕ_1 with α_1 =2.8, α_2 =3.3, E_k = 100 TeV, 20 < E_i <5,500 TeV, 1000 Missions

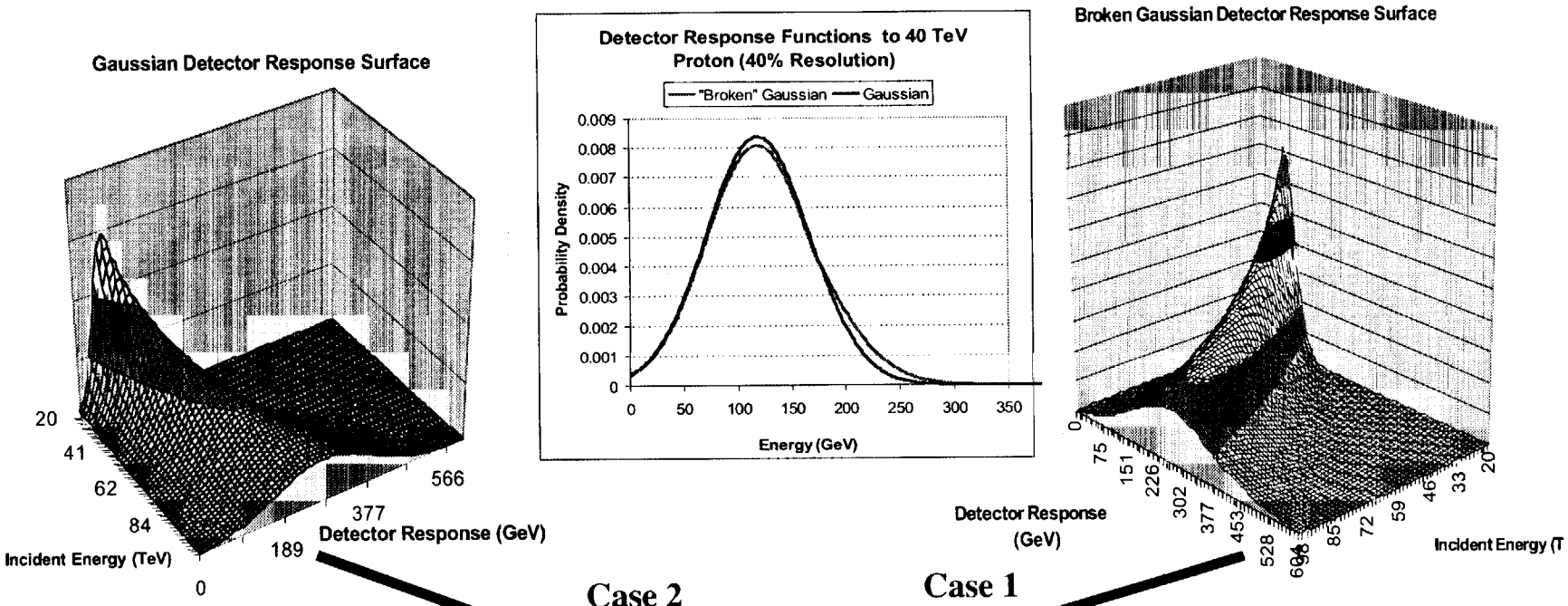

Case 2

Case 1

$$g(y_j;\alpha_1,\alpha_2,E_k)=\int g(y_j \mid E;\rho)\,\phi_1(E;\alpha_1,\alpha_2,E_k)\,dE$$

$$Min\ O(\alpha_1,\alpha_2,E_k)=-\log L=-\sum_{j=1}^{N}\log[g(y_j;\alpha_1,\alpha_2,E_k)]$$

Case 1: Assumed "Broken" Gaussian but really Gaussian. α_1 =2.98, α_2 =3.38, E_k=171 TeV

Case 2: Assumed Gaussian but really "Broken" Gaussian. α_1=2.53, α_2=3.21, E_k=67 TeV

1000- Mission Averages

NASA/MSFC

Uncertainties in Detector Response Models
Gaussian (40%) vs "Broken" Gaussian

ϕ_1 with $\alpha_{1,}$ =2.8, α_2 =3.3, E_k = 100 TeV, 20 < E_i <5,500 TeV, 25,000 Missions

Assumed Gaussian and *really* is Gaussian *(ref. Figure with events from* ϕ_1 α_1 =2.8, α_2 =3.3, E_k = 100)

α_1=2.80, α_2=3.21, E_k=128 TeV (25,000 mission averages)

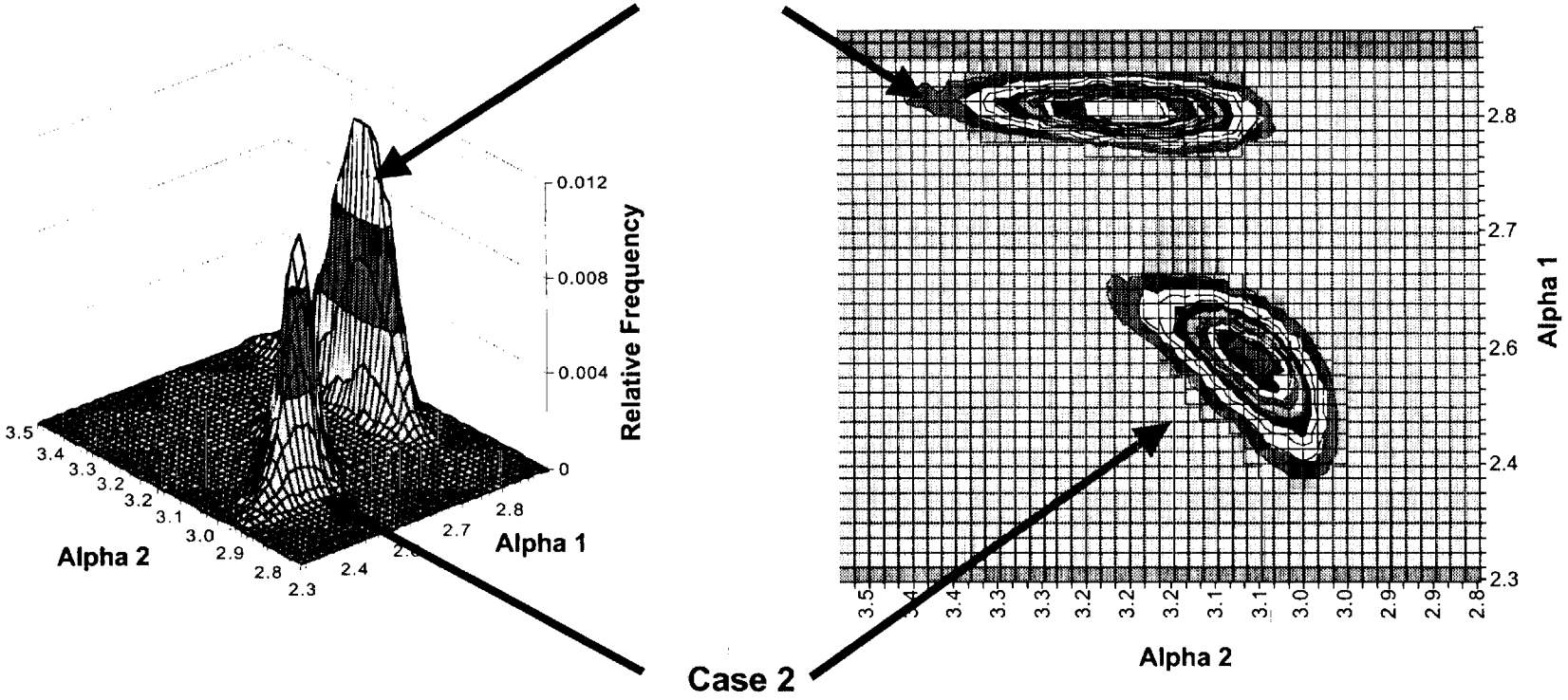

Case 2: Assumed Gaussian but really "Broken" Gaussian. α_1=2.53, α_2=3.1, E_k=66 TeV

NASA/MSFC

Uncertainties in Detector Response Models
Assumed Gaussian (40%) but Really "Broken" Gaussian – *Method 1*

ϕ_1 with α_1 =2.8, α_2 =3.3, E_k = 100 TeV, 20 < E_i <5,500 TeV

---

1. Analysis of Method 1– note that we simulated from 20 < E_i <5,500 TeV and kept all detector responses. If we lower the data analysis range to 5 TeV (634,083 events) then their responses to the Gaussian (40%) and Broken-Gaussian are:

Front end of histogram is an artifact of generating incident energies from the interval [5, 5500] and keeping all responses. A "real" spectrum doesn't have this front portion, but does look like from > 60 GeV .

This large mismatch of models in the front-end forces the estimate of α_1 to be far off, and then also E_k

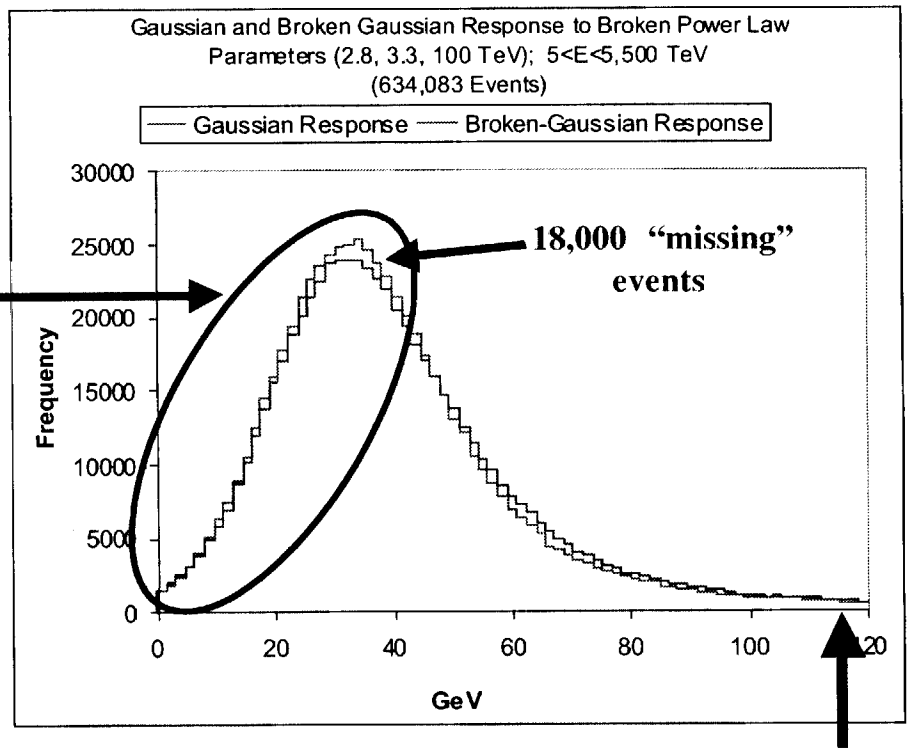

See next page for Log–Log Plot

Uncertainties in Detector Response Models: Log–Log Plot of Previous Chart

Assumed Gaussian (40%) but Really "Broken" Gaussian – *Method 2*

ϕ_1 with α_1, =2.8, α_2 =3.3, E_k = 100 TeV, 5 <E_i <5,500 TeV (634,083 events)

Method 2– Makes the response spectrum look more like a "real" spectrum by placing a cut Y_{cut} in the detector response data, dropping all simulated detector responses <Y_{cut}

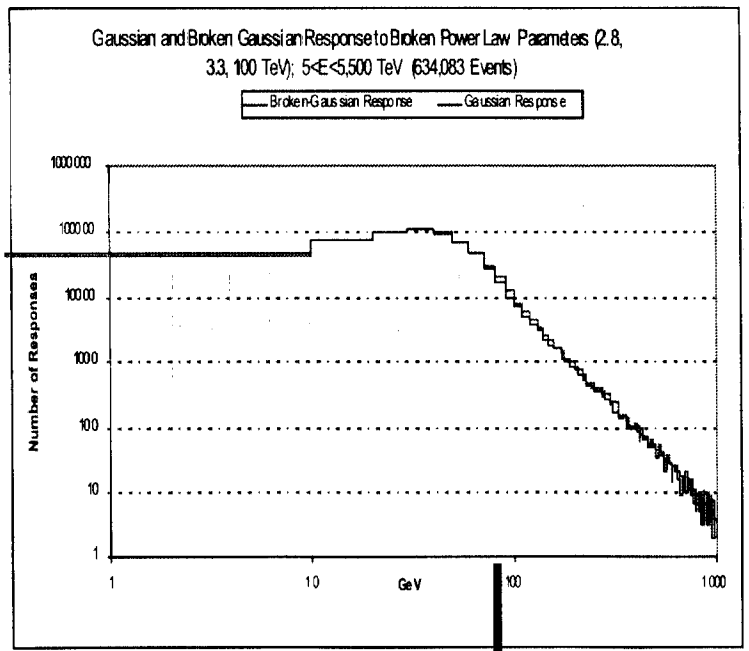

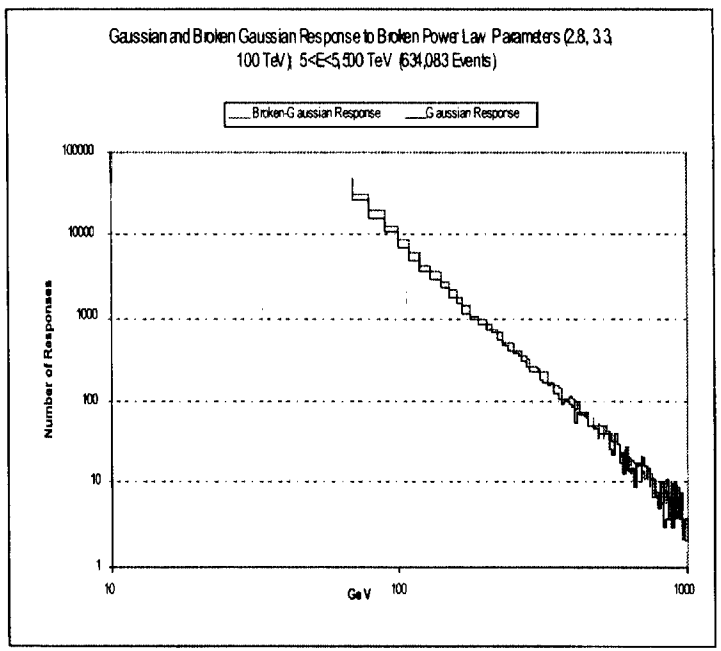

Cut at 60 GeV

NASA/MSFC

Uncertainties in Detector Response Models
Assumed Gaussian (40%) but Really "Broken" Gaussian – *Method 2*

ϕ_1 with α_1, =2.8, α_2 =3.3, E_k = 100 TeV, 5 < E_i <5,500 TeV (634,083 events)

Method 2– Makes the response spectrum look more like a "real" spectrum by placing a cut Y_{cut} in the detector response data, dropping all simulated detector responses < Y_{cut}

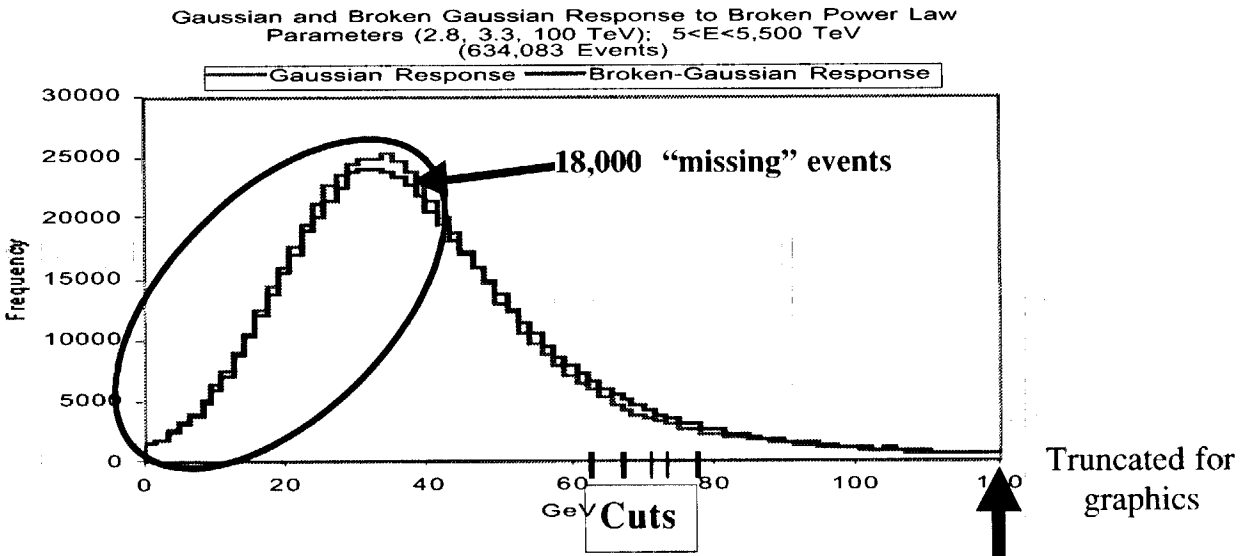

Results

Response Cutoff (keep $Y>Y_{cut}$)	Y_{cut}	N(events above Y_{cut}), Broken Gaussian	Pr{5 TeV event deposits>Ycut} Broken Gaussian	Pr{5 TeV event deposits>Ycut} Gaussian, 40% Resolution	Mean (1000 Missions) α_1	Mean (1000 Missions) α_2	Mean (1000 Missions) E_k	Std. Deviation α_1	Std. Deviation α_2	Std. Deviation E_k
μ(36 TeV)	110 GeV	23262	1.55E-09	6.09E-13	2.83	3.31	110	0.027	0.080	17.0
μ(30 TeV)	93 GeV	34450	8.69E-07	5.08E-09	2.84	3.32	112	0.018	0.079	16.7
μ(25 TeV)	80 GeV	49775	6.44E-05	2.30E-06	2.84	3.32	114	0.013	0.077	15.0
μ(20 TeV)	67 GeV	78900	2.01E-03	2.95E-04	2.85	3.32	116	0.009	0.078	14.6
μ(18 TeV)	62 GeV	98100	6.28E-03	1.45E-03	2.84	3.32	111	0.008	0.076	14.1
μ(15 TeV)	54 GeV	140650	2.71E-02	1.10E-02	2.79	3.24	83	0.033	0.079	14.2

Uncertainties in Detector Response Models

Assumed Gaussian (40%) but Really "Broken" Gaussian – *Method 2*

ϕ_1 with α_1 =2.8, α_2 =3.3, E_k = 100 TeV, 5 < E_i <5,500 TeV (634,083 events)

Method 2 – Make the response spectrum look more like a "real" spectrum by placing a cut in the detector response data. Simulate from 5 <E_i <5,500 TeV and ignore responses < y_{cut}

Results

Response Cutoff (keep Y>Y_{cut})	Y_{cut}	N(events above Y_{cut}), Broken Gaussian	Pr{5 TeV event deposits>Ycut} Broken Gaussian	Pr{5 TeV event deposits>Ycut} Gaussian, 40% Resolution	Mean (1000 Missions) α_1	Mean (1000 Missions) α_2	Mean (1000 Missions) E_k	Std. Deviation α_1	Std. Deviation α_2	Std. Deviation E_k
μ(36 TeV)	110 GeV	23262	1.55E-09	6.09E-13	2.83	3.31	110	0.027	0.080	17.0
μ(30 TeV)	93 GeV	34450	8.69E-07	5.08E-09	2.84	3.32	112	0.018	0.079	16.7
μ(25 TeV)	80 GeV	49775	6.44E-05	2.30E-06	2.84	3.32	114	0.013	0.077	15.0
μ(20 TeV)	67 GeV	78900	2.01E-03	2.95E-04	2.85	3.32	116	0.009	0.078	14.6
μ(18 TeV)	62 GeV	98100	6.28E-03	1.45E-03	2.84	3.32	111	0.008	0.076	14.1
μ(15 TeV)	54 GeV	140650	2.71E-02	1.10E-02	2.79	3.24	83	0.033	0.079	14.2

Must Modify the Objective Function *(to handle conditional probabilities)*

$$O(\alpha_1,\alpha_2,E_k) = -\log L = -\sum_{j=1}^{N} \log[g(y_j \mid y_j > y_c)]$$

$$g(y_j \mid y_j > y_c) = \frac{\int_{E_L}^{E_H} g(y_j \mid E;\rho)\,\phi_1(E;\alpha_1,\alpha_2,E_k)\,dE}{P(Y > y_c) = 1 - \int_0^{y_c} g(y;\alpha_1,\alpha_2,E_k)\,dy} \qquad y_j > y_c$$

Bonus 1: Does not require unique values for E_L and E_H (incident Energy Range). Pick E_L such that Pr{ Y(E_L)> y_{cut} }<ε (negligible number of events below E_L contribute to Y> Y_{cut}

This makes it applicable to "real" data sets

Bonus 2: Extends to multiple data sets/detectors with likelihood functions L_k, so that $O(\alpha_1,\alpha_2,E_k)$= - log L_k since **L** = ⊆L_k

NASA/MSFC

Glossary of Terms and Abbreviations

Notes: Some of the parameters in the figures may require further definition so they are defined here.

ML = Maximum Likelihood (the parameter estimation method used)

The symbol (Y|E) as in $\sigma(Y|E)$ or $\sigma_{Y|E}$ means the standard deviation of detector response (energy deposit) Y at the energy value E. Similarly, $\mu(Y|E)$ or $\mu_{Y|E}$ is the mean detector response (ED) at the energy value E.

ϕ_1 = A broken power law spectral form with the parameters α_1, α_2 and E_k and ϕ_0 is the simple power law with spectral parameter α_1

$N_{average}$ = the average number of cosmic rays measured in each mission, taken to be the mean of a Poisson distribution

μ_E is the mean energy of all the events in the broken power law spectrum between the upper and lower energy bounds (typically 20 to 5,500 TeV).

σ_E is the rms deviation of individual cosmic ray events in the spectrum from μ_E. Note that while $\sigma_E = \rho_E \mu_E$, it is important to not confuse ρ_E with ρ which is the fractional energy resolution with which the deposited energy is measured.

KLEM is a Russian concept for an energy-measuring device that uses the number and angular distribution of all secondaries from the first interaction of the cosmic ray to estimate energy. It gives somewhat poorer energy resolution but is very light weight so can be much bigger than a calorimeter.

A.1 Supplemental Charts

Broken Power Law Probability Density Function

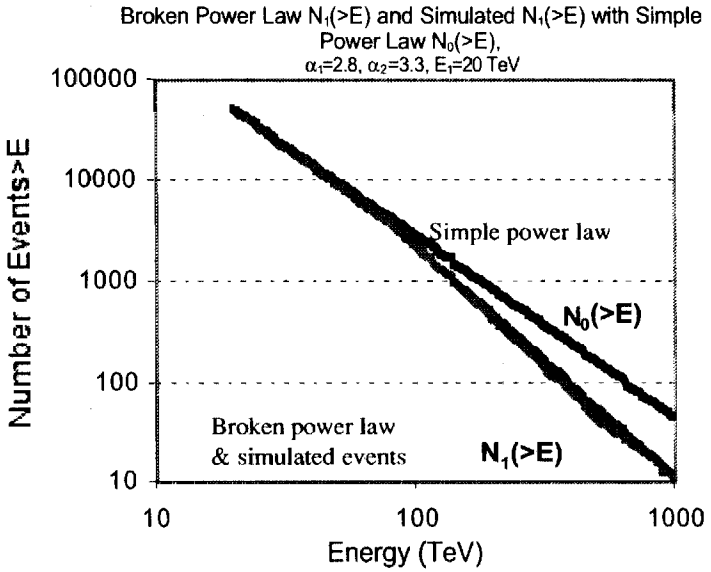

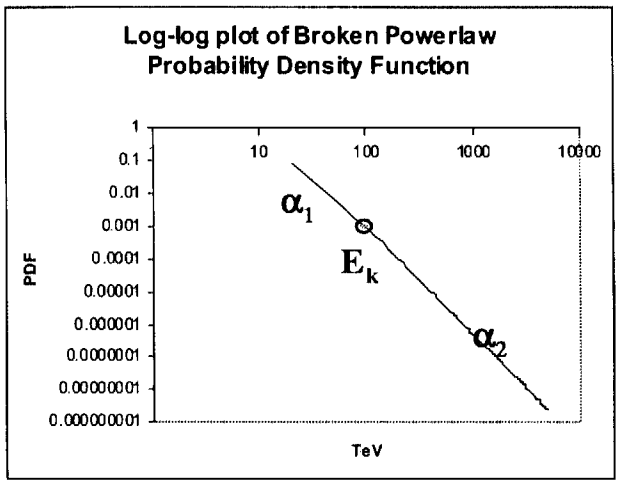

$$\phi_1(E;\alpha_1,\alpha_2,E_k)=\begin{cases} A\left(\frac{E}{E_k}\right)^{-\alpha_1} & for \quad E_1 \le E < E_k \\ A\left(\frac{E}{E_k}\right)^{-\alpha_2} & for \quad E_k \le E \le E_2 \end{cases} \qquad (XX)$$

$$A = A(\alpha_1,\alpha_2,E_k) = \frac{(\alpha_1-1)(\alpha_2-1)}{E_k\left[\alpha_1-\alpha_2+(\alpha_2-1)\left(\frac{E_1}{E_k}\right)^{1-\alpha_1}-(\alpha_1-1)\left(\frac{E_2}{E_k}\right)^{1-\alpha_2}\right]}$$

$$\left\langle E^m \right\rangle = \int_{E_1}^{E_2} E^m \phi_1(E)\,dE$$

$$= A\,E_k^{m+1}\left\{\frac{1}{m+1-\alpha_1}\left[1-\left(\frac{E_1}{E_k}\right)^{m+1-\alpha_1}\right]-\frac{1}{m+1-\alpha_2}\left[1-\left(\frac{E_2}{E_k}\right)^{m+1-\alpha_2}\right]\right\} \qquad (XX)$$

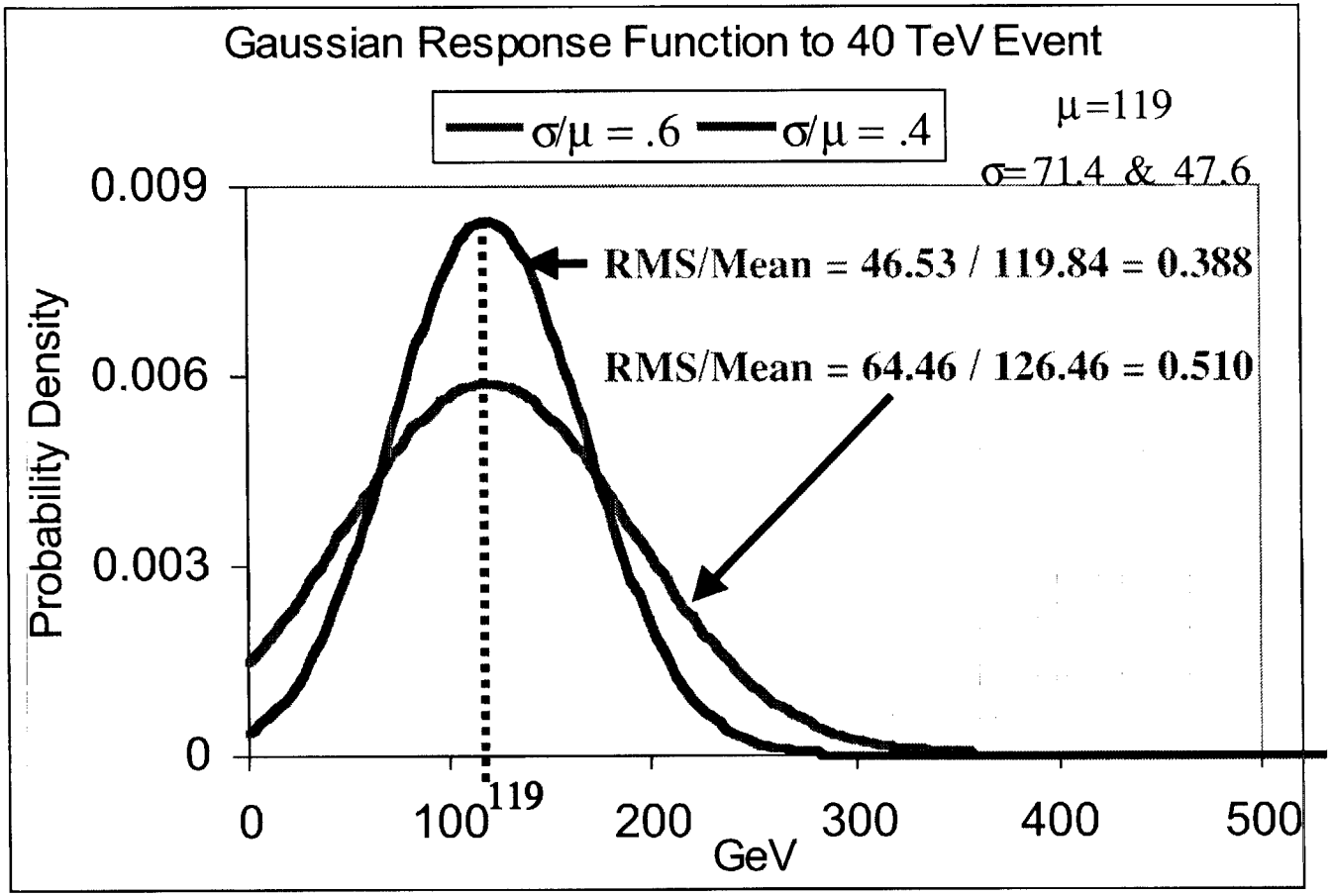

	Constant Resolution ρ					
	10%	20%	30%	**40%**	50%	**60%**
Truncated Probability	0	2.9E-07	0.00043	**0.00621**	0.02275	**0.04779**
η	1	1	1.00043	**1.00625**	1.02328	**1.05019**

Application to "Real" Data: use conditional distribution g(y|y>y_c)

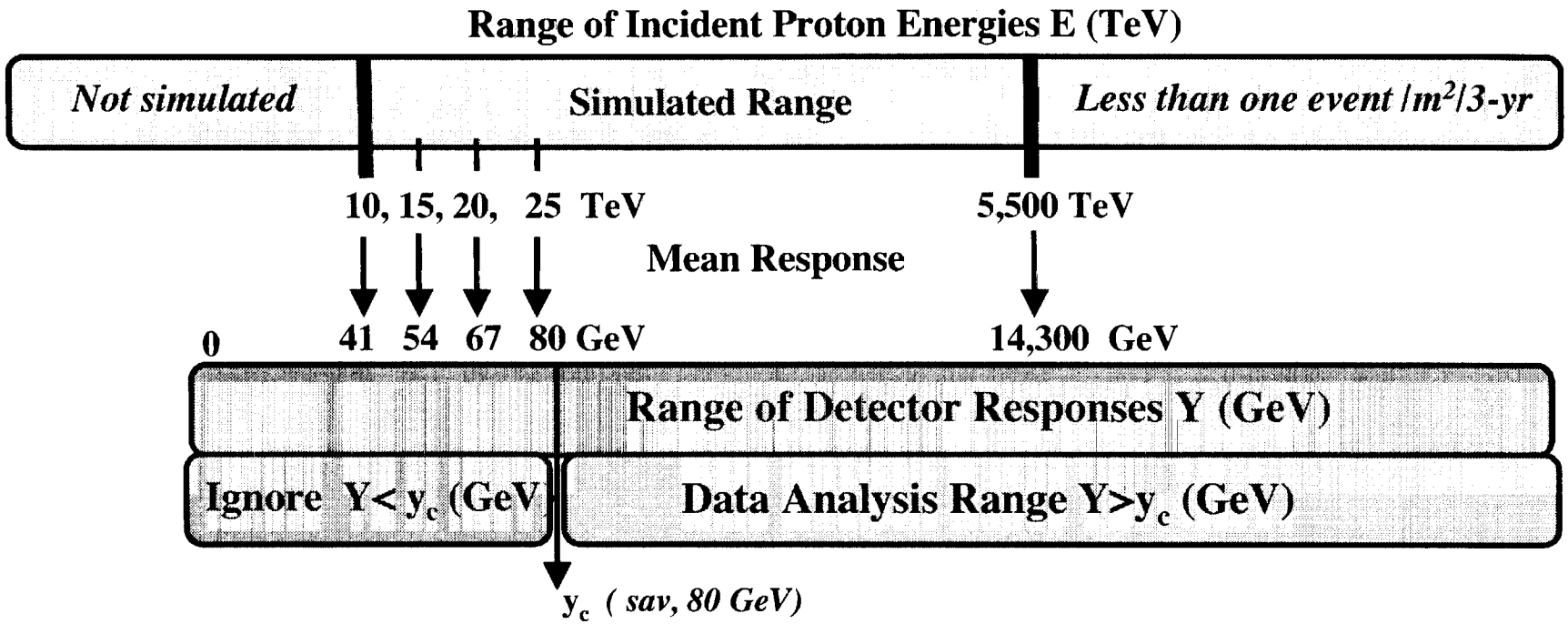

1. **Method 2** – Requires Modification to the Objective Function (conditional probabilities).

$$O(\alpha_1,\alpha_2,E_k) = -\log L = -\sum_{j=1}^{N} \log[g(y_j \mid y_j > y_c)]$$

$$g(y_j \mid y_j > y_c) = \frac{\int_{E_L}^{E_H} g(y_j \mid E;\rho)\,\phi_1(E;\alpha_1,\alpha_2,E_k)\,dE}{P(Y > y_c) = 1 - \int_0^{y_c} g(y\ ;\alpha_1,\alpha_2,E_k)\,dy}, \quad y_j > y_c$$

Bonus 1: Does not require unique values for E_L and E_H (incident Energy Range). Pick E_L such that $\Pr\{Y(E_L) > y_{cut}\} < \varepsilon$ (negligible number of events below E_L contribute to $Y > Y_{cut}$

This makes it applicable to "real" data sets

Bonus 2: Extends to multiple independent data sets/detectors with likelihood functions L_k, k= 1, 2, n.

$$O(\alpha_1,\alpha_2,E_k) = -\sum_{i=1}^{n} \log L_k \text{ since } L = \prod_{i=1}^{n} L_k$$

Estimating Spectral Parameters from Simulated Detector Responses

Simulate Incident Events

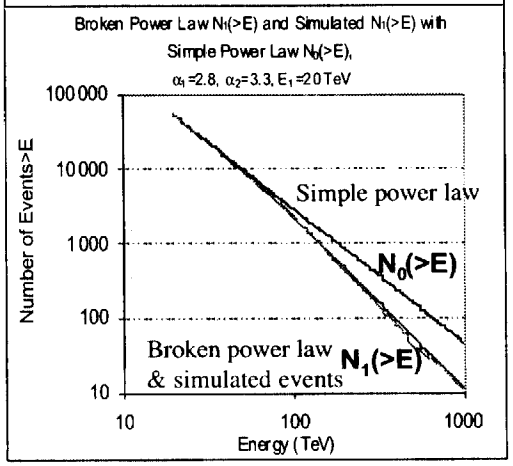

Gaussian Detector Response Surface

Simulate Detector Response GEANT

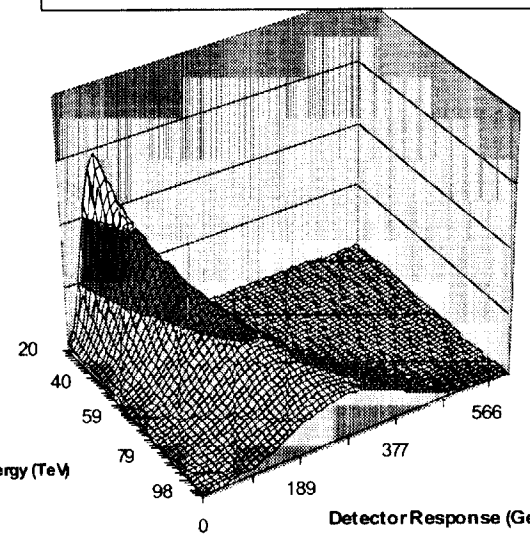

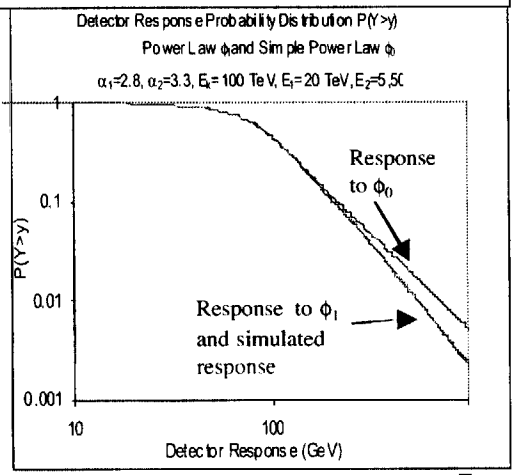

- Broken Power Law ϕ_1 *assumed*
  α_1, α_2, E_k (knee location)
- *Simple Power Law* ϕ_0
- *N (number of events) Poisson*
  Baseline collecting power - 1 m², 3 yr

Normally incident protons , linear mean response $\mu_{y|E} = a + bE$

- Gaussian uncertainty $g(y|E;\rho)$, function of resolution ρ
- *also gamma and "broken" Gaussian response functions*

Multiple missions

$(\alpha_1, \alpha_2, E_k)_{ML}$

Estimate the Spectral Parameters from Detector Responses $_i$Y

- Maximum Likelihood estimates* $(\alpha_1, \alpha_2, E_k)_{ML}$

- **Study the statistical behavior of $(\alpha_1, \alpha_2, E_k)_{ML}$ over these many missions**
- **Vary calorimeter size, resolution, response function, and spectral parameters, etc.**

* asymptotically minimum variance, consistent (unbiased for large samples), and normal. Kendall & Stuart Advanced Theory of Statistics

Calorimeter Size and Resolution Study: $20 < E_i < 5{,}500$ TeV

Events from ϕ_1 with $\alpha_{1,} = 2.8$, $\alpha_2 = 3.3$, $E_k = 200$ TeV, 1000 Missions

1. Baseline: ~ $1m^2$, 3 yr (top curve)
   $N_{average} = 52{,}025$ (~$650 > E_k$)

3. Double-size (bottom curve)
   $N_{average} = 104{,}050$ (~$1{,}300 > E_k$)

α_2

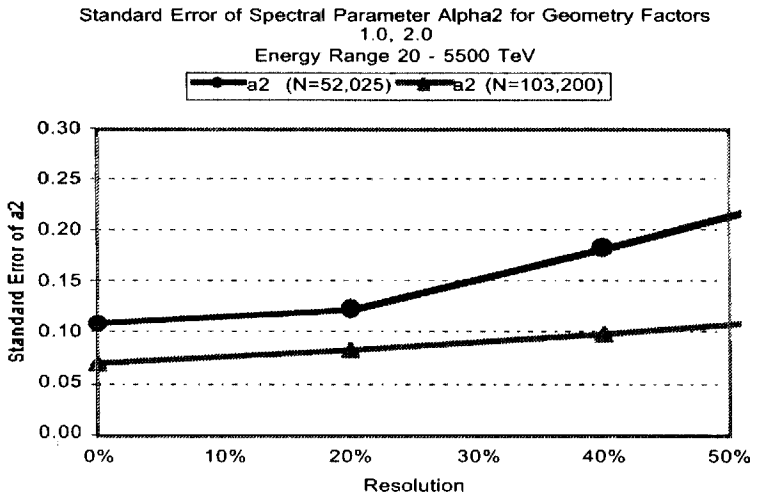

E_k

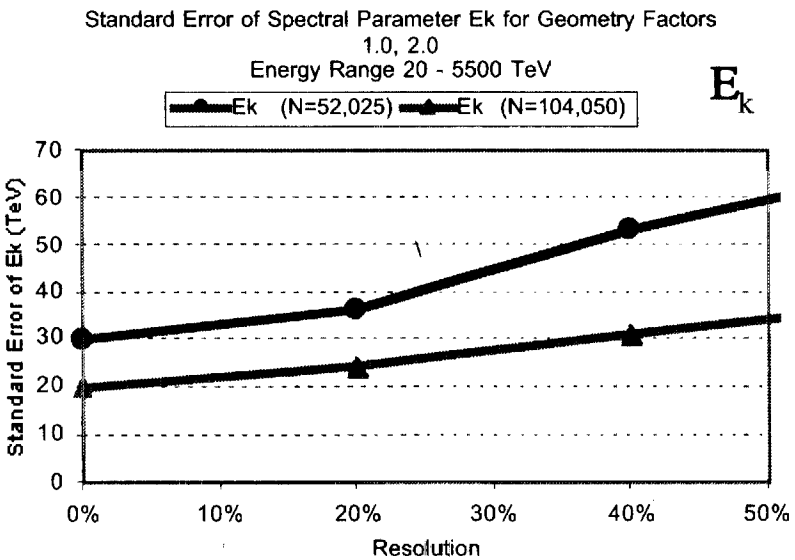

α_1

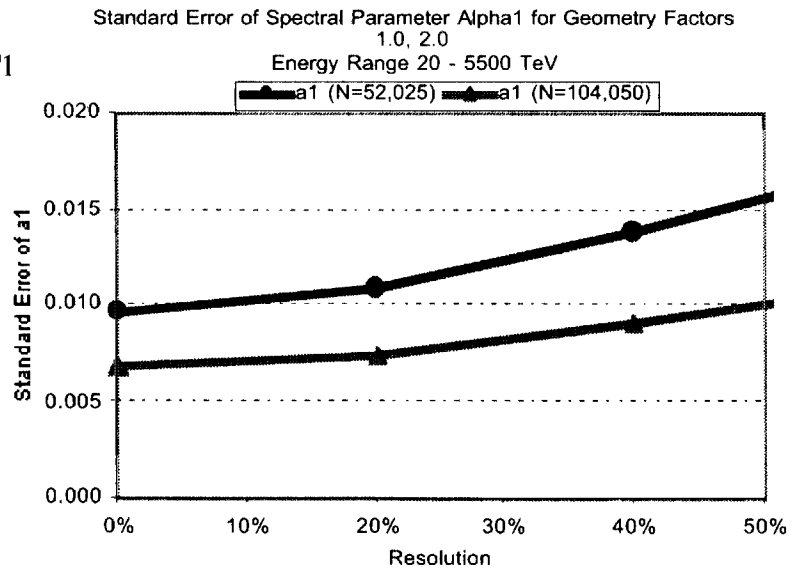

Detector Response Function Study: Gaussian, Gamma, "Broken"Gaussian

ϕ_1 with α_1 =2.8, α_2 =3.3, E_k = 200 TeV, 20 < E_i <5,500 TeV, 1000 Missions

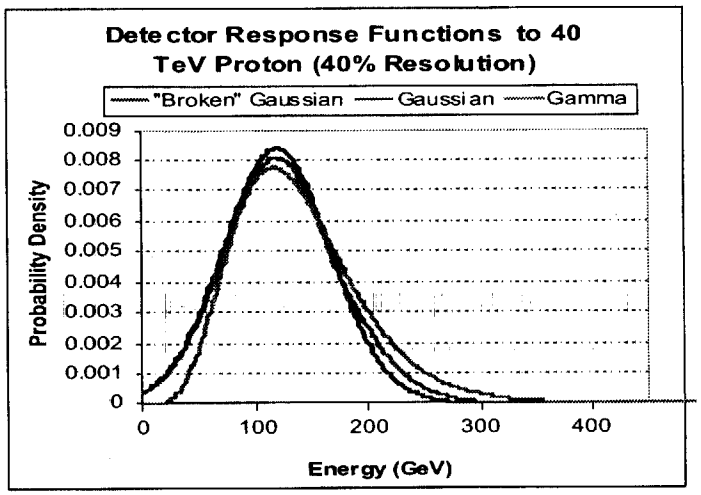

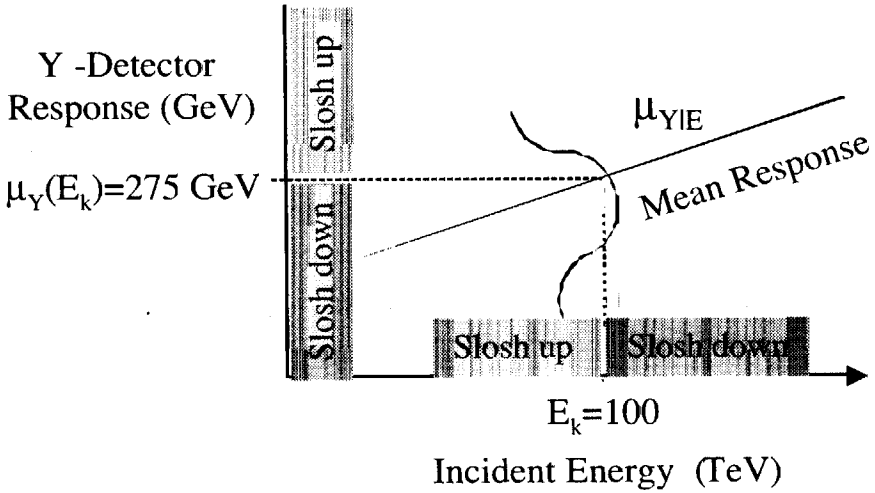

Sloshing of Events around the Kink E_k
(There are 2,250 events on average above 100 TeV)

E_k=100 TeV, α_1=2.8, α_2=3.3	Resolution			
Sloshing of Events around the Knee E_k	**0%**	**20%**	**40%**	**60%**
Gaussian: Average Number of Events sloshing Up	0	492	1104	1914
"Broken" Gaussian: Average Number of Events sloshing Up	0	597	1361	2391
Gaussian: Average Number of Events sloshing Down	0	362	582	655
"Broken" Gaussian: Average Number of Events sloshing Down	0	347	558	627

Simple Power Law: ML Estimation of α_1 -- 40% Resolution

Events from ϕ_0 with α_1, =2.8, 20 <E_i < 5,500 TeV, $N_{Average}$ = 52,200

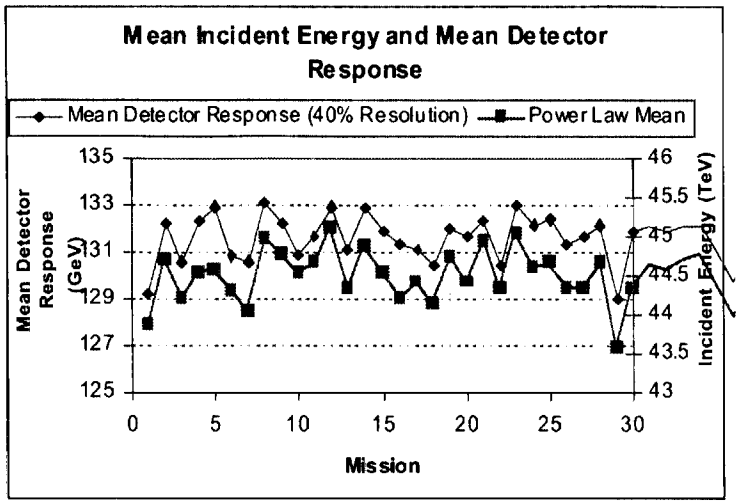

Mean detector response & mean incident energy

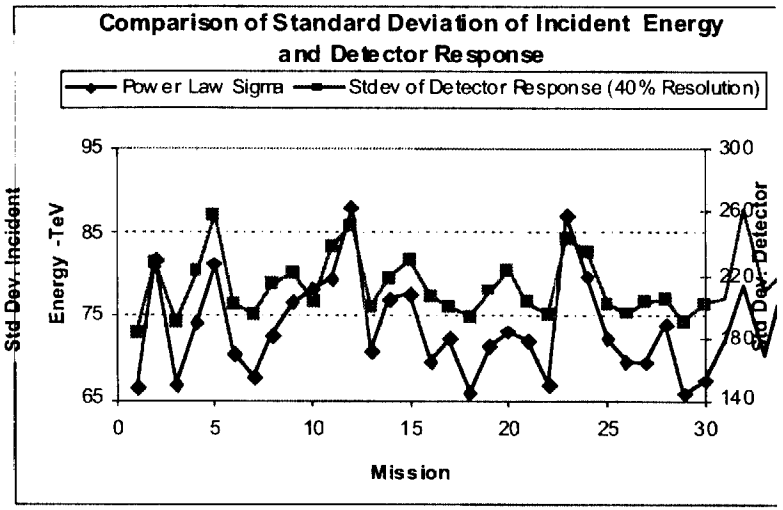

Standard Deviation of Incident Energy (σ_E) and of Detector Response (σ_Y)

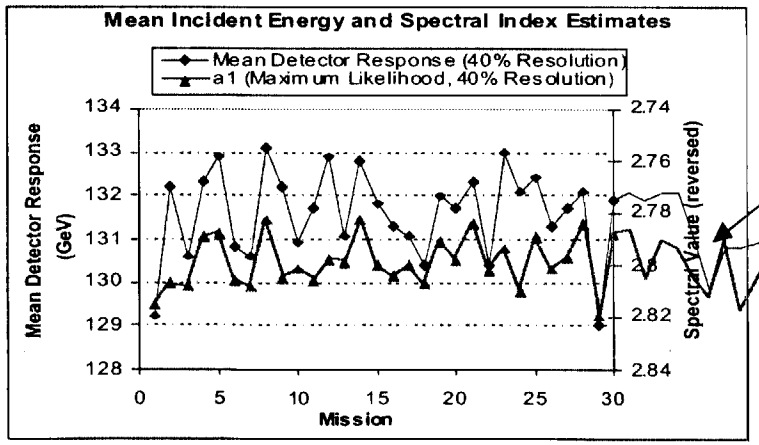

Note Reverse axis

ML estimate of α_1 (ρ=0.40) and Mean Incident Energy

Simple Power Law: ML Estimation of α_1 -- 40% Resolution

Events from ϕ_0 with α_1 =2.8, 20 <E_i < 5,500 TeV, $N_{Average}$ = 52,200

Maximum Likelihood estimate of α_1 ρ=0 and ρ=0.40

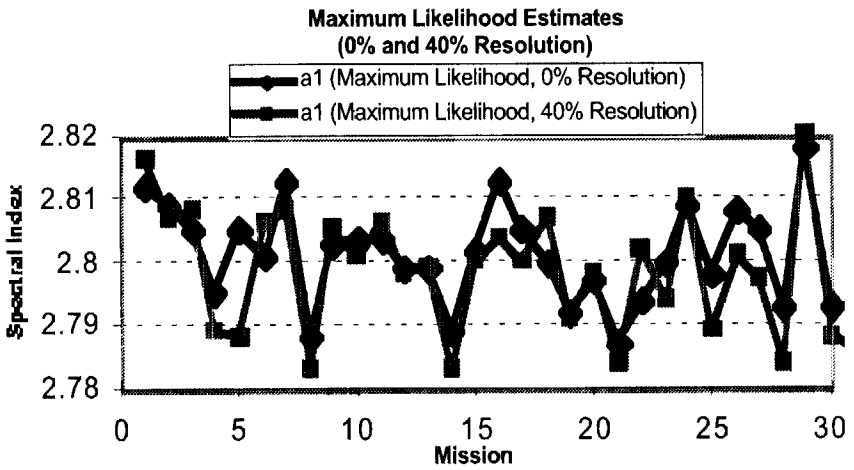

Size versus Resolution

5000 Missions

Resolution has less impact on standard error than for Broken Power Law, since σ_E is significantly larger. For this energy range, we have

σ_E = 74 TeV, α_1=2.8

σ_E = 54 TeV, α_1 =2.8, α_2 =3.1, E_k=100 TeV

σ_E = 46 TeV, α_1 =2.8, α_2 =3.3, E_k=100 TeV

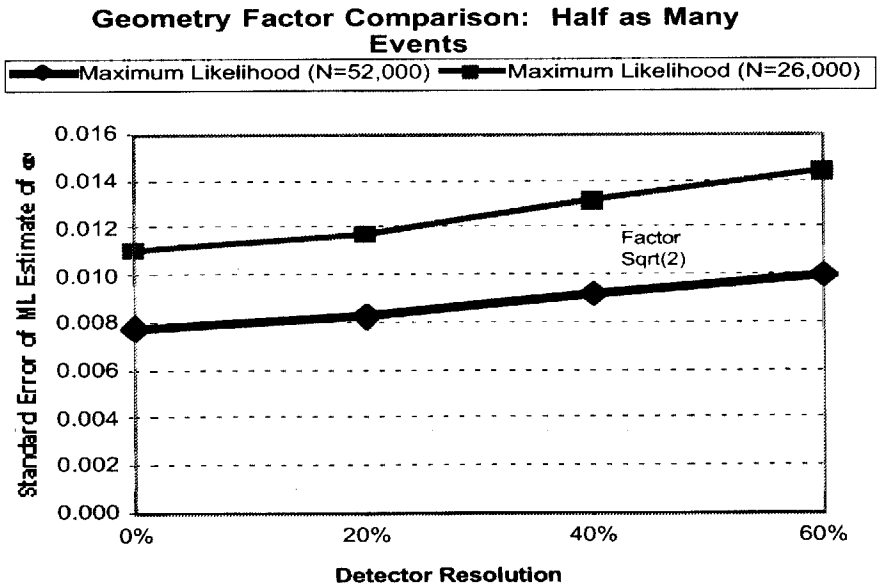

Checking the Maximum Likelihood Estimates $(\alpha_1, \alpha_2, E_k)_{ML}$

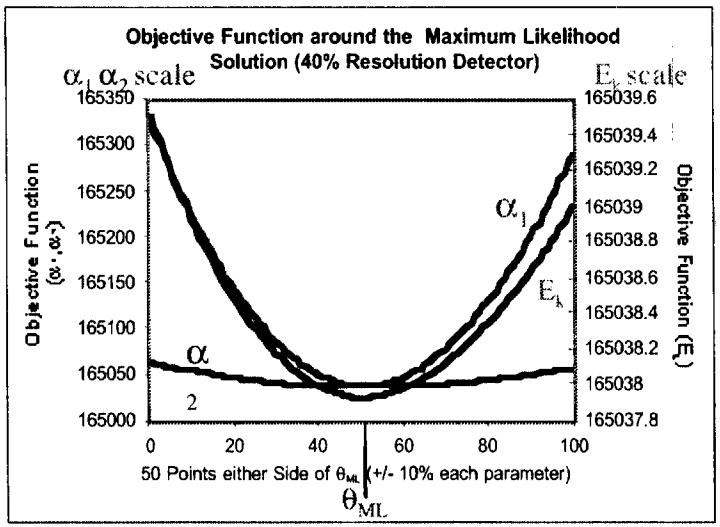

Objective function evaluated along orthogonal lines through $(\alpha_1, \alpha_2, E_k)_{ML}$

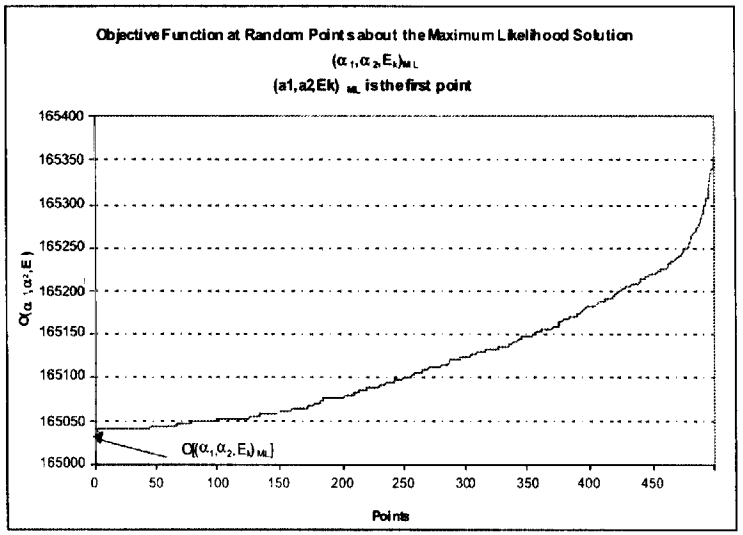

Objective function evaluated at random points in the vicinity of $(\alpha_1, \alpha_2, E_k)_{ML}$, then put in ascending order.

Objective Function in the Neighborhood of$(\alpha_1, \alpha_2, E_k)_{ML}$ (with α_1, fixed)

Events were simulated from ϕ_1 with α_1, =2.8, α_2 =3.3, E_k = 100 TeV, Resolution 0%

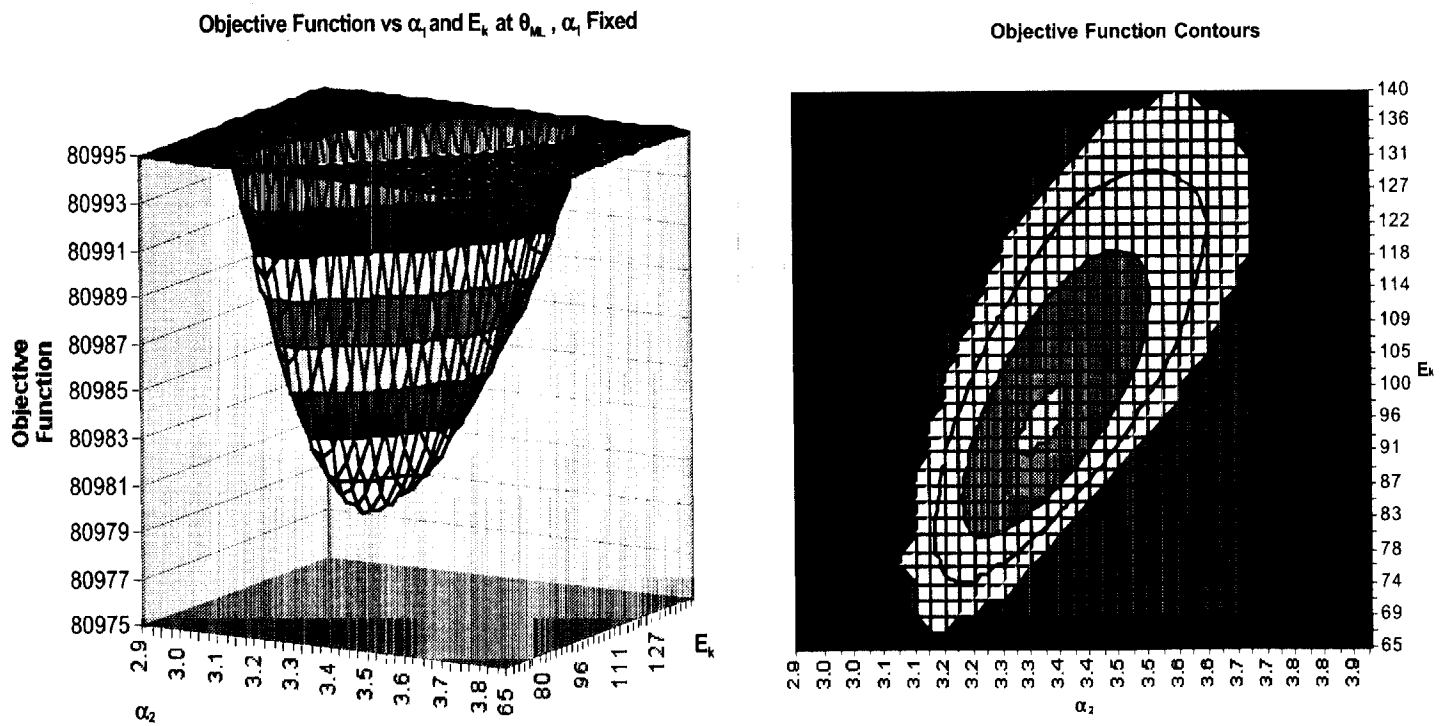

Objective Function in the Neighborhood of $(\alpha_1, \alpha_2, E_k)_{ML}$ (with α_1 fixed)

Events from ϕ_1 with $\alpha_1 = 2.8, \alpha_2 = 3.3, E_k = \mathbf{100\ TeV}$ over the range

$20\ TeV < E_i < 5{,}500\ TeV$, for which $N_{Average}$ 51,600 (2,250 > 100TeV) – *baseline detector*

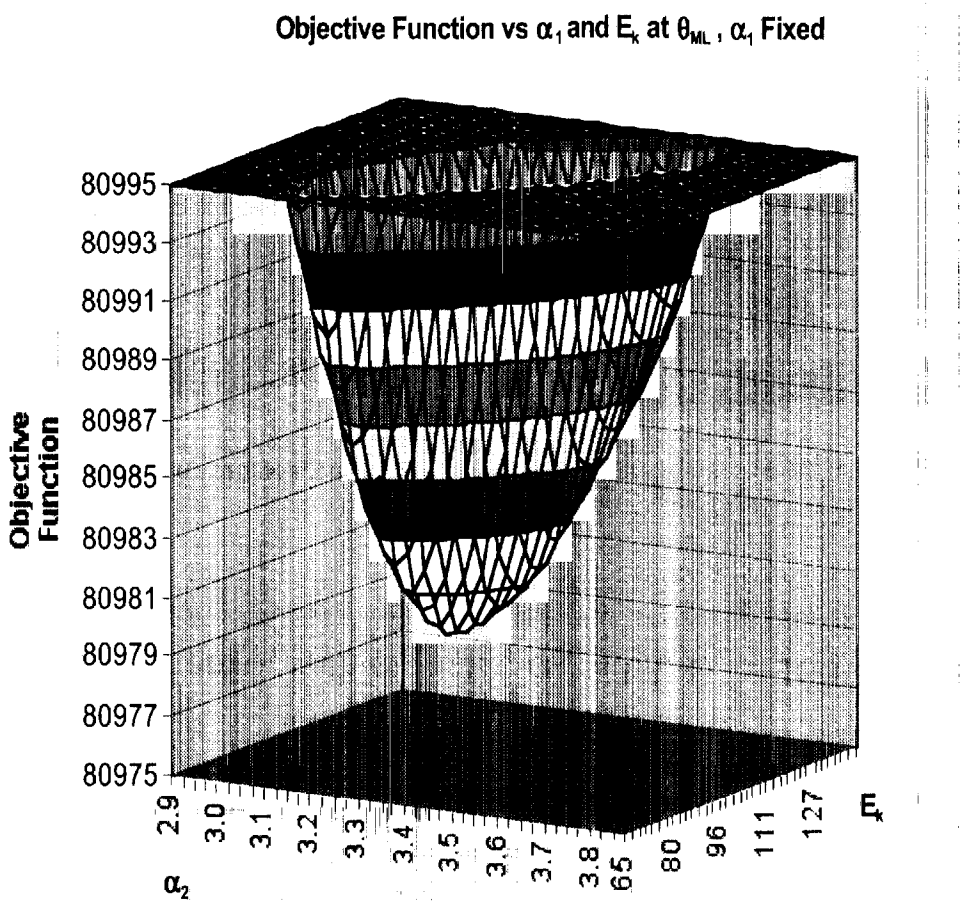

Objective Function in the Neighborhood of $(\alpha_1, \alpha_2, E_k)_{ML}$ (with α_1 fixed)

Events from ϕ_1 with $\alpha_1 = 2.8, \alpha_2 = 3.3, E_k = 200$ TeV over the range

$20 \text{ TeV} < E_i < 5{,}500 \text{ TeV}$, for which $N_{Average}$ 52,000 (650 > 200 TeV) – *baseline detector*

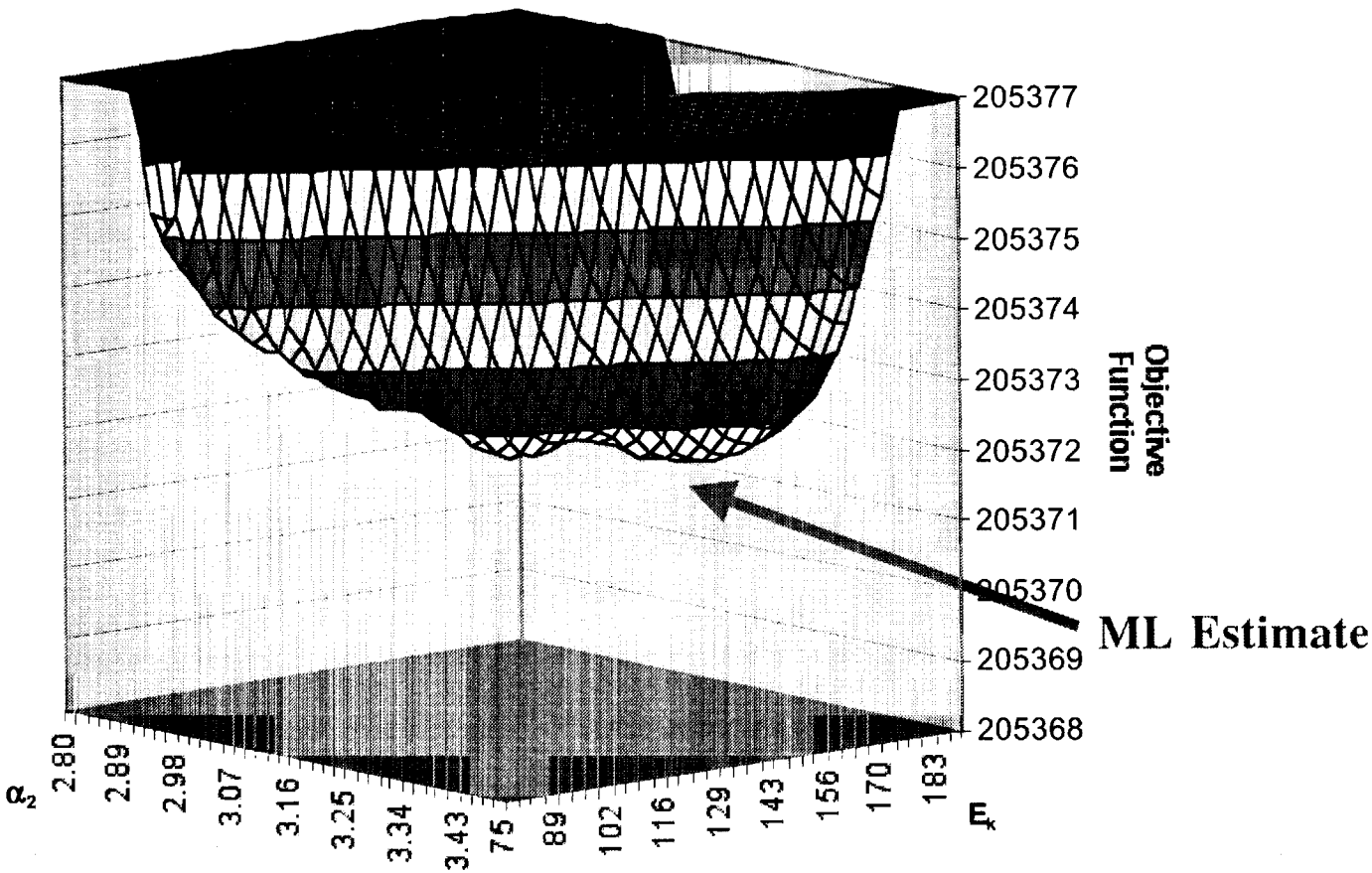

Objective Function in the Neighborhood of$(\alpha_1, \alpha_2, E_k)_{ML}$, (with α_1 fixed)

Events from ϕ_1 with $\alpha_1 = 2.8, \alpha_2 = 3.3, E_k = 200$ TeV over the range

$20 \text{ TeV} < E_i < 5{,}500$ TeV, for which $N_{Average}$ 52,000 (650 > 200 TeV) – *baseline detector*

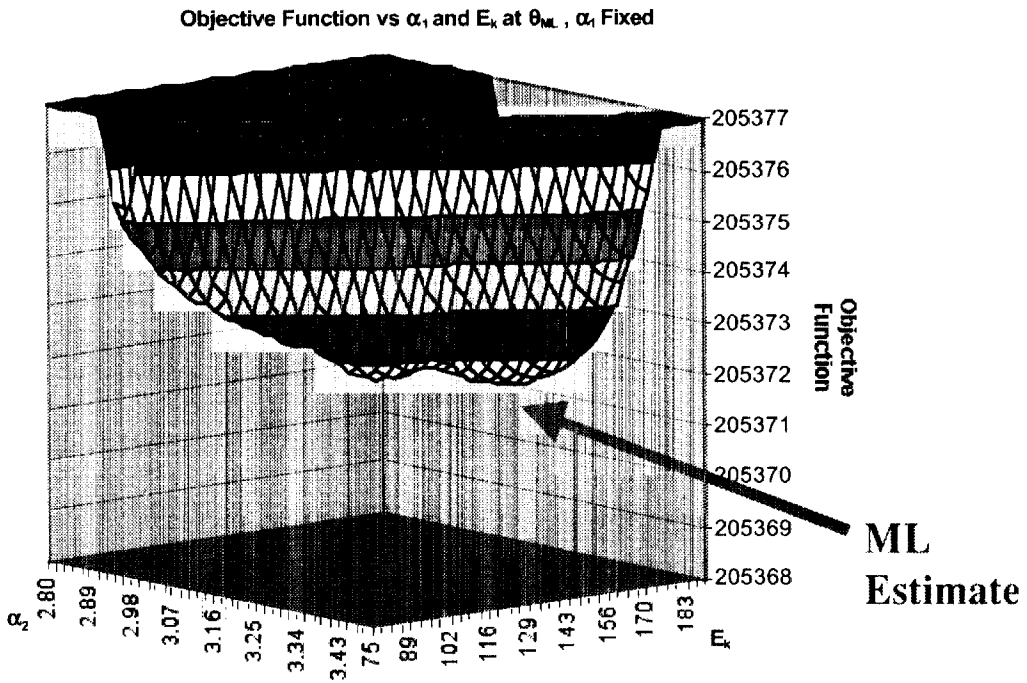

$$O(\theta) = -L(\theta) = -N \log A(\theta) + \alpha_1 \left(\sum_{E_i < E_k} \log\left[\frac{E_i}{E_k}\right] \right) + \alpha_2 \left(\sum_{E_j \geq E_k} \log\left[\frac{E_j}{E_k}\right] \right), \; E_1 \leq E_{i,j} \leq E_2, \qquad (XX)$$

$$O(\theta) = -N \log A(\theta) - \alpha_1 N_1 \log E_k - \alpha_2 N_2 \log E_k + \alpha_1 \left(\sum_{E_i < E_k} \log E_i \right) + \alpha_2 \left(\sum_{E_j \geq E_k} \log E_j \right)$$

$$A = A(\alpha_1, \alpha_2, E_k) = \frac{(\alpha_1 - 1)(\alpha_2 - 1)}{E_k \left| \alpha_1 - \alpha_2 + (\alpha_2 - 1)\left(\frac{E_1}{E_k}\right)^{1-\alpha_1} - (\alpha_1 - 1)\left(\frac{E_2}{E_k}\right)^{1-\alpha_2} \right|}$$

Objective Function in the Neighborhood of $(\alpha_1, \alpha_2, E_k)_{ML}$ (with α_1 fixed)

Events from ϕ_1 with $\alpha_1 = 2.8, \alpha_2 = 3.3, E_k = 300$ TeV over the range $20 \text{ TeV} < E_i < 5{,}500 \text{ TeV}$, for which $N_{Average}$ 52,100 (300 > 300 TeV) – *baseline detector*

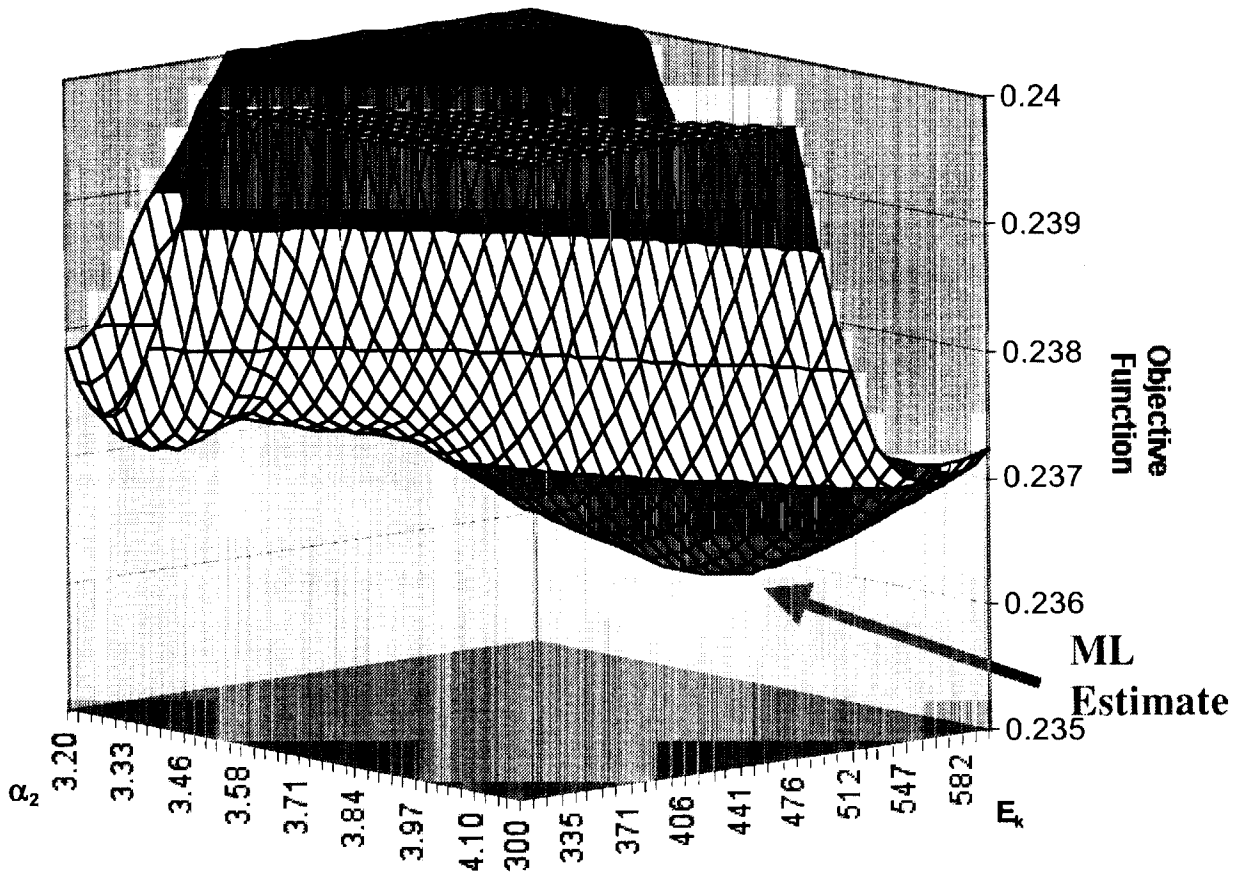

Objective Function in the Neighborhood of $(\alpha_1, \alpha_2, E_k)_{ML}$ (with α_1 fixed)

Events from ϕ_1 with $\alpha_1 = 2.8, \alpha_2 = 3.3, E_k = 300$ **TeV** over the range $20\ \text{TeV} < E_i < 5{,}500\ \text{TeV}$, for which N_{Average} 52,100 (300 > 300 TeV) – *baseline detector*

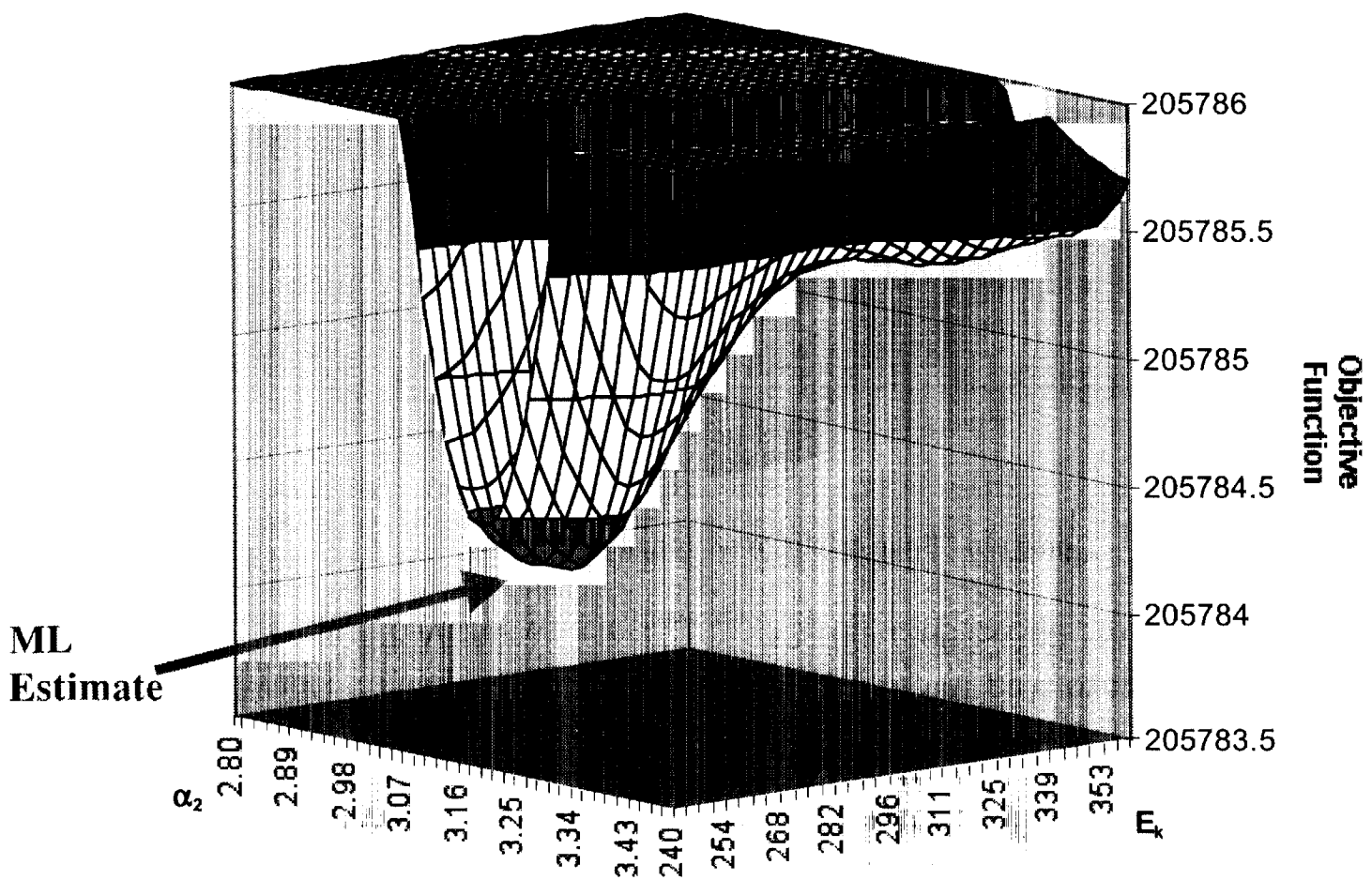

Objective Function in the Neighborhood of$(\alpha_1, \alpha_2, E_k)_{ML}$ (with α_1, fixed)

Events from ϕ_1 with α_1, =2.8,α_2 =3.3,E_k = **300 TeV** over the range 20 TeV < E_i < 5,500 TeV, for which $N_{Average}$ 52,100 (300 > 300 TeV) – *baseline detector*

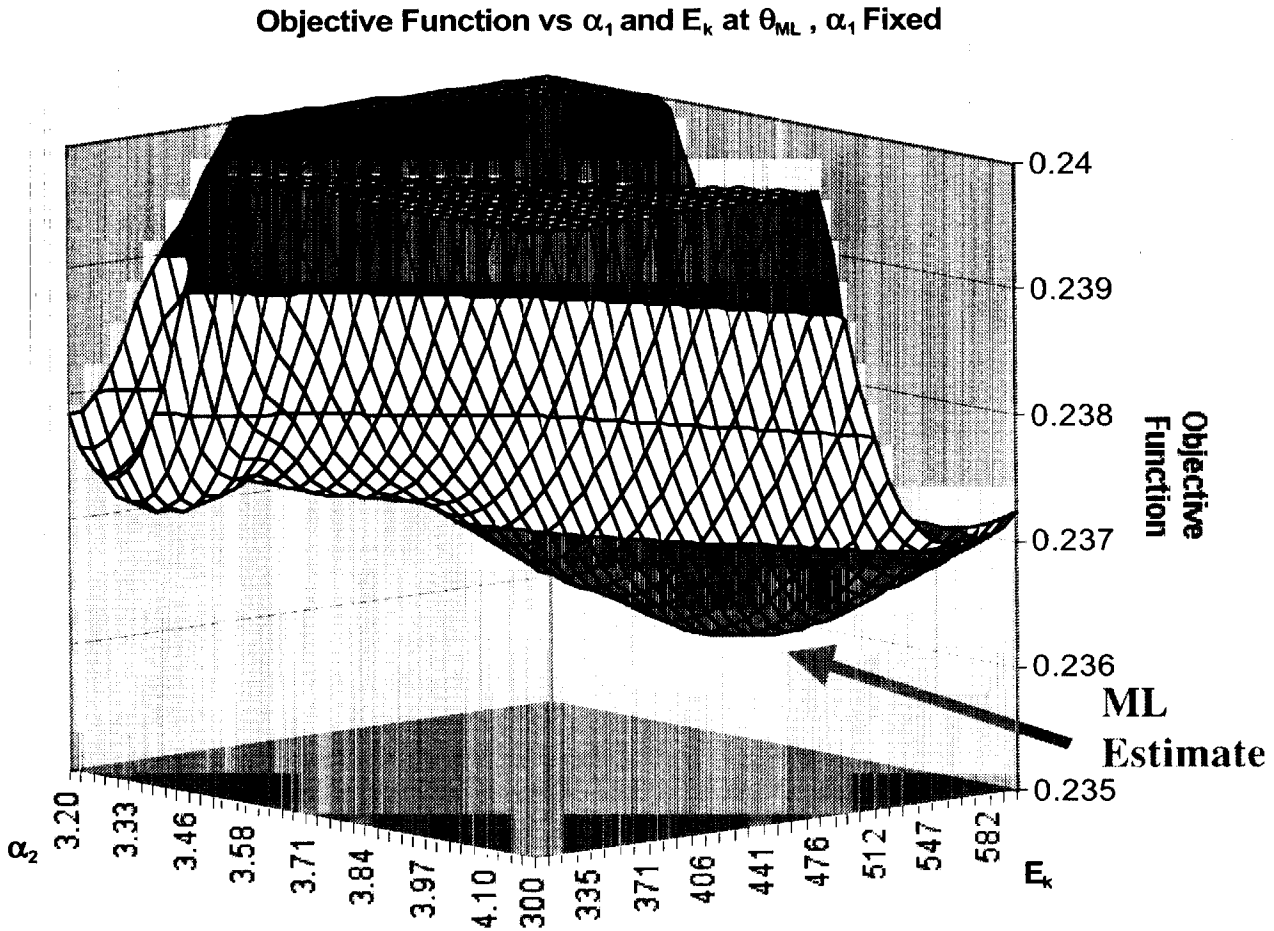

Detector Response Surface: Gaussian

Energy Range 20 – 100 TeV, 40%-resolution

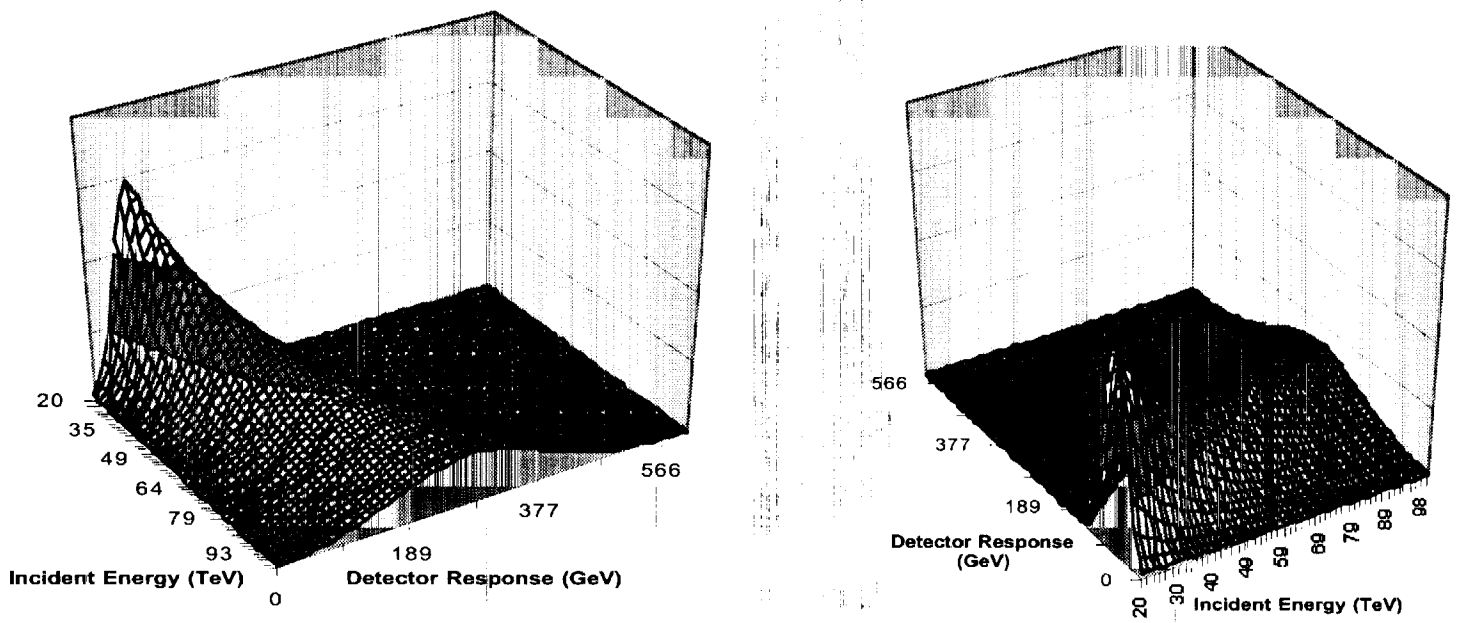

Detector Response Surface: Gamma

Energy Range 20 – 100 TeV, 40%-resolution

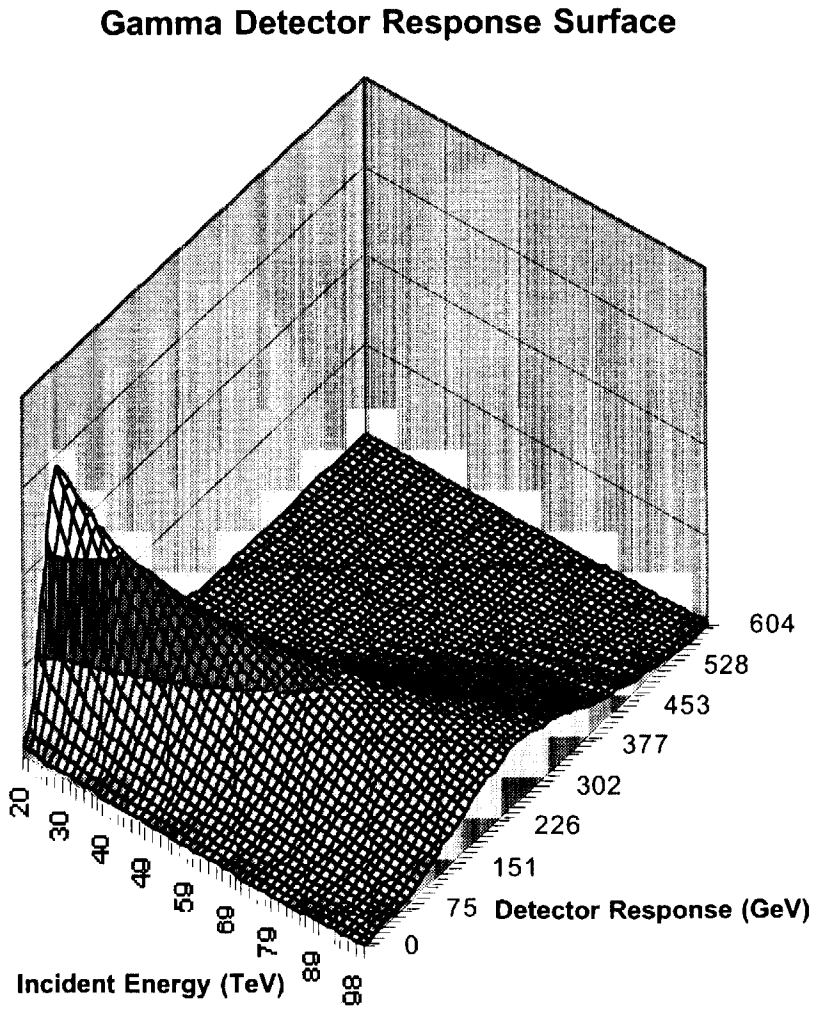

Detector Response Surface: BrokenGaussian

Energy Range 20 – 100 TeV, 40%-resolution

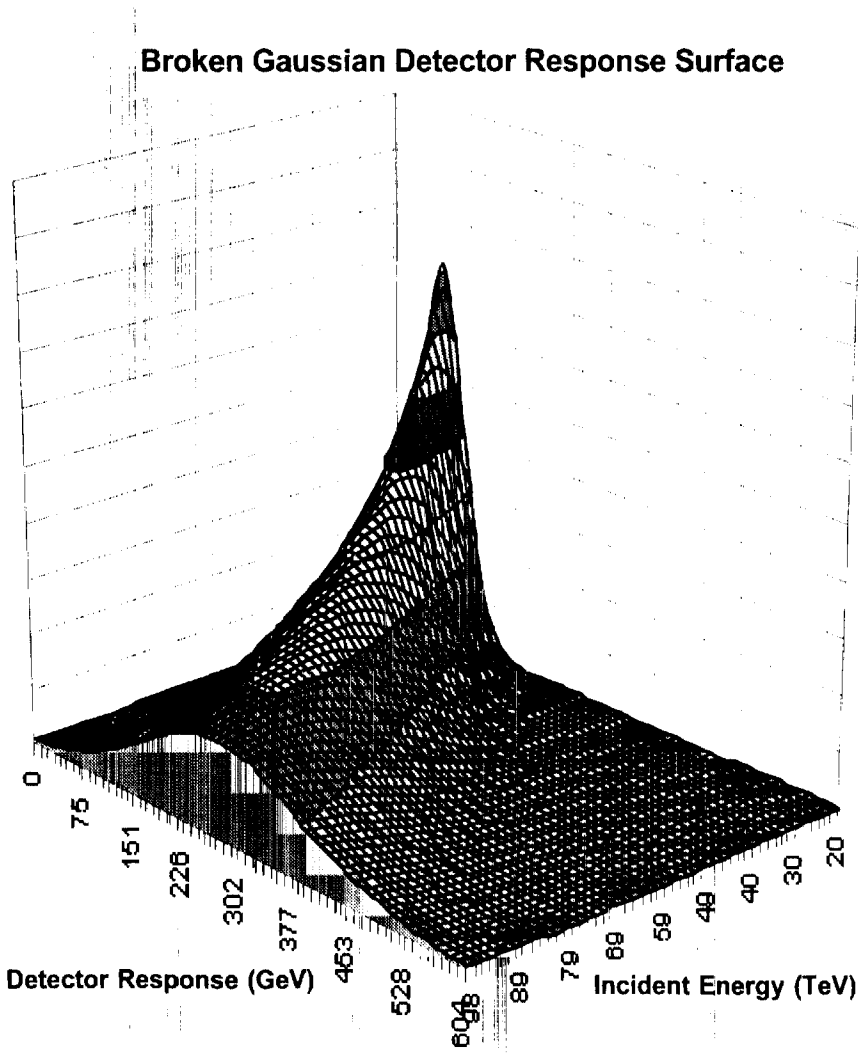

Histograms of the Three Spectral Indices α_1, α_2 , E_k for1000 Missions

Events were simulated from ϕ_1 with α_1 =2.8, α_2 =3.1, E_k = 100 TeV

Resolution 0%

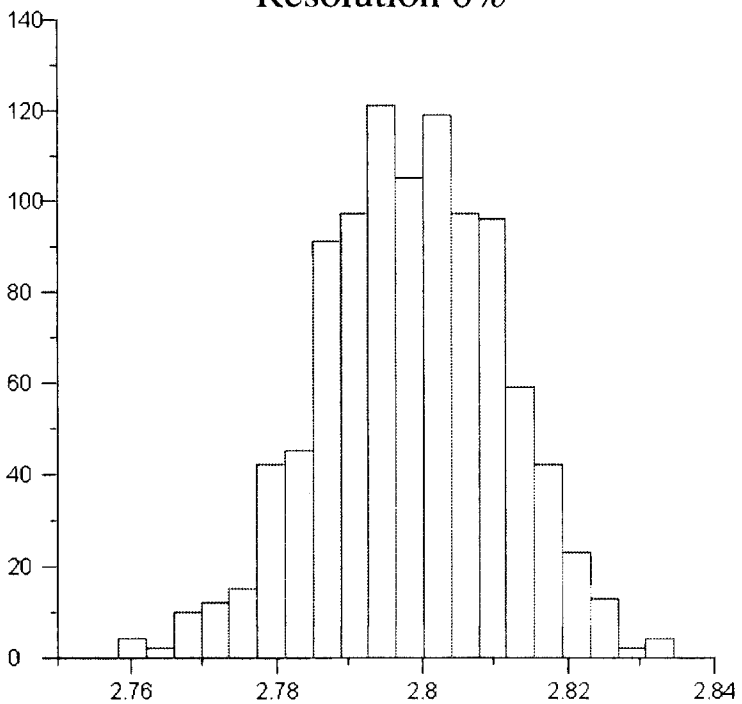

Alpha 1

Resolution 20%

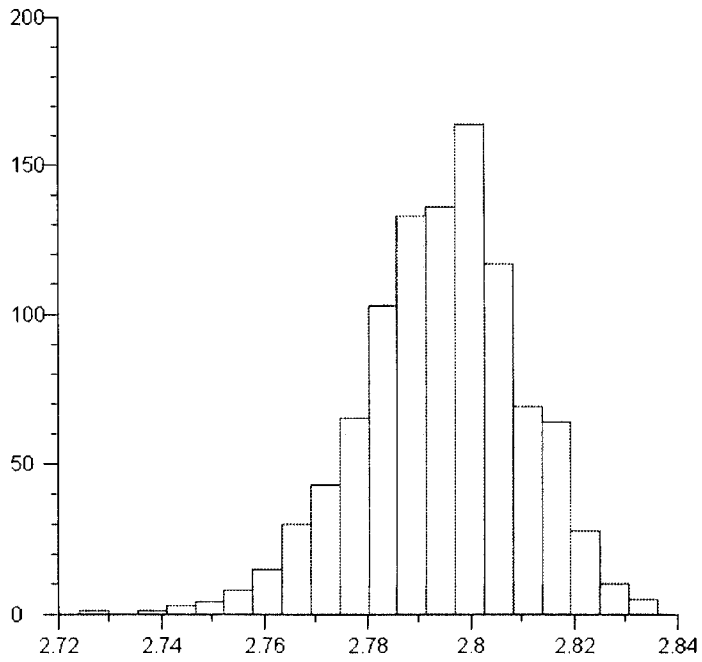

Alpha 1

Estimation of the Three Spectral Indices α_1, α_2 , E_k for1000 Missions

Events were simulated from ϕ_1 with α_1 =2.8, α_2 =3.1, E_k = 100 TeV

Resolution 0%

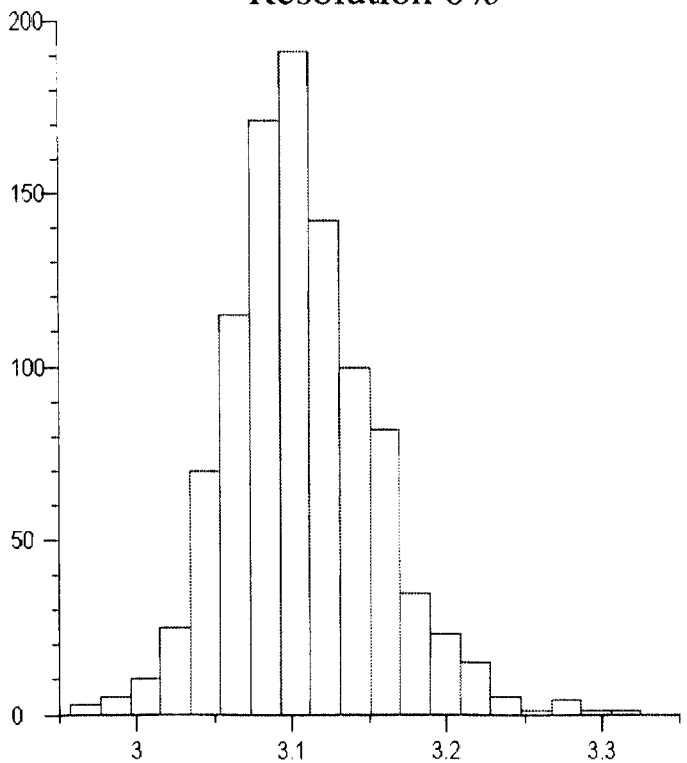

Alpha 2

Resolution 20%

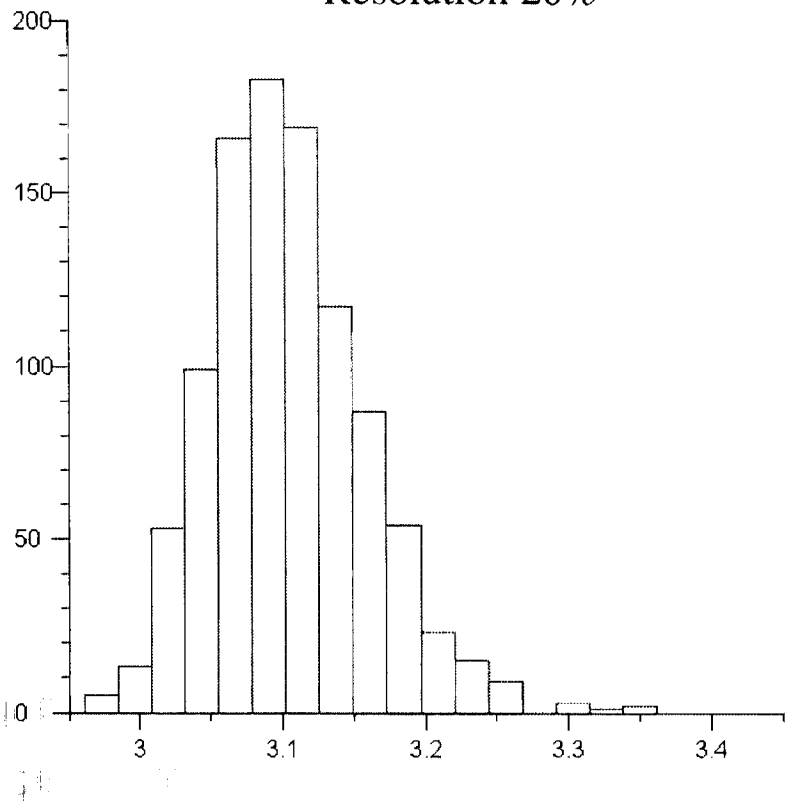

Alpha 2

Estimation of the Three Spectral Indices α_1, α_2 , E_k for1000 Missions

Events were simulated from ϕ_1 with α_1 =2.8, α_2 =3.1, E_k = 100 TeV

Resolution 0%

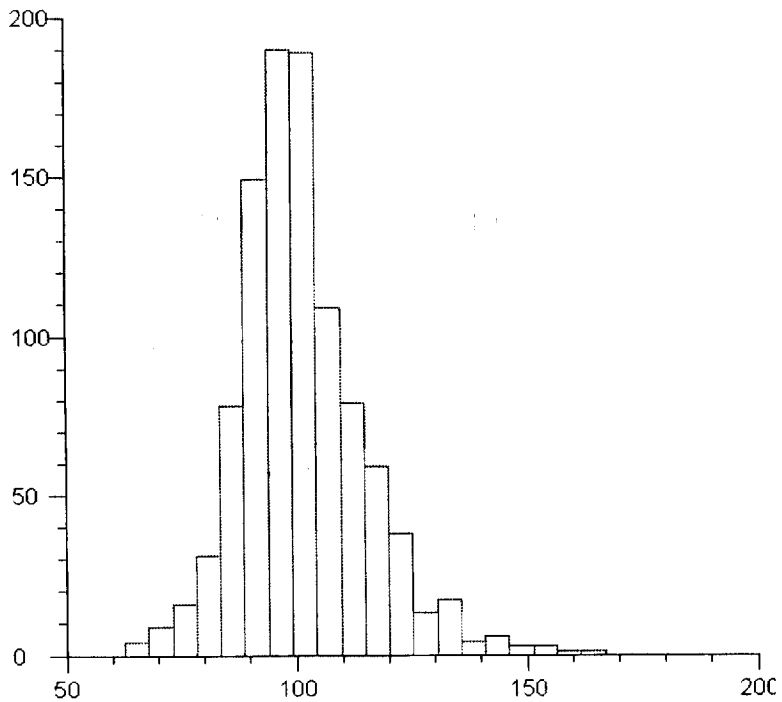

Resolution 20%

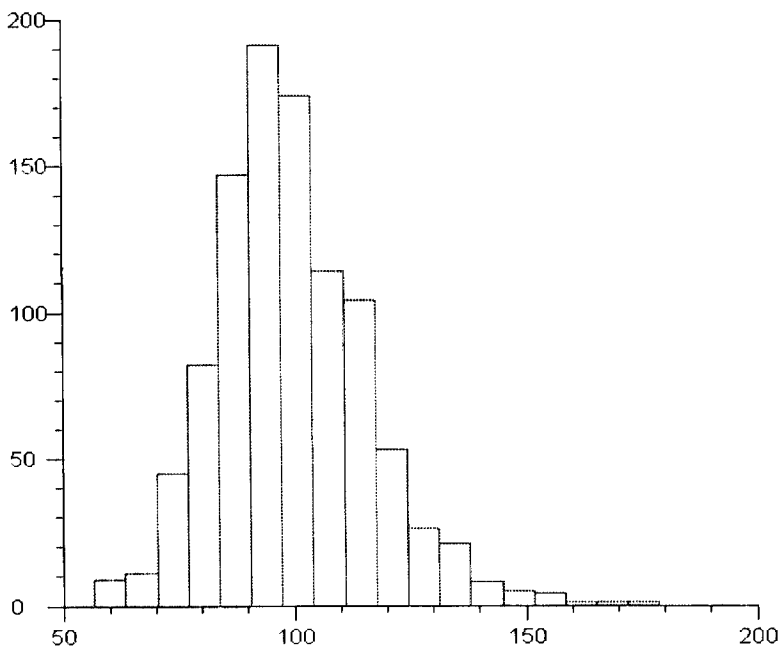

Shows Cramer-Rao Lower bound for the standard deviation of any estimator of the knee location Ek and for a2 (slope above knee) as a function of true knee location for ideal detector with $\rho=0$. α_1 is fixed at 2.8, α_2 =3.1 and 3.3, $100 < E_k < 600$, and data analysis range 20-5,500 TeV.

Note that the Cramer-Rao lower bound for α_2 estimator (second figure) is smaller when the true α_2 goes from 3.3 to 3.1. This is because the number of the events above the knee increases when α_2 goes from 3.3 to 3.1, despite the fact that the variance of the incident energies increases (which would tend to increase the variance of the estimator)

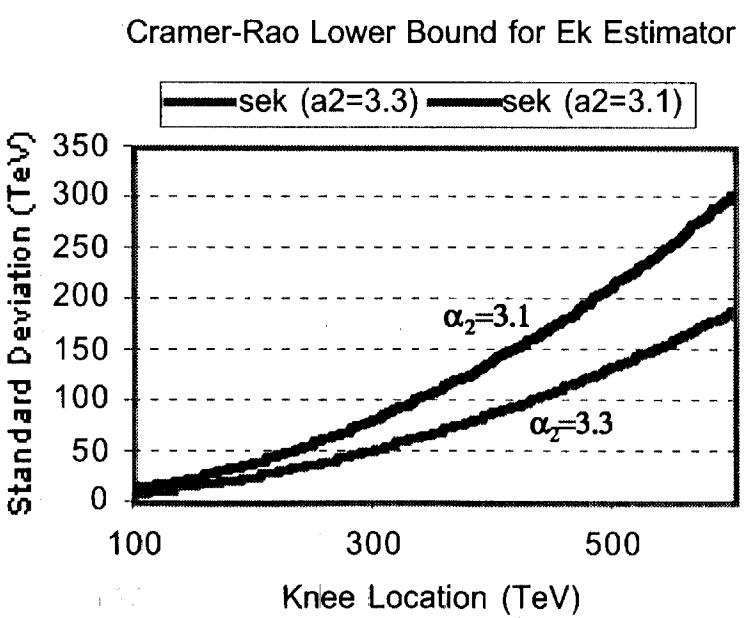

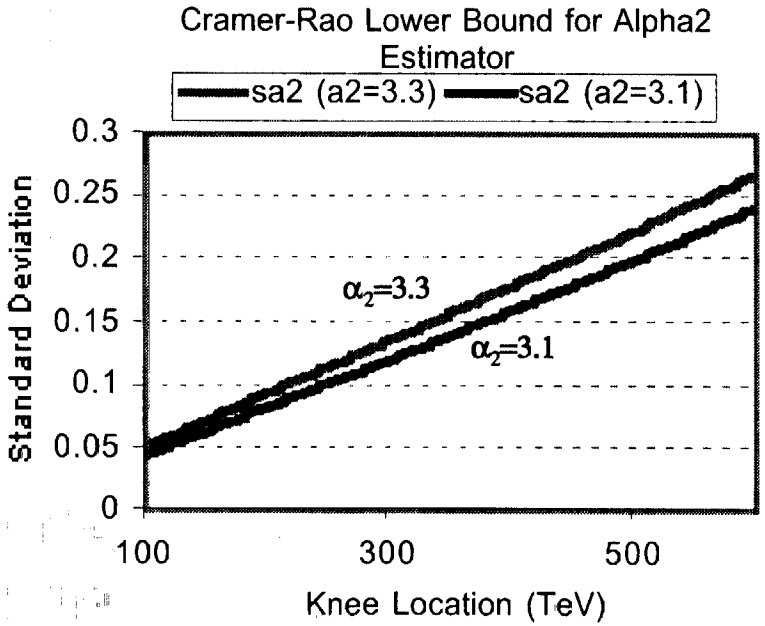

Shows where $(\alpha_2 - 2\,\sigma_{\alpha 2,CR})$ cross with $(\alpha_1 + 2\,\sigma_{\alpha 1,\,CR})$ as a function of knee location for ideal detector with $\rho=0$ (and a half-size detector). This is**NO** substitute for hypothesis testing, but might suggest "a trouble zone" even for the zero resolution detector**AND** using the Cramer-Rao lower bound in $\pm 2\sigma$ (recall $\sigma_{ML} \_ \sigma_{CR}$ for all parameters) . Data analysis range 20-5,500 TeV

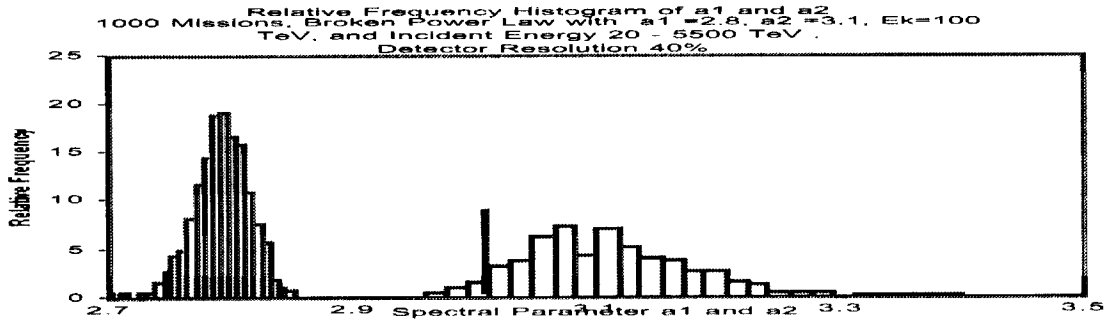

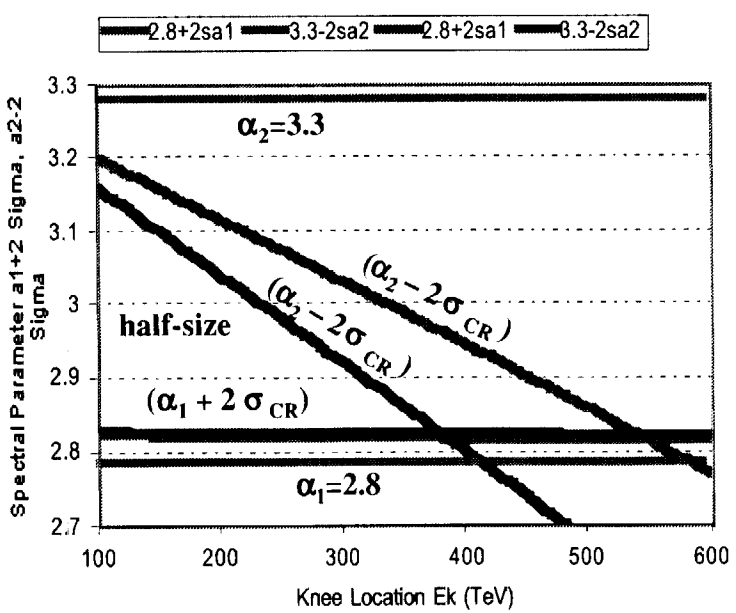

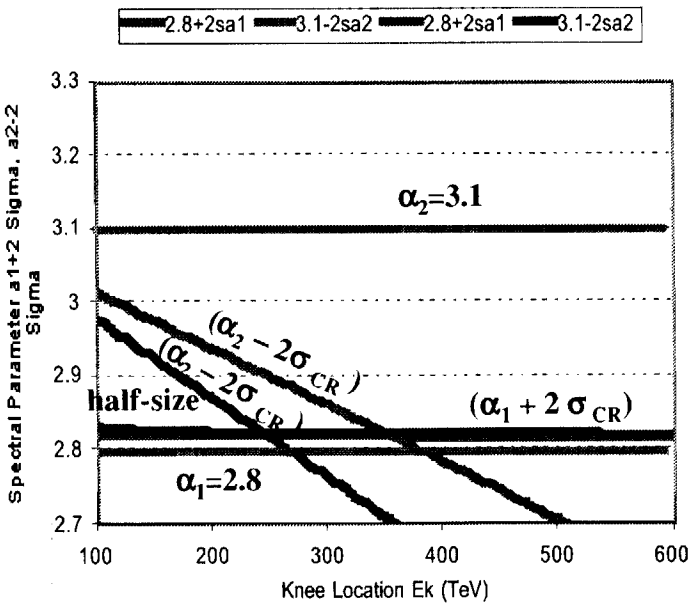

Calorimeter Size and Resolution Study: $20 < E_i < 5{,}500$ TeV

ϕ_1 with $\alpha_{1,} = 2.8$, $\alpha_2 = 3.3$, $E_k = 100$ TeV, Gaussian Response Function 1000 Missions

1. Baseline: ~ $1m^2$, 3 yr (middle curve)
   $N_{average} = 51{,}600$ (~$2{,}250 > E_k$)
2. Half-size (top curve)
   $N_{average} = 25{,}800$ (~$1{,}125 > E_k$)
3. Double-size (bottom curve)
   $N_{average} = 103{,}200$ (~$4{,}500 > E_k$)

α_1

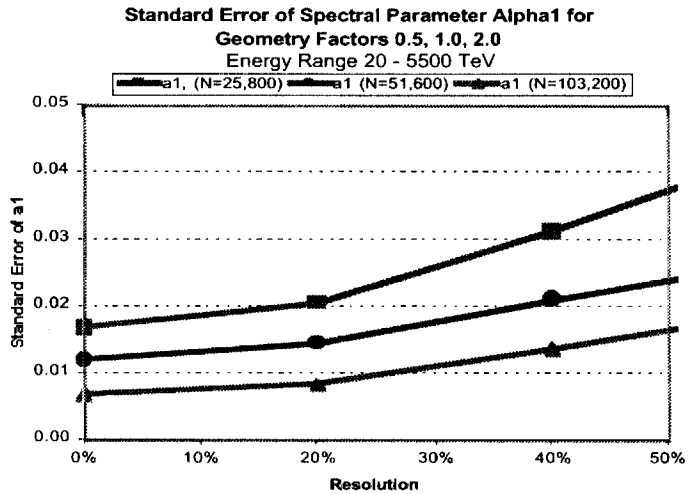

E_k

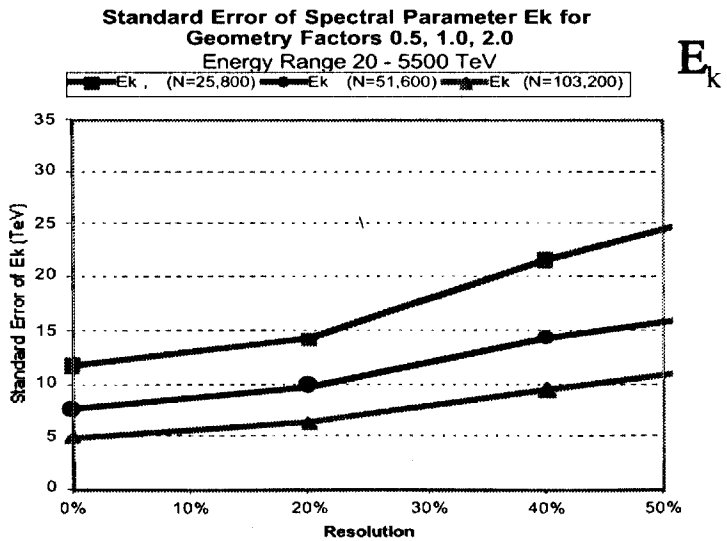

α_2

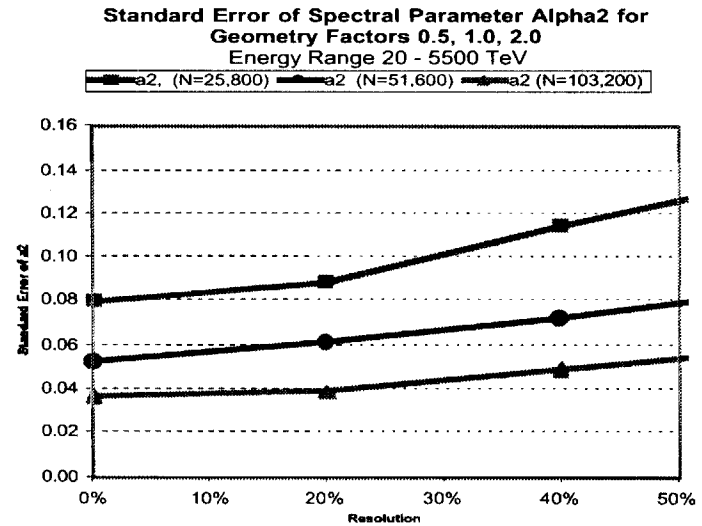

Recall that RMS/Mean is 51% when $\sigma/\mu = 0.6$ for Gaussian response function

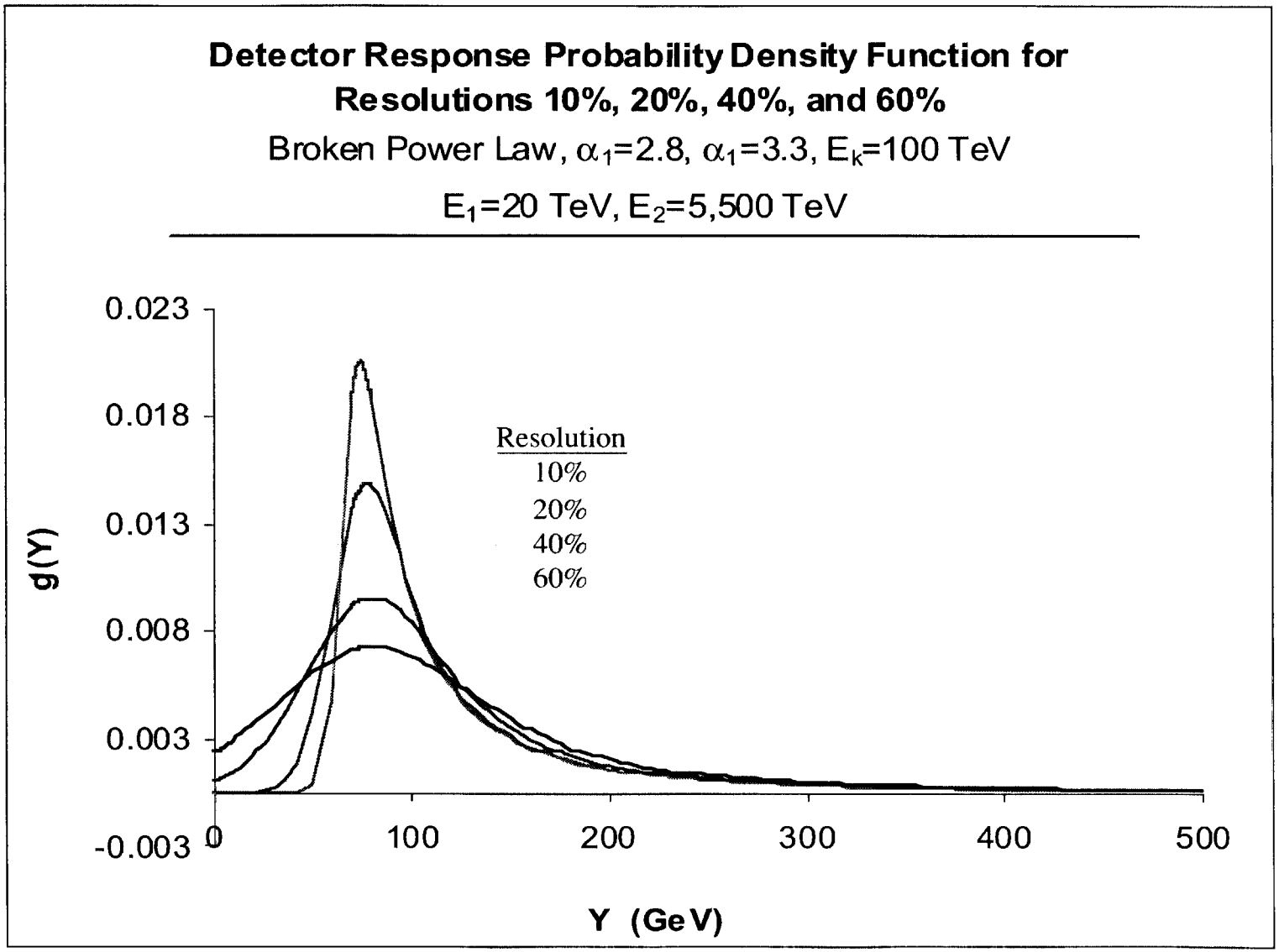
Detector Response Probability Density Function for
Resolutions 10%, 20%, 40%, and 60%
Broken Power Law, α_1=2.8, α_1=3.3, E_k=100 TeV
E_1=20 TeV, E_2=5,500 TeV
0.023
0.018
0.013
0.008
0.003
-0.003
g(Y)
Resolution
10%
20%
40%
60%
0
100
200
300
400
500
Y (GeV)

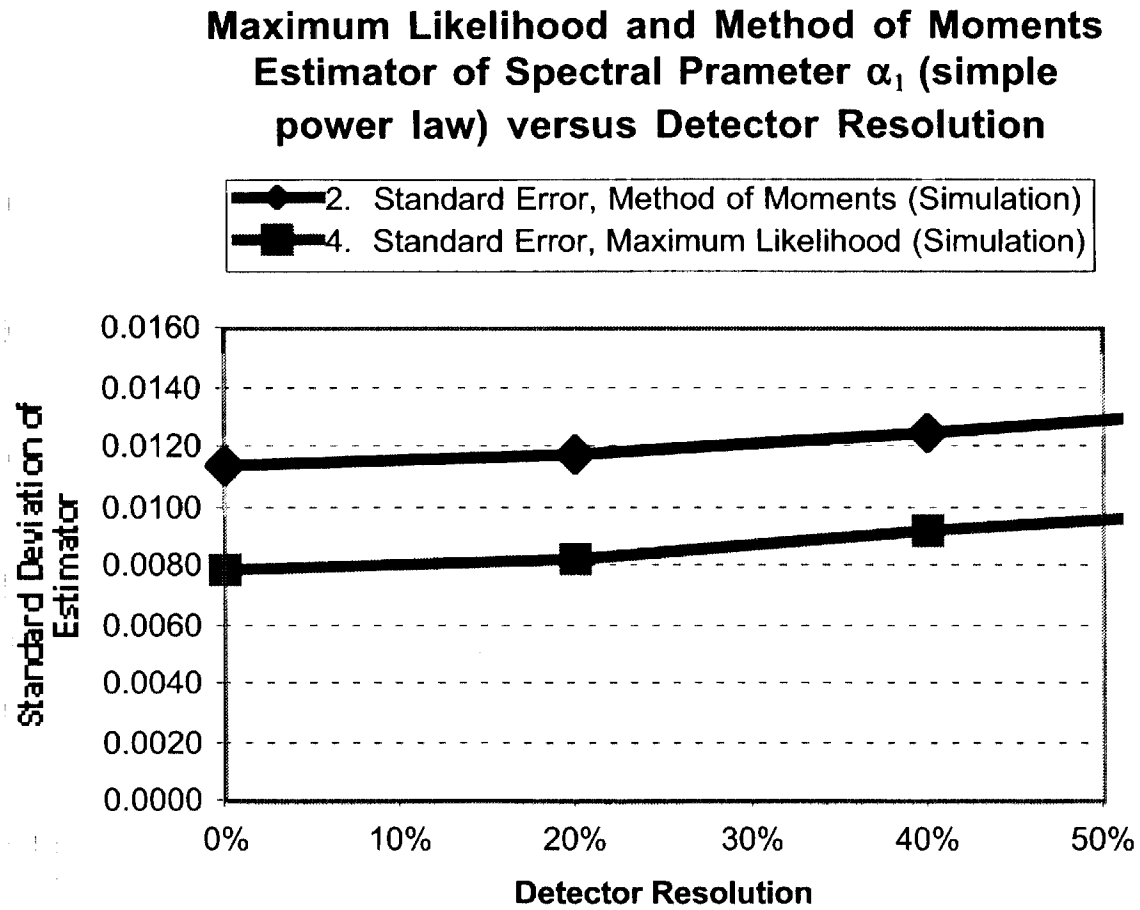
Maximum Likelihood and Method of Moments Estimator of Spectral Prameter α_1 (simple power law) versus Detector Resolution
2. Standard Error, Method of Moments (Simulation)
4. Standard Error, Maximum Likelihood (Simulation)
Standard Deviation of Estimator
0.0160
0.0140
0.0120
0.0100
0.0080
0.0060
0.0040
0.0020
0.0000
0%
10%
20%
30%
40%
50%
Detector Resolution

REFERENCES

1. Sina, R.; and Seo, E.S.: "How Well Can a Cosmic Ray Spectral Kink be Measured?" *COSPAR 32*, Nayoya, Japan, 1998.

2. Kendall, M.G.; and Stuart, A.: *The Advanced Theory of Statistics*, Vol. 1, 2nd ed., Hafner Publishing Company, New York, p. 243, 1963.

3. Kendall, M.G.; and Stuart, A.: *The Advanced Theory of Statistics*, Vol. 2, 2nd ed., Hafner Publishing Company, New York, pp.8–45, 1963.

4. Rheinfurth, M.; and Howell, L.W.: "Probability and Statistics in Aerospace Engineering," *NASA TP—1998–207194*, Marshall Space Flight Center, AL, 1998.

5. Lee, J.; Watts, J.; and Howell, L.: "Simulations of a Thin Sampling Calorimeter With GEANT/FLUKA," *J. Nuclear Instruments*, in press, 2001.

6. Harris, B.: *Theory of Probability*, Addison-Wesley, Reading, Massachusetts, p. 128, 1966.

7. *Numerical Recipes in FORTRAN*, Cambridge University Press, New York, NY, p. 402, 1992.

8. Ormes, J.: Laboratory for High Energy Astrophysics, Goddard Space Flight Center, Greenbelt, MD, Private Communication, 2000.

REPORT DOCUMENTATION PAGE

Form Approved
OMB No. 0704-0188

Public reporting burden for this collection of information is estimated to average 1 hour per response, including the time for reviewing instructions, searching existing data sources, gathering and maintaining the data needed, and completing and reviewing the collection of information. Send comments regarding this burden estimate or any other aspect of this collection of information, including suggestions for reducing this burden, to Washington Headquarters Services, Directorate for Information Operation and Reports, 1215 Jefferson Davis Highway, Suite 1204, Arlington, VA 22202-4302, and to the Office of Management and Budget, Paperwork Reduction Project (0704-0188), Washington, DC 20503

1. AGENCY USE ONLY *(Leave Blank)*	2. REPORT DATE	3. REPORT TYPE AND DATES COVERED
	April 2001	Technical Publication

4. TITLE AND SUBTITLE

Estimating Cosmic-Ray Spectral Parameters From Simulated Detector Responses With Detector Design Implications

5. FUNDING NUMBERS

6. AUTHORS

L.W. Howell

7. PERFORMING ORGANIZATION NAMES(S) AND ADDRESS(ES)

George C. Marshall Space Flight Center
Marshall Space Flight Center, AL 35812

8. PERFORMING ORGANIZATION REPORT NUMBER

M–1014

9. SPONSORING/MONITORING AGENCY NAME(S) AND ADDRESS(ES)

National Aeronautics and Space Administration
Washington, DC 20546–0001

10. SPONSORING/MONITORING AGENCY REPORT NUMBER

NASA/TP—2001–210962

11. SUPPLEMENTARY NOTES

Prepared by Space Science Department, Science Directorate

12a. DISTRIBUTION/AVAILABILITY STATEMENT

Unclassified-Unlimited
Subject Category 90
Standard Distribution

12b. DISTRIBUTION CODE

13. ABSTRACT *(Maximum 200 words)*

A simple power law model consisting of a single spectral index (α_1) is believed to be an adequate description of the galactic cosmic-ray (GCR) proton flux at energies below 10^{13} eV, with a transition at knee energy (E_k) to a steeper spectral index $\alpha_2>\alpha_1$ above E_k. The maximum likelihood procedure is developed for estimating these three spectral parameters of the broken power law energy spectrum from simulated detector responses. These estimates and their surrounding statistical uncertainty are being used to derive the requirements in energy resolution, calorimeter size, and energy response of a proposed sampling calorimeter for the Advanced Cosmic-ray Composition Experiment for the Space Station (ACCESS). This study thereby permits instrument developers to make important trade studies in design parameters as a function of the science objectives, which is particularly important for space-based detectors where physical parameters, such as dimension and weight, impose rigorous practical limits to the design envelope.

14. SUBJECT TERMS

cosmic rays, maximum likelihood, simple power law, broken power law

15. NUMBER OF PAGES

116

16. PRICE CODE

A06

17. SECURITY CLASSIFICATION OF REPORT	18. SECURITY CLASSIFICATION OF THIS PAGE	19. SECURITY CLASSIFICATION OF ABSTRACT	20. LIMITATION OF ABSTRACT
Unclassified	Unclassified	Unclassified	Unlimited

NSN 7540-01-280-5500

Standard Form 298 (Rev. 2-89)
Prescribed by ANSI Std. 239-18
298-102